NBSIR 80-2083

Development of In-Situ Techniques for the Detection and Measurements of Corrosion of Copper Concentric Neutrals in Underground Environments

J. Kruger, U. Bertocci, E. Escalante, and J. L. Mullen

Corrosion and Electrodeposition Group
Chemical Stability and Corrosion Division
Center for Materials Science
National Bureau of Standards
U.S. Department of Commerce
Washington, D.C. 20234

January 1980

Final Report

Issued June 1980

NBSIR 80-2083

DEVELOPMENT OF IN-SITU TECHNIQUES FOR THE DETECTION AND MEASUREMENTS OF CORROSION OF COPPER CONCENTRIC NEUTRALS IN UNDERGROUND ENVIRONMENTS

J. Kruger, U. Bertocci, E. Escalante, and J. L. Mullen

Corrosion and Electrodeposition Group
Chemical Stability and Corrosion Division
Center for Materials Science
National Bureau of Standards
U.S. Department of Commerce
Washington, D.C. 20234

January 1980

Final Report

Issued June 1980

Development of IN-SITU Techniques for the Detection and Measurement
of Corrosion of Copper Concentric Neutrals in Underground Environments

Final Technical Report for Period January 15, 1976 to January 15, 1979

J. Kruger, U. Bertocci, E. Escalante, and J. L. Mullen

1. Introduction

This is the final report of a three-year project, whose objective was
to develop techniques and instrumentation for detecting and measuring the
extent of corrosion of the copper concentric neutral (CCN) wires of buried
electric cables without removal of the cables from the soil. By being able
to locate the sites where the rate of corrosion is high, preventive measures
such as altering the environment (e.g., by backfilling with different soils),
developing new CCN materials, application of cathodic protection, or other
yet to be determined ways, can be applied.

The approach to this problem consisted in finding first, by means of
laboratory tests, the conditions that promote a high corrosion rate, and
subsequently to create those conditions on buried cables in order to compare
laboratory and field results. Also necessary was the development of background
knowledge, such as the role of a.c. in promoting corrosion, in order to provide
a basis for various measurement methods.

Measurements methods such as the recording of polarization curves and
electrode potential were evaluated with respect to their ability to detect
and measure corrosion of buried cables. Also, at the same time, other proposed
methods, such as a.c. impedance and electrochemical noise measurements, were
developed and evaluated in the laboratory. The measurement techniques were then
applied in the field to corroding and non-corroding cables, and their potential
for detecting corrosion assessed.

Specifically, our accomplishments were as follows:

1) The development of methods for the determination of corrosion rates
by polarization measurements;

2) The assessment of potential measurements as a means for detecting
corrosion;

3) The demonstration that polarization measurements can be used to
detect and measure in-situ corrosion of CCN wires;

4) The identification of the environmental factors that affect corrosion
of CCN wires;

5) The development of a theory and the experimental validation of that
theory of the effect of a.c. on CCN corrosion;

6) The development of equipment and methodology to make electrochemical
noise and a.c. impedance measurements in the laboratory.

This final report describes the details of the above accomplishments by collecting together reprints of published papers that describe the work carried out on this project. It also includes preprints of papers that are accepted or have been submitted for publication.

The work described in this report has been successful in identifying and overcoming the most difficult aspects of the problem of in-situ detection and measurement of CCN corrosion. For example, as mentioned above, it has demonstrated that it is possible to make in-situ polarization corrision rate measurements on underground cables. There still remain, however, a number of tasks to be accomplished before enough information is available to provide the basis for the development of simple easy-to-operate field instruments for use by utility personnel. To accomplish this remaining need, the work initiated by the DOE project is to be continued under the sponsorship of the Electric Power Research Institute (EPRI). The new EPRI project, which has been set up for a period of two years, was initiated in October 1979. The new EPRI project seeks to accomplish the following:

1) Adaptation and evaluation of the corrosion noise technique in the field.

2) Interpretation of the corrosion noise technique and its correlation with corrosion rates measured by other means.

3) Completion of the development of polarization corrosion rate measurement techniques by carrying out more extensive current distribution and corrosion rate measurements.

4) Evaluation of polarization and noise measurements on operating cables.

CORROSION/77

ELECTROCHEMICAL AND CORROSION STUDIES ON COPPER CONCENTRIC NEUTRAL WIRES

By

Ugo Bertocci and Jasper L. Mullen
Corrosion and Electrodeposition Section
Metallurgy Division
Institute for Materials Research
National Bureau of Standards
Washington, D.C. 20234

In February 1976 the NBS started work for ERDA to develop methods for the in situ detection of corrosion occurring on copper concentric neutral wires buried underground.

The purpose of these studies is to find an easily applicable test that can detect the locations where corrosion is taking place and can measure the rate of corrosion. By being able to detect such sites, preventive measures such as altering the environment (e.g. by backfilling with different soils), application of cathodic protection, or other yet to be determined ways, can be applied.

Approach to the Problem

For the detection of underground corrosion, it is necessary to assume that the corroding wires send out electrical signals different from those emitted by non-corroding wires or that they respond differently to electrical stimuli. Therefore, the approach to the problem consists in trying a number of measurement methods on buried cables under corroding and non-corroding conditions, and to compare the results.

Four methods have been proposed; two of them are passive, and do not require the application of an external signal, and two are active techniques. They are:

1) Potential Measurements. These measurements are the most simple to carry out and have been already used in the examination of power cable systems,[1] but their reliability is open to question.

2) Noise Measurements. This method as the previous one is a passive method and consists in analyzing the fluctuations in potential in terms

of amplitude and frequency. Although noise measurements are well known in many areas, very little has been done so far to apply them to electrochemical or corrosion systems.[2] This method is therefore a novel one, and although very interesting, it is impossible to predict its usefulness.

3) Polarization Techniques. These techniques, consisting in recording the current-potential response of an electrode-electrolyte half-cell have been extensively and successfully applied by NBS to corrosion rate measurements on metal in the soil.[3] These techniques, under various slightly different forms, galvanostatic, potentiostatic, or potentiodynamic, are the most likely to be successful in discriminating between corroding and non-corroding buried wires.

4) A.C. Impedance Methods. These methods may be considered a special case of the previous one, where the stimulus applied is a sinusoidal signal of various frequencies. These methods are widely used in electrochemistry,[4] but have not been used in underground corrosion studies and their usefulness is unknown.

Before starting with the field tests, however, a considerable amount of work at the laboratory scale is necessary. The objectives of this laboratory work are to provide the necessary knowledge for creating the desired corroding conditions at the field test sites, in other words, to know which environments are conducive to corrosion, and to collect information on what responses and values are to be expected from the measurements in the field.

The purpose of this paper is to present the results of the laboratory tests carried out so far, and to discuss their implications as to the causes of the concentric neutral wire corrosion and as to the prospective value of the field test methods proposed.

Experimental Methods

On the basis of an examination of the situation and of previous published studies[5] on the corrosion of concentric neutrals, it was decided to investigate the effect of the following parameters:

1) presence or absence of oxygen,
2) presence or absence of chloride ions in solution,
3) presence or absence of convective motion in the electrolyte,
4) presence or absence of an a.c. signal,
5) coupling of the metal wire to conducting polyethylene (CPE).

As basic electrolyte solution for the corrosion tests and the current-potential measurements, it was decided to choose a neutral 2% solution of Na_2SO_4 adding, in a number of cases, 1% NaCl. Later on, following indication by others[6] that sulfur in some forms could be a significant factor in causing corrosion, tests were carried out also in 0.42 m $NaClO_4$.

As material to submit to the corrosion tests, tinned copper wire coming from the same cable to be used for the field tests was chosen. For the current-potential measurements, experiments were also carried out on pure copper and on a massive piece of an alloy containing 90% Pb and 10% Sn, equal to the composition of the tinning bath.

The effect of oxygen was studied by running tests both under an O_2 and an N_2 atmosphere. To study the influence of convective motion, some corrosion tests were carried out in solution gels obtained by adding 1% agar, as done by Schick[5].

Since in the actual buried cables it is likely that alternating current is leaking from the neutral wire into the soil, its effect upon corrosion was examined by applying a voltage signal between the wire under study and on counterelectrode. The circuit employed is shown in Fig. 1. By using a very small resistance (10Ω) for the current measurements, a very large capacitance ($110~\mu F$), and a large counterelectrode to working electrode surface area, a condition approaching a potentiostatic system was achieved.

Cells and circuits used for the electrical measurements are of conventional design, and will not be described here. For the noise measurements, which are still at a preliminary stage, two circuit schemes are being tested. The first, shown in Fig. 2, is based essentially on the use of a spectrum analyzer particularly built for low frequencies. The instrument employed has 200 channels and at its lowest frequency range is 5 Hz with a resolution of 0.025 Hz, this being also the lowest frequency measured. Problems arising from d.c. coupling of the amplifier tend to restrict the lowest measurable frequency to 0.1 Hz. The second method has the capability of detecting signals whose amplitude is below that of the noise of the electronic equipment employed, and operates by introducing the noise signal to be measured in two parallel amplifying and filtering channels, as shown in Fig. 3. The output signals of the two channels go to a multiplying amplifier with averaging capability. Each channel signal is the sum of the source noise and of the instrument noise, but since the instrument noise if uncorrelated, the average of its product is zero and the output of the multiplying amplifier should be only the square of the source noise.

Experimental Results

A) Current-Potential Measurements.

Potentiodynamic scans have been carried out on wire samples as well as on copper and Pb-Sn alloy in various solutions. Figs. 4 and 5 give the results for tinned wire, Figs. 6 and 7 give the scans for pure copper in Na_2SO_4, Fig. 8 in $NaClO_4$, and Figs. 9, 10, and 11 in Na_2SO_4 and NaCl. Finally, Figs. 12, 13, and 14 report the results for the Pb-Sn alloy. All data were taken at room temperature, 23°C.

B) Corrosion Tests.

Wire samples were immersed in the various solutions chosen for testing and left there for times up to and exceeding 2000 h, in the presence or absence of combinations of the parameters under examination, i.e., oxygen, chloride ions, CPE coupling, and a.c. signal. In a number of cases, agar was added so as to prevent convection in order to simulate more closely the conditions in the soil. If the samples were electrically connected to the CPE, the short circuit current was also monitored. In the cases where an a.c. signal was superimposed, a.c. cell voltage and a.c. current were recorded.

At the end of the tests the wires were examined optically, and in some cases with a scanning electron microscope. Analysis of the surface material was carried out in some instances by means of x-ray energy dispersion.

Some of the results are presented here. Figs. 15, 16, 17, and 18 are photos of the electrode potential versus time obtained in a number of corrosion tests. Other results are summarized in Table I, dealing with the observed short circuit currents between tinned Cu wire and CPE and Table II, relative to a batch of tests with superimposed a.c. The rest potential versus time of CPE and of a massive piece of Pb-Sn alloy have also been monitored under various conditions. The results are shown in Fig. 19.

C) Noise Measurements.

The work done so far on the detection of electrochemical noise for corrosion studies has been concentrated on the testing and calibration of the instrumentation, and on exploratory work to establish the units of sensitivity of the systems. The work is at too early a stage to allow much discussion. As an example of the results obtained with the method described in Fig. 2, two typical spectra are shown in Fig. 20.

Discussion of the Results

The extrapolation from laboratory tests to the actual behavior underground is always risky, and requires comparison of the results of measurements in both environments to be sufficiently reliable. For the time being, therefore, we will discuss the results drawing a minimum of conclusions.

The potentiodynamic scans taken on the tinned wire are rather complex in shape, particularly in the presence of Cl^- ions, but comparison with the results on pure copper and on Pb-Sn alloy enables us to separate the different contributions. Essentially all the peaks observed at potentials more negative than approximately -200 mV vs. S.C.E. are due to the tinning coat and are absent on copper, and tend to disappear rather rapidly on the tinned wire itself, if dissolution due to extensive potential cycling is allowed to occur.

When the results on copper are observed, it is clear that no adherent passive film tends to form in neutral solutions (pH is always close to 7). Although the copper ions produced anodically eventually precipitate as hydroxide, no protective layer is formed and the anodic branch of the scan increases monotomically in sulfate and in perchlorate. The situation is somewhat different in the presence of Cl^-, since CuCl precipitates immediately on the surface, so that at times peaks and inflexion points are observed on the anodic sides. The layer, however, affords no protection, and anodic current densities are as large or larger than in other solutions. The precipitate is, however, on the electrode surface so that part of it can be reduced during the cathodic sweep, causing a characteristic peak between -200 and -400 mV.

The results of the corrosion tests indicate that presence of oxygen and of Cl^- ions tends to increase the rate of attack. In a number of instances pit formation was observed under large salt encrustations. The data summarized in Table II show that more rapid attack can be caused by an a.c. signal, but it is not evident that serious corrosion cannot occur without it. Observation of the wires after the tests showed that the specimens under N_2 were covered with a Cu_2O deposit, and that the tinning had disappeared. Surface analysis has confirmed that the tinning coat might be lost eventually, possibly because of failure to totally prevent oxygen leakage.

Galvanic coupling with CPE has also been suspected as a possible contributing cause to corrosion of the wires. Some results, reported in Table I, show that in some instances the short circuit current is cathodic on the wire. The anodic reaction on the CPE electrode might be the oxidation of intermediate corrosion products such as Cu^+ migrating from the metal wire.

By observing the data in Figs. 16, 17, 18, and 19 some general trends can be found. More positive potentials occur in the presence of oxygen and in the absence of chlorides. Coupling with CPE generally raises the potential, which is consistent with the data of Fig. 17, showing that the rest potential of CPE is close to 200 mV. Exceptions, however, are observed, notably in oxygenated chloride solutions where coupling lowers the potential,

compared with the corresponding test without coupling. Interestingly, in these cases the wire is cathodic with respect to the CPE, except for the solution containing agar, where transport of the corrosion products to the CPE is much more difficult.

The results obtained so far give a fair idea of the parameters that enhance wire corrosion. As far as their implications on predicting the feasibility of detecting corrosion of buried cables by electrical measurements, comparison with field experiments is necessary. Some general trends can probably be spotted by potential measurements, but current-potential measurements hold more promise of giving useful indications, if the response of underground wires is analogous to that of the specimens in our laboratory beakers.

REFERENCES

1)   D.H. Kroon, Mat. Perf. 15, N.8, 19 (1976).

2)   G. Okamoto, T. Sugita, S. Nishiyama, K. Tachibana, Bōshokugijutsu, 23, 439 (1974); S. Nishiyama, K. Tachibana, G. Okamoto, T. Sugita, ibid. 23, 445 (1974).

3)   See, for instance, W.J. Schwerdtfeger, J. Res. NBS, 65C, 271 (1961).

4)   See, for instance, M. Sluyters-Rehbach, J.H. Sluyters, in "Electro-analytical Chemistry", Vol. 4, A.J. Bard, ed., p. 1 (1970).

5)   G. Schick, Paper N. 128, Intern. Corr. Forum, Toronto (1975).

6)   R. Latanision, Private communication.

Table 1

Corrosion current (c) $\mu A/cm^2$, and electrode potential (E), mV vs. SCE for tinned copper coupled to CPE

conditions of the test				Time, h					
chloride	atm.	ac	Agar		0	48	164	212	308	329
No	O_2	No	Yes	C E	+0.13 +21	+0.23 +21	+0.04 +21	+0.03 +20	-0.01 +19	-0.03 +20
Yes	O_2	No	Yes	C E	+7.8 -83	+9.4 --	+6.8 -88	+6.8 -90	+6.8 -89	+6.8 -91
Yes	N_2	No	No	C E	+0.65 -148	+0.73 -150	+0.57 -153	+0.59 -158	+0.57 -156	+0.51 -156
Yes	N_2	No	No	C E	+0.17 -174	+0.14 -166	+0.15 -167	+0.36 -164	+0.50 -163	+0.40 -169
No	N_2	No	No	C E	-0.01 -315	-0.03 --	-0.02 -310	-0.02 -305	-0.01 -281	-0.01 -275
Yes	O_2	No	No	C E	-0.21 -31	-0.22 --	-0.13 -18	-0.11 -19	-0.14 -10	-0.18 -10

TABLE 1 continued....

conditions of the test					Time, h					
chloride	atm.	ac	Agar		0	48	164	212	308	329
No	O_2	No	No	C	+0.09	+0.06	+0.10	+0.12	+0.14	+0.17
				E	+16	+8	+7	+7	+5	+7
No	O_2	No	No	C	+0.19	+0.23	+0.16	+0.16	+0.21	+0.21
				E	+9	+9	+9	+9	-3	+11
Yes	N_2	Yes	No	C	+0.5	+3.5	+0.7	+1.1	+1.4	+2.5
				E	-119	-122	-126	-129	-130	-129
No	N_2	Yes	No	C	+1.6	+0.94	+1.1	+0.93	+0.79	+0.81
				E	-24	--	-13	-28	-15	-7
Yes	O_2	Yes	No	C	-1.0	-0.46	-0.14	-0.14	-0.14	-0.36
				E	-55	-55	-53	-55	-55	-51
No	O_2	Yes	No	C	+4.0	+1.2	+0.68	+0.57	+0.71	+0.93
				E	+28	--	+41	+31	+25	+27

Table II

Data concerning 12 corrosion tests, lasting 2000 hours, a.c. superimposed

| No.	Atm.	Cl⁻	CPE coupling	Agar	d.c. mV	a.c. mA/cm^2	short circ. $\mu A/cm^2$	Optical Examination
1	N_2	*			-240	8		Rather uniform Cu_2O layer
2	N_2	*			-220	8		
3	N_2				-50	4 to 2		Cu_2O layer
4	N_2		*		0	2	+1/+2	Cu_2O crystals
5	N_2	*	*		-140	8	+2/+5	Cu_2O, Cu deposit. Less attack
6	O_2	*	*		-50	1	-0.2	Small green crystals, Cu_2O
7	O_2		*		+30	0.8	+1/-0.2	Thin layer of green crystals
8	O_2			*	-20/+5	2		Green scale. Red blisters
9	O_2	*		*	-150/-60	6 to 2		Similar to 8
10	O_2				+20	2.5		Sheets and mounds of green salt. Pits full of Cu_2O
11	O_2				+20	2		
12	O_2	*			-50	2 to 1		Large green mounds
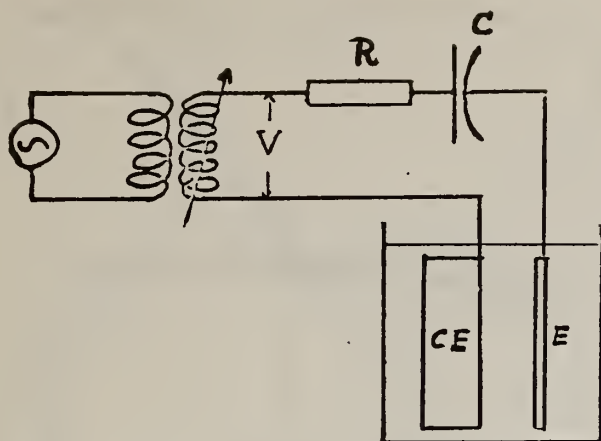
Fig. 1   Schematic circuit for corrosion tests with superimposed a.c.
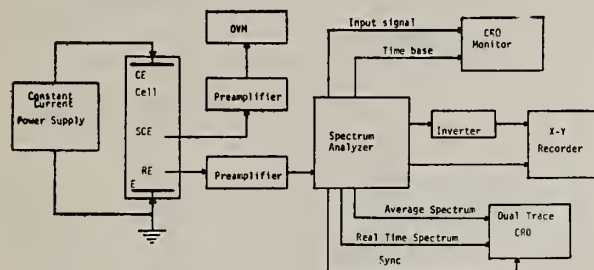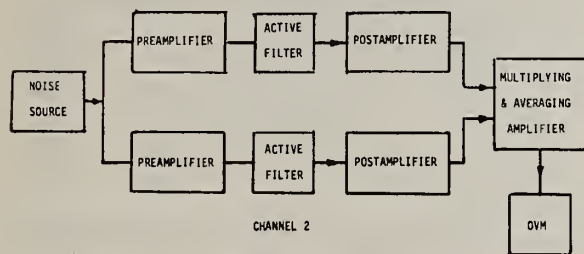

Fig. 2   Schematic circuit for noise measurements.
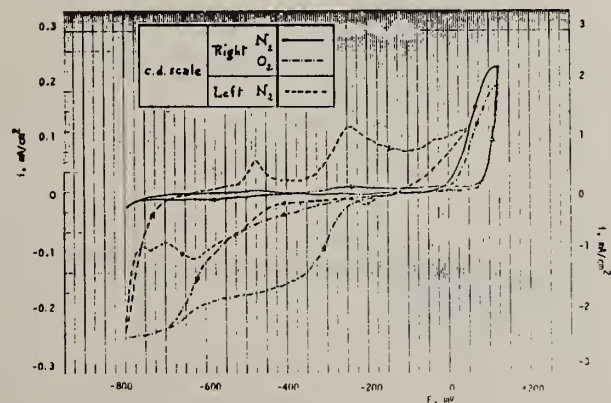

Fig. 3   Noise measuring circuit.

Fig. 4   Potentiodynamic scans for tinned Cu in 2% Na$_2$SO$_4$. Scan rate 4 mV/sec. Dashed curve is expansion of solid curve and refers to c.d. scale on left.
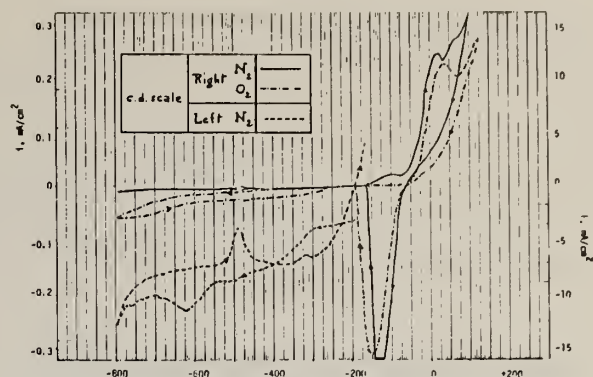

Fig. 5   Potentiodynamic scans for tinned Cu in 2% Na$_2$SO$_4$ + 1% NaCl. Scan rate 4 mV/sec. Dashed curve is expansion of solid curve and refers to c.d. scale on left.
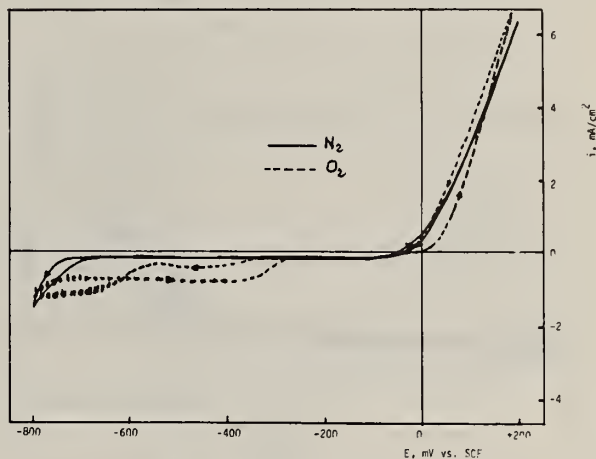

Fig. 6   Potentiodynamic scans for Cu in 2% Na$_2$SO$_4$. Scan rate 4 mV/sec.

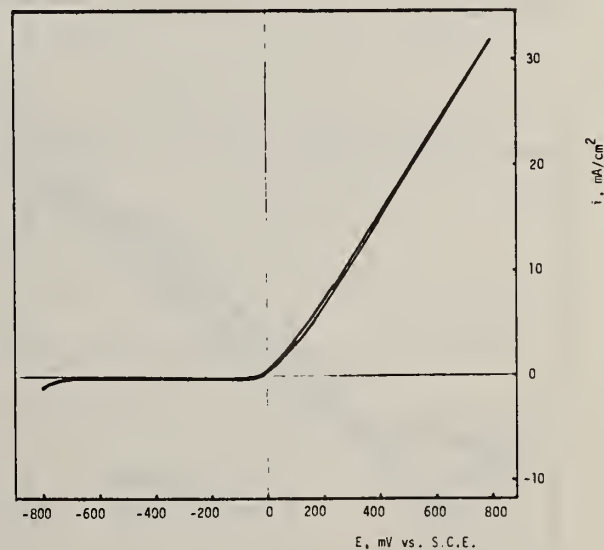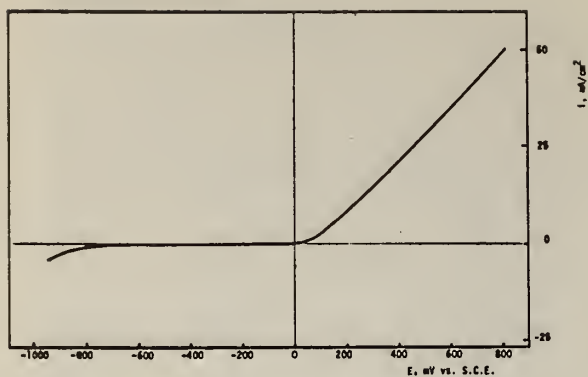Fig. 7   Potentiodynamic scan for Cu in 2% Na$_2$SO$_4$ up to 800 mV. Scan rate 4 mV/sec.

131/7

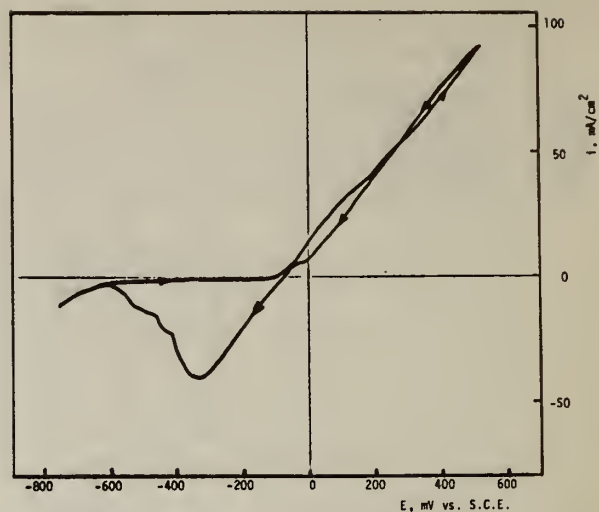Fig. 8 Potentiodynamic scan for Cu in 0.4m NaClO₄. Inert atmosphere. Scan
rate 4 mV/sec.

Fig. 11 Potentiodynamic scan for Cu in 2% Na₂SO₄ + 1% NaCl. Inert atmosphare.
Scan rate 40 mV/sec.
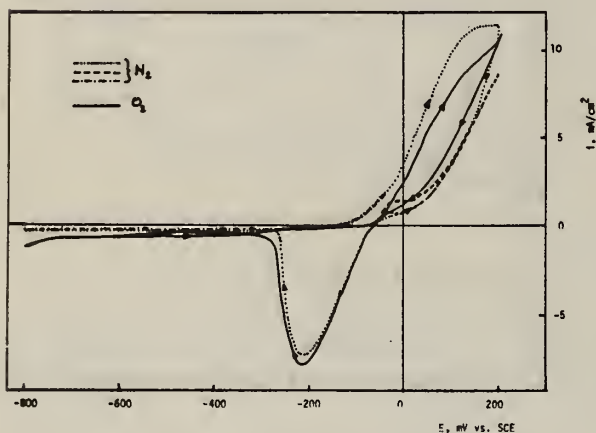

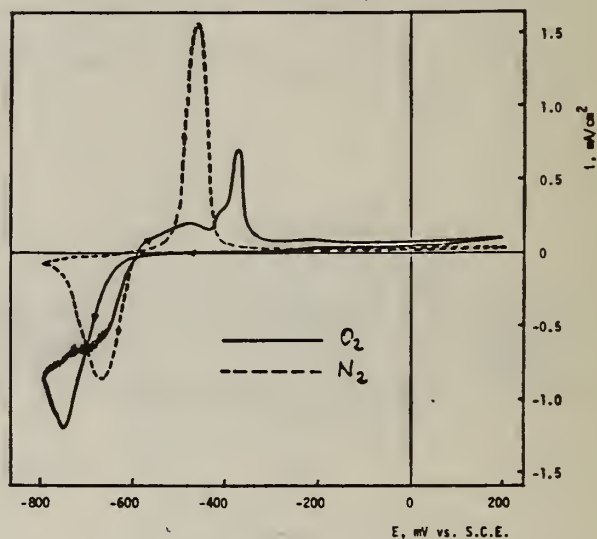Fig. 9 Potentiodynamic scans for Cu in 2% Na₂SO₄ + 1% NaCl. Scan rate 4 mV/sac.

Fig. 12 Potentiodynamic scans for Pb-Sn alloy in 2% Na₂SO₄. Scan rate 4 mV/sac.
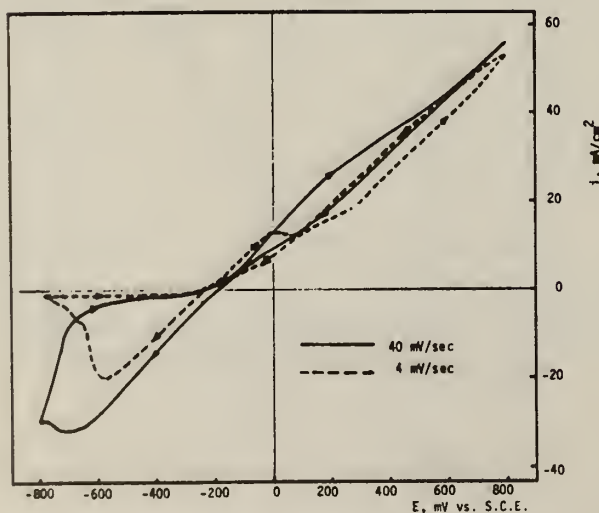
Fig. 10 Potentiodynamic scans for Cu in 2% Na₂SO₄ + 1% NaCl. Inart atmosphere.
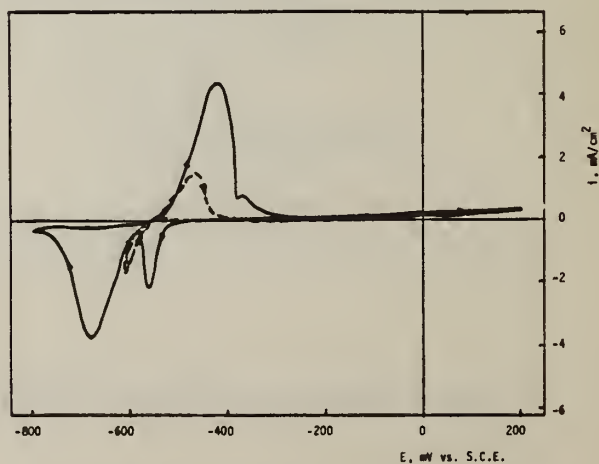
Fig. 13 Potentiodynamic scans for Pb-Sn alloy in 2% Na₂SO₄ + 1% NaCl. Inert
atmosphare. Scan rate 4 mV/sec.

131/8
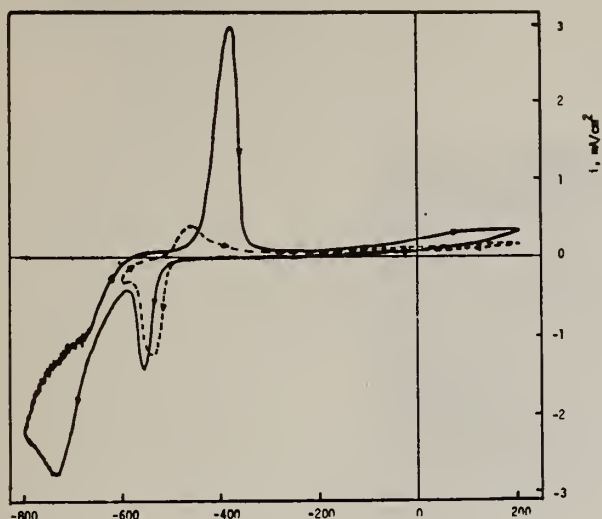
Fig. 14 Potentiodynamic scans for Sn-Pb alloy in 2% Na_2SO_4 + 1% NaCl. Scan rate 4 mV/sec. Oxygen atmosphere.
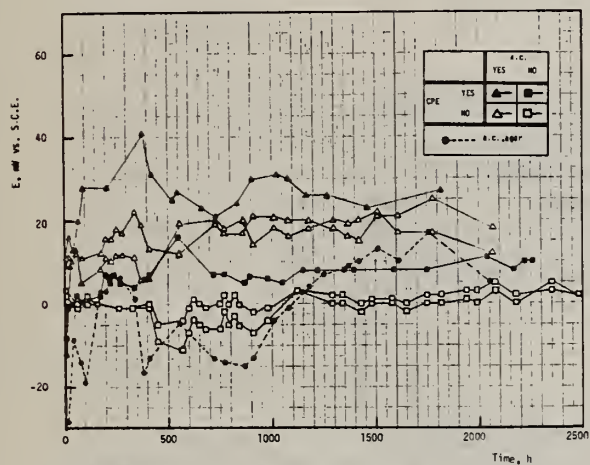
Fig. 15 Electrode potential vs. time for tinned Cu wire in 2% Na_2SO_4. O_2 atmosphere.
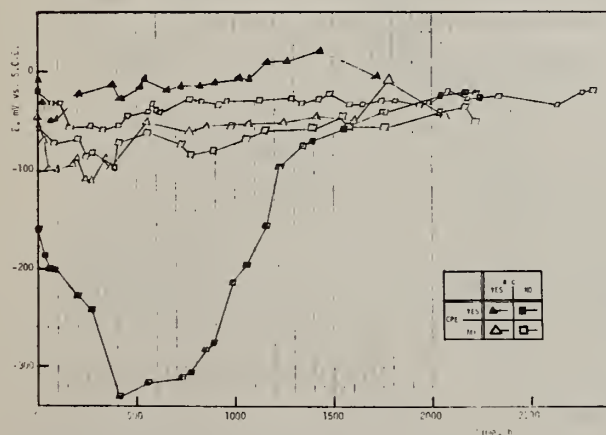
Fig. 16 Electrode potential vs. time for tinned Cu wire in 2% Na_2SO_4. N_2 atmosphere.
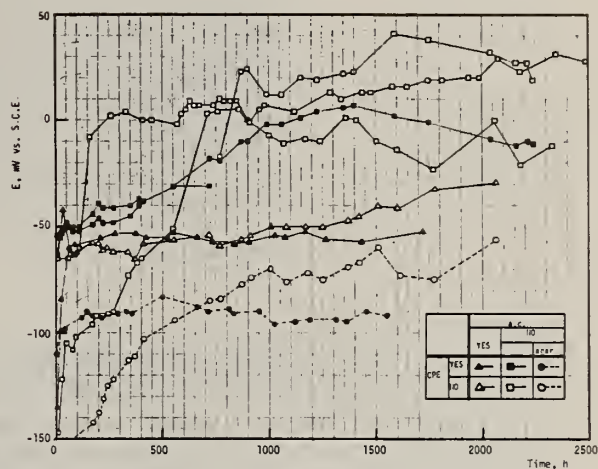
Fig. 17 Electrode potential vs. time for tinned Cu wire in 2% Na_2SO_4 + 1% NaCl. O_2 atmosphere.
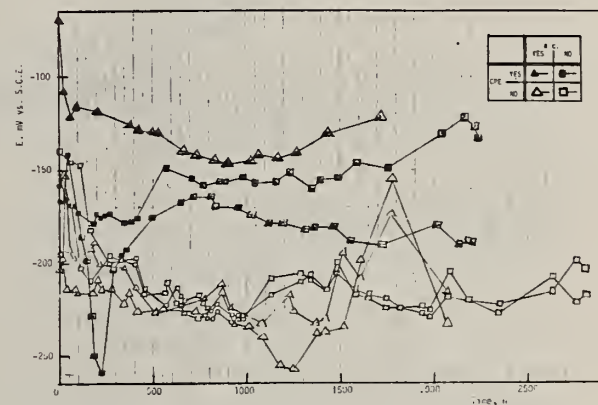
Fig. 18 Electrode potential vs. time for tinned Cu wire in 2% Na_2SO_4 + 1% NaCl. N_2 atmsophere.
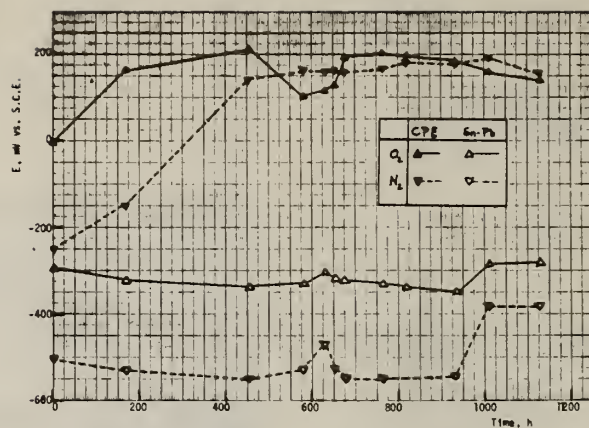
Fig. 19 Rest potential vs. time for CPE and Pb-Sn alloy in 2% Na$_2$SO$_4$ + 1% NaCl.
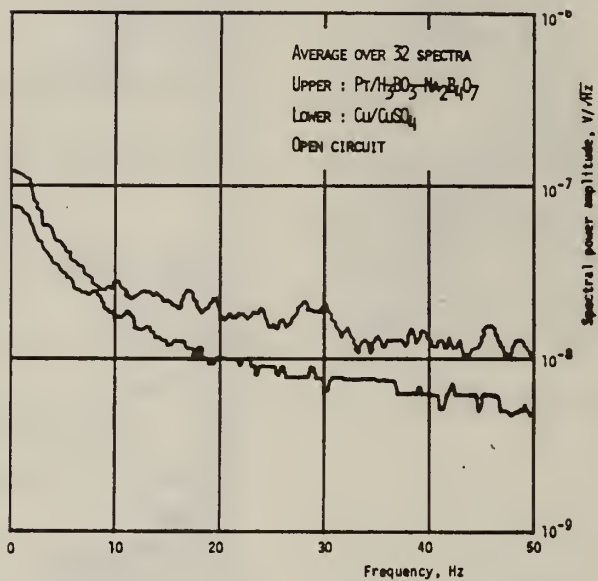
Fig. 20 Noise spectrum at open circuit. 1) Cu in CuSO$_4$. 2) Pt in borate.

CORROSION/79

A Field Study on the Corrosion of
Concentric Neutral Cable

E. Escalante, U. Bertocci, J. Mullen
Corrosion and Electrodeposition Section
National Bureau of Standards
Washington, D.C. 20234

INTRODUCTION

The corrosion of the outer metallic members of electric cable in under-
ground distribution networks is a threat to the safety and longevity of these
systems. Though the corrosion problem is apparently not widespread, it can be
a serious threat in the local areas where it is found. In fact, realizing
that a corrosion situation exists is a problem in itself. Often times the
corrosion of the cable is found by accident when the cable is excavated for
reasons not related to corrosion. Thus, an important part of this study is to
be able to detect the existence of corrosion on the cable and measure the
extent of deterioration.

MATERIALS AND ENVIRONMENT

The cable used for this study was chosen on the basis of the cable
design most widely used throughout the United States as determined from the
sales of three major cable manufacturers. The specifications were as follows:

#2 AWG stranded conductor in cross-linked, thermosetting polyethylene
insulation with ten strands of #14 AWG coated copper concentric neutral
wires manufactured within AEIC #5 and IPCEA S-61-402 specifications.

Figure 1 illustrates the cross sectional configuration of the cable.

For our purposes the inner stranded conductor and its polyethelene
insulation are of little consequence since they do not play an active role in
the corrosion process. The carbon filled polyethelene jacket around the
insulator is of interest because of its relatively low resistivity and the
chemically noble nature of carbon in the electromotive series. The average
film thickness of this jacket is 0.8 mm, and its resistivity, which was
measured to be 50 ohm cm, changed when mechanically flexed during handling and
increased by as much as a factor of two in an irreversible way.

The ten outer strands of coated copper concentric neutral wire are spirally wound around the jacket making one complete turn every 22.5 cm of cable. Ideally these wires do not touch one another and generally they remained separated in the 330 meters of cable we received. The diameter of the wire including the coating is 1.63 mm. During its manufacture, the wire is coated by passing it through a 90% Pb, 10% Sn bath and then drawing it through a die to remove the excess molten material. The resulting film is a Cu Sn intermetallic with some Pb.

In addition to the cable, bare copper wire and an ingot of the tinning alloy was obtained from the cable supplier. The wire was identical to that used on the cable, but without the coating. Chemical analysis of the ingot indicated that antimony was the single major impurity (0.3%) and the sum of all other impurities was less than 0.7%.

The underground test site is located on the NBS grounds in an area that was found to have the lowest soil resistivity. The ground is slightly inclined with good drainage and an average soil resistivity of 10,000 ohm cm. Soil ph has been found to be between 5.5 to 6.0. The first 0.5 m is a brown loamy, well aerated soil which becomes more clay like with increasing depth. Below 1 m the soil is distinctly clay like and changes to a grey color.

EXPERIMENTAL PROCEDURE

Four cable specimens were cut to a length of 15 m. The ends of each cable were wrapped with 5 turns of 0.5 mm copper wire which was then soldered to each one of the ten concentric neutral wires. The entire end was then coated with a silicon adhesive, thus, reducing the development of local galvanic cells. Copper wire was also wrapped and soldered around the cable at a point midway between the ends of the cable. To this was attached an insulated 14 AWG wire which extended out of the ground after burial and served as an electrical contact to the concentric neutral wires. Silicon adhesive was also applied to this joint.

In order to evaluate the electrochemical interaction of the cable components, sections of cable were cut to a length of 1 m. The concentric neutral wires were removed from the body of the cable and reassembled as illustrated in Figure 2. The ends of the wires were soldered to a copper conductor and coated with silicon adhesive. An insulated electrical conductor which extended above ground was attached to one corner of the specimen. Similar specimens were made from the uncoated copper wire. The remaining body of the cable which was jacketed with the carbon loaded polyethylene was coated on the ends with adhesive. At a midpoint between the ends, copper wire was tightly wrapped around the jacketed cable, coated with adhesive, and connected to an insulated conductor leading above ground. The 90% Pb, 10% Sn ingot was rolled down to strips 0.5 cm thick. Specimens were cut from this such that their total surface area was equal to the total surface area of the concentric neutral wires on a 1 m section of cable (512 cm^2). The 90% Pb, 10% Sn sheet specimens were then attached to insulated conductors leading above ground.

The specimens were buried to a depth of 1 m in trenches approximately 0.6 m wide and of sufficient length to hold the 15 m cables and cable components. Figure 3 is a top view of the burial plan. Two parallel cables were located in each trench and positioned against the side walls so that they were approximately 0.6 m apart along the length of the trench. A wooden post located between the cables at their midpoint, extended above ground and supported the electrical conductors attached to the cables. After burial a 60 Hz, 45 acV signal was applied between two of the cables in one trench (cables 1 and 2). This developed an alternating current of 0.7 mA/cm^2 on the concentric neutral wires. Current control was accomplished by using a variable transformer.

Isolation was found necessary to remove undesired direct current (dc) coming through the ac line. The second set of cables (cables 3 and 4) had no imposed ac, however, the soil was locally modified as will be described. In an effort to increase localized corrosion which could subsequently be detected and monitored by our measurements on cables 3 and 4, a cubic meter of soil was removed from a section of these cables which were visually inspected at this time. Laboratory studies indicated that the corrosion rate on the concentric neutral cable could be raised by increasing aeration in the presence of chlorides. After visual inspection, the excavation was backfilled with a mixture of equal volumes of soil and sand. As the layers of soil-sand mixture were added, a solution of sodium chloride was poured over each layer. A total of four kilograms of sodium chloride were added to the backfill material. Three months after the modification, the soil was qualitatively tested for chloride content and the soil resistivity measured at three locations at the site and at three depths at each location. The chloride evaluation was made by taking 100 g of soil and mixing it with 200 ml of distilled water. After standing for 30 minutes the mixture was filtered so that a clear solution resulted. 1 ml of a saturated solution of silver nitrate was added to the filtrate causing any chloride to precipitate as silver chloride.

MEASUREMENTS

Two types of measurements were made on the 15 m cables. These consisted of open circuit potential survey measurements and polarization measurements.

Open circuit potential surveys consisted of soil surface potential measurements made at the intersections of an 18 m x 2 m grid at 1 m intervals along the length of each buried cable using a $Cu-CuSO_4$ reference electrode. Every point on the grid is marked at the field site with a permanent aluminum marker imbedded in the ground. With these markers it is possible to make repeated measurements over several months at the same point. The survey allows one to detect potential changes that may occur along the length of the cable.

The circuit diagram being used for polarization measurements is illustrated in Figure 4. This diagram can be thought of as two separate circuits with the section to the left of the specimen providing and measuring the current for polarization while the circuit to the right measures the resultant potential change of the specimen. Ac filtering circuits are included so that polarization measurements can be made in the presence of the ac signal imposed on cables 1 and 2.

The section on the left has a dc power supply whose current output to the specimen is controlled by a voltage divider circuit not shown in the illustration. In addition to this voltage divider there is a variable resistor which also assists in current control. Two switches in parallel, as illustrated, can completely isolate the specimen from the current circuit. The normally open (N.O) switch is a push button microswitch used for intermittent current control. The on-off switch bypasses the N.O. switch when needed for longer term current applications. The output of the dc power supply is measured by a zero resistance ammeter. Notice that the ammeter is in parallel with a capacitor which serves as an ac filter for the ammeter, and allows most of the ac to travel to ground through the counter electrode without affecting the dc current measurement.

The section of the circuit shown to the right of the specimen in Figure 4 is used to measure the potential of the specimen with respect to the $Cu-CuCO_4$ reference electrode. The potential is measured across a Wheatstone bridge which is used to measure and compensate for any IR error.

The high impedance voltmeter is isolated from the background ac by means of a two-pole low-pass filter circuit which reduces the 60 Hz signal by as much as a factor of 5000.

Measuring the corrosion rate of a finite length of a metallic member in an electrolyte such as soil is, in general, not difficult using techniques developed here and elsewhere (1,2). However, measuring the corrosion rate of what amounts to be an infinite length of metal poses a special problem. The problem is that of not knowing how much of the metallic specimen is being polarized. If the surface area being polarized is not known, then corrosion current densities cannot be calculated.

To get around this problem polarization measurements were made at four points along each cable. The positions of the electrodes were changed for each measurement as illustrated in Figure 5. The currents necessary to polarize each section of cable to an overpotential of 6 mv are then compared. The amount of current required to polarize each section of cable 6 mv is directly related to the corrosion rate of the section.

In order to determine current distribution, current was applied to a cable from a counter-electrode driven into the ground at a given distance from the cable, and potential measurements made over the length of the cable. The change in potential with and without polarizing current applied was then plotted for each point along the cable.

Of secondary interest to the study was the electrical interaction of the cable components. Though single specimens were included in the study, most data was obtained from the galvanic couples whose galvanic current was measured with a zero impedance ammeter. This data gives the magnitude of the current and the direction of flow.

RESULTS AND DISCUSSIONS

The primary objectives of this study were twofold. The first objective was to detect the presence of localized corrosion on a buried cable and, second, to evaluate the intensity of the deterioration. The three conditions of exposure for the 15 m cables were as follows. One set of cable (1 and 2) had an imposed ac signal of 0.7 mA/cm^2. The second set of cables (3 and 4) was buried without any imposed ac. And finally, the corrosion of a small section of the cables without ac was increased by a local modification of the soil.

Initially a considerable amount of time was spent in improving our ability to make measurements in the presence of the imposed ac and other interfering signals. By using the filtering circuits described earlier, these interferences were essentially removed from the measuring circuit allowing us to observe the dc signal of interest. The effect of the imposed ac on the open circuit potential of cables 1 and 2 was observed over several months. The first measurements were made before the ac signal was applied as is shown for cable 1 in Figure 6. This figure illustrates the potential along the cable at intervals (positions) of 1 m. This potential was unstable for the first few weeks after the ac was applied but later stabilized as the three month data show. Throughout the next several months the potential fluctuated slightly and gave little indication of what was happening to the cable. Similar open circuit potential measurements were made on cables 3 and 4 that had no imposed ac but did have the local soil modification. Again the potentials remained very stable even in the area of the soil modification as the data for cable 3 in Figure 7 illustrates. The only change observed was that the overall potential of the cable became more positive (noble) with time.

Polarization measurements were made on the cables 1 and 2 before the ac was turned on with the results shown at the bottom of Figure 8. Without ac the polarizing current was less than 500 μA. After applying the ac signal, however, the polarizing current began to increase with time until one section of the cable reached a polarizing current of 12,500 μA after 3 months. Ten months later the polarizing current still averaged over 5,000 μA with a high of 8,000 μA. At this time the ac was turned off and the measurements repeated immediately. The polarizing current remained essentially unchanged. Two months later with the ac still off the polarizing current had dropped to an average of less than 2,000 μA.

The same polarization measurements were made on cables 3 and 4 which were free of ac. The data for cable 3 over a period of more than 12 months is shown in Figure 9. In every case the polarizing current was below 600 μA or a factor of ten times less than that measured on the cables exposed to ac. The suggestion is that the imposed ac has dramatically increased the corrosion of the concentric neutral cables. These cables were excavated and inspected after the last measurements were made. Figure 10 is a photograph of a concentric neutral cable that had imposed ac. The surface is corroded and pitted and is representative of how the entire cable appears. Figure 11 is also a representative section of the cable without ac. Some attack is visible but clearly not of the magnitude observed with ac. The measurement in Figure 9 also indicates that the modified soil increased the corrosion of that section by 20 to 40% as compared to the sections around it. Figure 12 is a photograph of a section of the concentric neutral cable that was in the modified soil.

In order to evaluate the distribution of current over the cable during polarization, the change in potential over the length of the cable was measured as current was applied from a vertical steel rod in the ground. The distance of the current source was varied from 0.5 m to 1 m. The resulting data, illustrated in Figure 13, indicate that from a distance of 1 m the current is distributed over the 15 m cable with little concentration of current in the vicinity of the source located at position 5. As the current source (counter-electrode) is moved to within 0.5 m of the trench, the current distribution begins to show a distinct concentration around the source with an applied current of 1.8A. When a current of 0.9A is applied at a distance of 0.5 m, 85% of the current is concentrated along 9 m of the 15 m cable. As the current is increased the distribution becomes more uniform. This type of information which describes the current distribution during polarization is necessary for corrosion rate determinations. However, more data is needed before current densities can be calculated with confidence.

The galvanic current measurements made on the cable components are listed in Table 1. This table shows the average galvanic current measured over the period of burial and the polarity of the components. As expected, the data clearly indicates that the carbon filled polyethylene is cathodic to the coated copper wire, the bare copper wire, and to the 90% Pb, 10% Sn alloy, but the galvanic current generated is of such low magnitude that it caused only minor damage to the metals. Examination of these components after removal verified that they had suffered minor corrosion attack. However, the coating alloy sheet developed severe attack when connected to the bare copper wire, a condition that was expected judging from the current measurements.

SUMMARY AND CONCLUSIONS

It has been found that differences in degree of corrosion along a 15 m cable can be detected by polarization techniques. This method was used to determine that the cables with an imposed ac were deteriorating ten times faster than similar cables without ac, and that the section of cable in the modified soil was corroding only slightly more than other sections of the same

cable. These measurements were substantiated by visual examination of the cable after excavation. The distribution of polarizing current along a cable can be determined so that current densities and corrosion rates may be calculated, but more work is needed on this phase of the study. The measurements also revealed that potential readings give no indication of the condition of the cable.

The galvanic couples of the cable components indicate that the carbon filled polyethylene is cathodic to the coated copper wire, the bare copper wire, and to the 90% Pb, 10% Sn alloy, but the galvanic current generated is of such low magnitude that it caused only minor damage to the metals.

References

1)   Schwedtfeger, W. J., A Study by Polarization Techniques of the Corrosion Rates of Aluminum and Steel Underground for 16 months, J. Res. Nat. Bur. Stand. (U.S.), 65C, No. 4, 271-276 (Oct.Dec. 1961).

2)   Jones, D. A. and Lower, T. A., ASTM Journal of Materials; "Polarization Methods for Measuring the Corrosion of Metals Buried Underground, p. 600, Sept. 1969.

Table 1

Galvanic Currents of Cable Components

Specimens	Average Current μA	Polarity
Bare copper wire connected to carbon filled polyethylene	2.8	Bare copper wire anodic
Bare copper wire connected to coating alloy sheet	682	Coating alloy sheet anodic
Coated copper wire connected to carbon filled polyethylene	8.8	Coating copper wire anodic
Coating alloy sheet connected to carbon filled polyethylene	49	Coating alloy sheet anodic
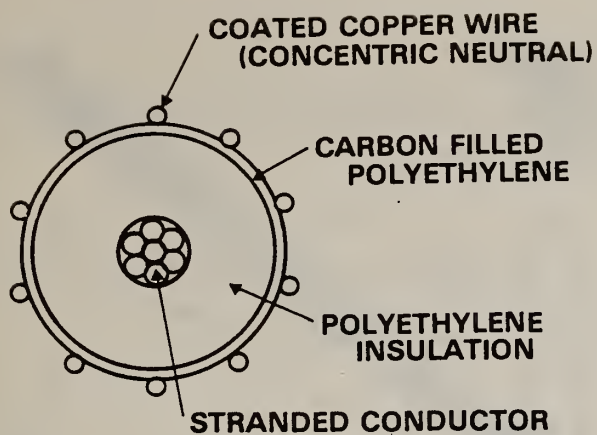
FIGURE 1 - Cross-section of concentric
neutral cable.
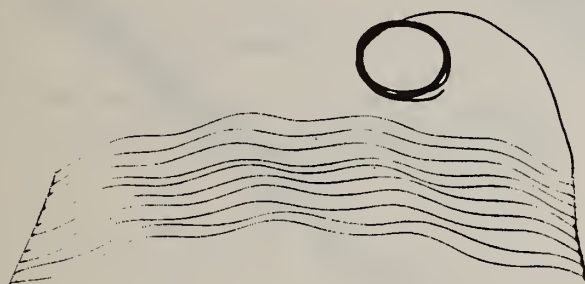
FIGURE 2 - Concentric neutral wires as
assembled for burial.
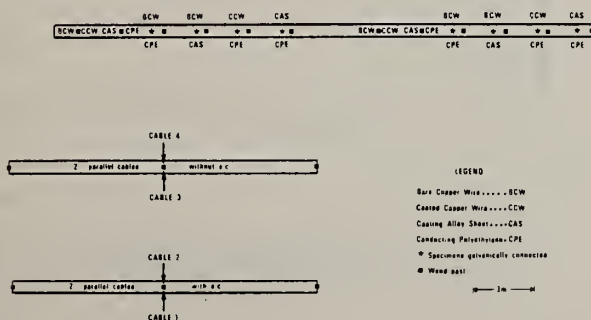
FIGURE 3 - Top view of NBS test site.
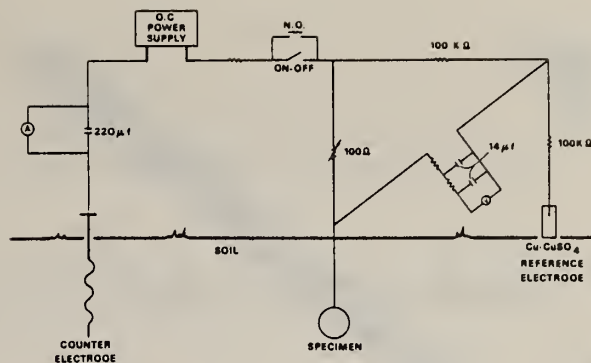
FIGURE 4 - Electrical diagram of polarization
circuit.
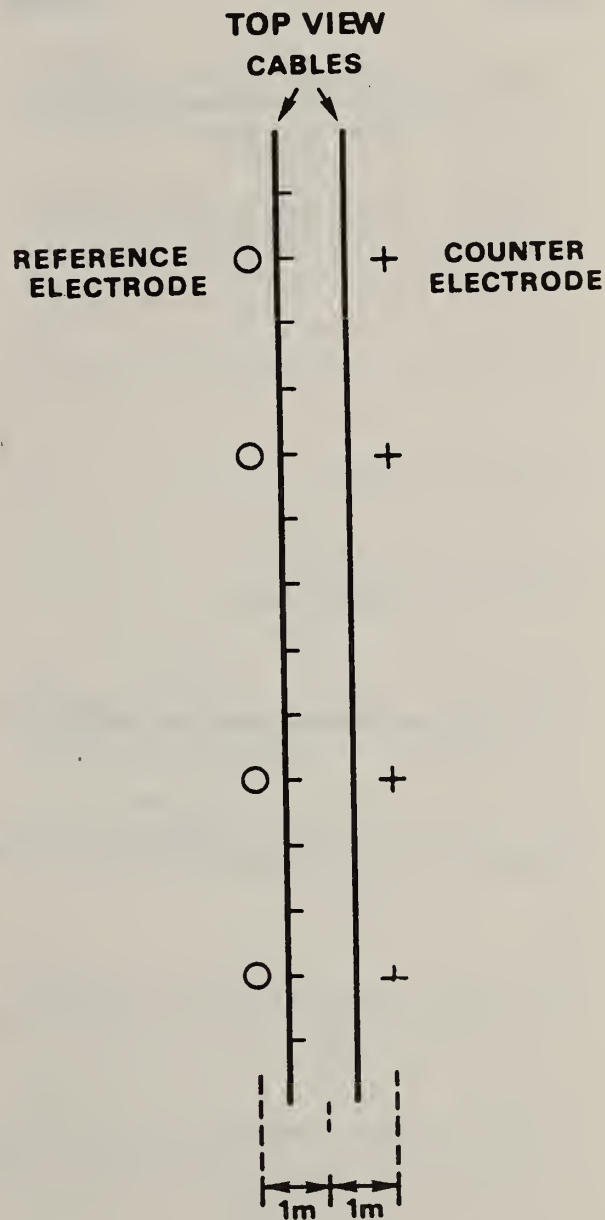
FIGURE 5 - The positions of the electrodes
during polarization.

244/7
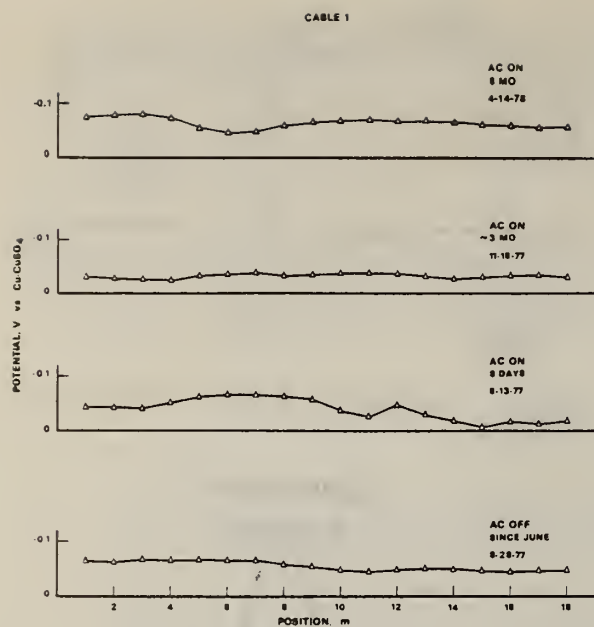
FIGURE 6 - The potential along cable 1 at different burial times.

FIGURE 8 - The current required to polarize cable 1 6 mV at four positions and at different burial times.

FIGURE 7 - The potential along cable 3 at different burial times.
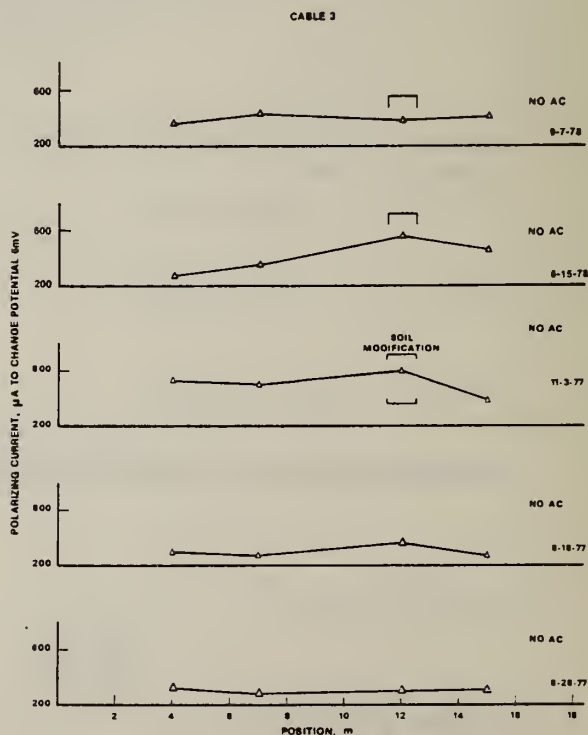
FIGURE 9 - The current required to polarize cable 3 6 mV at four positions at different burial times.
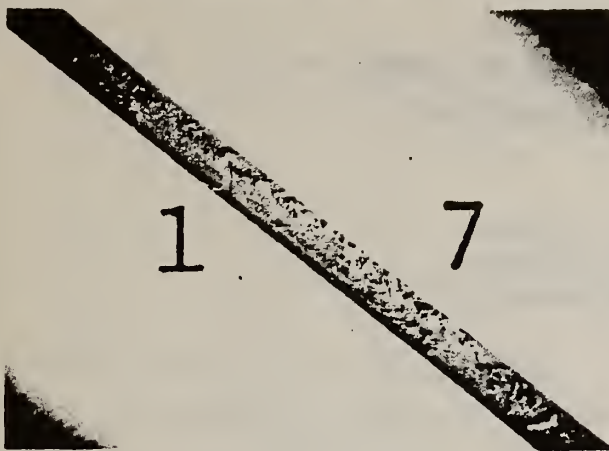
FIGURE 10 - Section of concentric neutral wire with imposed ac.
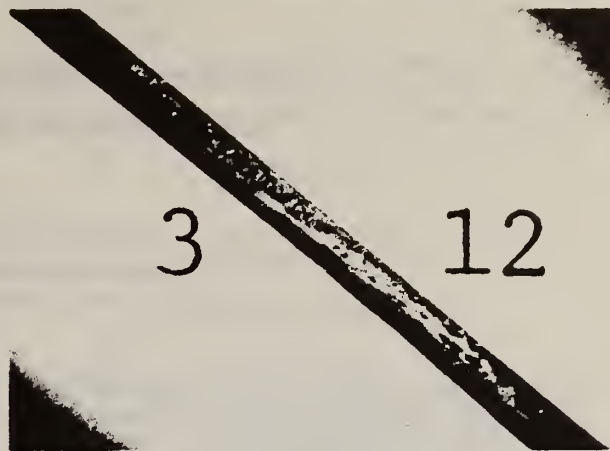
FIGURE 12 - Section of concentric neutral wire without ac in modified soil.
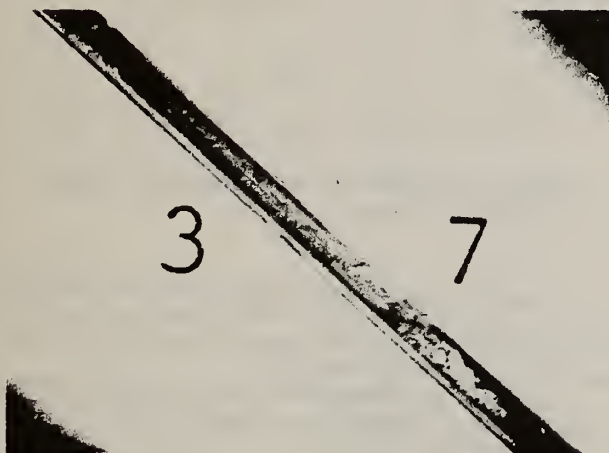
FIGURE 11 - Section of concentric neutral wire without ac.
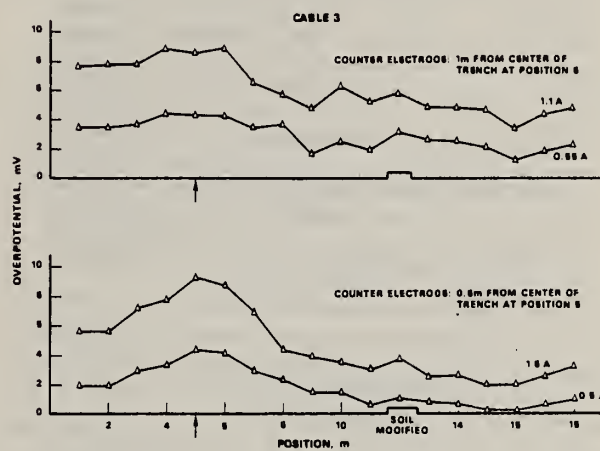
FIGURE 13 - The distribution of polarizing current along the cable as indicated by the change in overpotential.

Laboratory Corrosion Studies on Tinned
Copper Concentric Neutral Wires*

U. BERTOCCI and J. L. MULLEN
Corrosion and Electrodeposition Section,
National Bureau of Standards, Washington, DC

Results are given of corrosion tests up to 2500 hours of tinned Cu neutrals such as are used for grounding residential underground distribution systems. Data were compared for couples between tinned Cu neutrals and conductive polyethylene also. Environmental variables included compositions of electrolytes (Na sulfate and perchlorate) and superimposed AC. Data were taken when oxygen was present and absent and when there was convective motion of the solution. Pitting was found on specimens carrying superimposed AC, more in nonoxygenated than in oxygenated environments. Chlorides intensified attack and bottom pitting was extensive when they were present. Potentiodynamic scans were made also to determine the current-potential behavior of the electrodes. A specimen of 90 Pb-10 Sn alloy (used for tinning the wires) was tested also with results indicating irreversible reduction of a Pb sulfate film occurred. The quantity of tin removed during the tests was measured. AC attack was impeded when corrosion products were present and no significant difference was found between the effects of perchlorate and sulfate environments. Differential aeration may contribute to effects noted. Field tests are contemplated.

THIS PAPER REPORTS the results of laboratory experiments carried out on "tinned" copper concentric neutral (CCN) wires at the National Bureau of Standards (NBS) under contract with the Department of Energy (formerly ERDA).

The aim of the research was to develop methods for the detection of corrosion on CCN wire buried underground, and for this purpose a number of techniques are being investigated, both in the laboratory and in the field. However, before starting the field tests, a considerable amount of laboratory work was necessary to provide the knowledge for creating the desired corrosion conditions at the field test sites, and to collect information on what results can be expected in the field tests. Moreover, the results obtained in these studies can shed some light on the possible causes of corrosion of buried CCN cables.

Experimental Methods

Materials

Materials used for these studies were mainly "tinned" (*i.e.*, Pb/Sn) copper wires with a diameter of 1.5 mm, taken from a CCN cable obtained from a major manufacturer of such cables. When immersed in an electrolyte, the wire ends were masked with a protective paint. Some experiments involved the use of specimens of conductive polyethylene (CPE) which covers the insulating sheath of a CCN cable. These were also cut from a piece of the same cable, and electrical contact was made by electrodepositing copper on the CPE and then winding copper wire tightly over it. The contact was masked with insulating paint. Some measurements were carried out on bare copper wires. In this case, oxygen free, high conductivity (OFHC) copper was used.
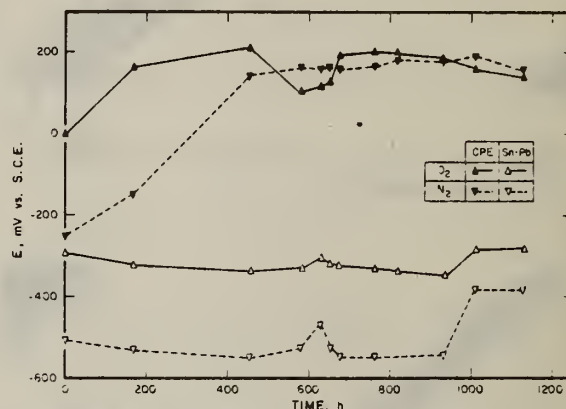
FIGURE 1 — Rest potentials vs time of CPE and Pb-Sn alloy in 2% Na_2SO_4 + 1% NaCl.

The cable manufacturer also provided a sample of the alloy used in the "tinning" process for the Cu wire. The alloy was found to be 90% Pb and 10% Sn with small amounts of impurities. This alloy was employed in some experiments.

The open circuit potential of CPE and of the tinning alloy was monitored for an extended period in various environments. The results are presented in Figure 1.

On the basis of previously published studies,[1-4] several environmental variables were tested for their influence on corrosion susceptibility. These were:

Composition of the Electrolyte. Four laboratory test solutions were employed: 2% Na_2SO_4, 2% Na_2SO_4 + 1% NaCl, 0.42M $NaClO_4$, and 0.42M $NaClO_4$ + 1% NaCl. The pH of all solutions was approximately neutral. These solution compositions were chosen to determine the influence of a sulfate ion (thought not to be particularly aggressive), both in the presence and absence of chloride ions (which are considered to be corrosive in soil). Solutions containing another nonaggressive salt—perchlorate, instead of sulfate were also tested, because of reports that sulfur in some form could be a significant factor in causing corrosion.[5]

Composition of the Gaseous Atmosphere in Contact with the Solution. Both oxygen and nitrogen atmospheres were tested, the latter to simulate poor soil aeration.

Convective Motion in Solution. Since convective transport in the soil is negligible compared to that in a solution, some corrosion tests were carried out in 1% agar gel to simulate soil conditions. In this case, the solution had the same composition given above.

Superimposed AC. Since with actual buried cables, it is likely that alternating current is leaking from the neutral wire into the soil, its effect upon corrosion was examined by applying an AC voltage between the wire under study and a counter electrode. The circuit employed had a small resistance in series (10 Ω) for the current measurements and a very large capacitance (110 μF) to stop direct

TABLE 1 – Solution: 2% Na$_2$SO$_4$

Exper. No.	CPE	AC	Agar	Gas	DC mV	AC R, $\Omega \cdot cm^2$	Short Circuit Current Density $\mu A/cm^2$	Visual Observation
3		•		N$_2$	-50 ± 20	180		Cu$_2$O layer, tin coat excellent underneath.
4	•	•		N$_2$	-20 ± 30	185	1.0	Cu$_2$O crystals, tin coat underneath. No visible attack.
101				N$_2$	-50 ± 20			Tiny red spots. Otherwise excellent condition.
103				N$_2$	-30 ± 10			Excellent condition.
104	•			N$_2$	-300/-30		+0.04	Almost unchanged.
7	•	•		O$_2$	+30 ± 10	590	+1/0.2	Thin layer of green crystals. Some small pits. Large part of tin coat still in good condition.
8		•	•	O$_2$	+5 ± 20	330		Green scale. Red blisters. Some pitting under scale.
10		•		O$_2$	+20 ± 10	240		Sheets and mounds of green salt. Extensive pitting with Cu$_2$O in pits.
11		•		O$_2$	+20 ± 10	250		Same as 10.
106				O$_2$	0 ± 5			Good condition.
107				O$_2$	0 ± 5			Good condition.
109			•	O$_2$	+35 ± 5			A few pits (2 or 3) under green mounds. Otherwise good.
115	•			O$_2$	+10 ± 5		+0.14	Green crystals, white patine. Tinning in excellent condition.
117	•			O$_2$	+15 ± 5		+0.2	Green crystals. Tinning excellent.
118	•		•	O$_2$	+18 ± 5		-0.14	White-green patina. Excellent.

currents. With a large counter electrode-to-working electrode surface ratio, a condition approaching a potentiostatic system was achieved. With such a circuit, the cell voltage and current density could not be maintained constant. Variations in voltage and current between 150 and 450 mV and 1 and 8 mA/cm^2, respectively, were observed. In the tables that summarize the results, an AC resistance is reported, calculated as the ratio between the average cell voltage and the electrode current density. This number indicates the ease of AC flow between the wire and the solution. A smaller resistance leads to a larger current density, and vice versa.

Coupling with Conductive Polyethylene (CPE). The outer part of the insulating sheath of the cable is covered with CPE (formed by carbon powder embedded in polyethylene), which is in electrical contact with the neutral wire. Since the open circuit potential of CPE tends to be fairly positive (Figure 1), the effect of coupling the CCN wire with CPE was also examined. In these experiments, the short circuit current flowing between CCN wire and CPE was periodically measured by inserting a current-to-voltage converter between the two. Since the internal resistance of the instrument was effectively zero, it was possible to measure the short circuit without affecting its magnitude.

Both open circuit and current-potential measurements were carried out using a saturated calomel as reference electrode. Conventional instrumentation and cells were employed for the measurements.

Experimental Results

Long Term Corrosion Tests

A number of specimens of CCN wire were subjected to long term corrosion tests for times often in excess of 2500 hours. During the tests, the open circuit potential was measured at short intervals. The alternating current and voltage were also measured for the specimens with superimposed AC, as well as the short circuit current for the specimens coupled with CPE. Some of these corrosion tests were in duplicate. At the end of the tests, the wires were examined under a low power optical microscope. Some were also examined with a scanning electron microscope. The results obtained are summarized in Tables 1-4. Examples of the potential-time records are given in Figures 2 and 3.

The results show that under a nitrogen atmosphere, the rate of corrosion was slower than in the presence of oxygen. The electrode potentials, as a consequence, tended to be more negative; if the tin coating was continuous, the potential could remain at low voltages, -400 to -500 mV vs SCE, for fairly long periods. The tin coating on the CCN wire used in this work always had many small flaws, and very low potentials were not maintained for long times. The steady state values were higher in the absence of Cl$^-$ ions (about 0 mV in NaClO$_4$ and -50 mV in Na$_2$SO$_4$) than in their presence (from -130 to -220 mV in Na$_2$SO$_4$ and from -100 to -200 mV in NaClO$_4$). Potentials were shifted towards more positive values by oxygen, and

TABLE 2 – Solution: 0.42M NaClO₄

TABLE 2 – Solution: 0.42M $NaClO_4$

Exper. No.	CPE	AC	Agar	Gas	DC mV	AC R, $\Omega \cdot cm^2$	Short Circuit Current Density $\mu A/cm^2$	Visual Observation
3		*		N_2	-40 ± 20	67		Almost black. Some indications of attack on extrusion lines, no pits. Perhaps some tin coat left.
4	*	*		N_2	-40 ± 10	186	+1.5	Dark green with protrusions. Extensive attack underneath. Small, shallow pits uniformly distributed.
101				N_2	-200/+10			Excellent condition. Thin white patina.
103				N_2	+10 ± 10			Almost unchanged.
112	*			N_2	+20 ± 20		+0.14	Most tin coat can be removed by brushing. Otherwise little attack.
7	*	*		O_2	+85 ± 10	180	2.3	Green and black scale. Attack is not localized. Copper exposed in large areas, but some tinning still present.
8		*	*	O_2	+40 ± 20	420		Only one pit, with Cu_2O inside. Fairly extensive attack, but some tinning still on.
10		*		O_2	+55 ± 15	260		Green-black scale. Pits under blisters.
11		*		O_2	+55 ± 20	220		Same as 10. Tinning is intact on large areas.
106				O_2	+55 ± 10			White-green patina in places. Excellent condition.
107				O_2	+55 ± 10			More stains and black blisters than 106, but little attack underneath.
109			*	O_2	+70 ± 10			Green patina in places. Tin coat can be removed by scratching, showing Cu_2O formation, in one spot.
115				O_2	+65 ± 10		0.35	Tin coat in good condition. Most red spots can be removed by scratching.
117			*	O_2	+70 ± 15		0.22	Tin coat in excellent condition.
118	*		*	O_2	+70 ± 10		0.35	Good condition. Some loss of tin coat.

they were higher in the absence of chlorides, where $NaClO_4$ solutions showed, as under a N_2 atmosphere, higher values (+40 to 80 mV) than Na_2SO_4 solutions (from 0 to +30 mV). When chlorides were present, the differences were also much less pronounced because the spread was larger. In sulfate solutions, the potential ranged from +30 to -60 mV, and in perchlorate from +50 to -80 mV, with the agar gels showing the lowest values, due to the lower availability of oxygen.

The AC resistance showed a definite tendency towards lower values in nitrogen than in oxygen. Chlorides in solution had the effect of decreasing the resistance of the electrode even more. When these findings were compared with the results of visual inspection of the wires after the test, it was clear that a high AC resistance was associated with, and probably caused by, extensive scale formation. Low resistance specimens in general were only slightly corroded. Chlorides, on the other hand, promoted corrosion, but evidently

contributed to the formation of more conductive corrosion products than those formed in their absence. Comparison of the results in sulfate and perchlorate solutions showed that, all other conditions being equal, the extent of corrosion was greater in perchlorate.

Preliminary experiments had shown that corrosion in agar gel under an N_2 atmosphere was very small, and, therefore, it was decided to examine the effect of preventing convective motion only under oxygen atmosphere. Corrosion was found to be rather small in the absence of chlorides although some pitting was detected. In solutions containing chlorides, however, extensive pitting was found towards the bottom of the wire, with a pattern suggesting differential aeration. This was true both in sulfate and perchlorate.

The superposition of AC did not have a clear effect on the electrode potential but definitely increased the amount of corrosion. In particular, pitting (as opposed to a more uniform attack)

TABLE 3 — Solution: 2% Na$_2$SO$_4$ + 1% NaCl

Exper. No.	CPE	AC	Agar	Gas	DC mV	AC R, $\Omega \cdot cm^2$	Short Circuit Current Density $\mu A/cm^2$	Visual Observation
1		*		N$_2$	-200 ± 40	16		Uniform Cu$_2$O layer, pits underneath, but also some tin coat left, some attack under the coat.
2		*	·	N$_2$	-220 ± 40	30		Similar to 1.
5	*	*		N$_2$	-130 ± 20	14	+3.2	Cu$_2$O, Cu deposit. Some small pits.
102				N$_2$	-220 ± 10			Very little attack.
104				N$_2$	-220 ± 10			Little attack. Some loss of tin coat.
111	*			N$_2$	-150 ± 10		+1.4	Light green patina. Part of the tin coat can be removed by scratching. Underneath is Cu$_2$O, and probably pit initiation.
113	*			N$_2$	-170 ± 10		+1.4	Similar to 111, but little can be removed by scratching.
6	*	*		O$_2$	-55 ± 5	420	-0.18	Only one pit, distributed attack, considerable tin coat left. Small green crystals.
9		*	*	O$_2$	-150/-60	173		Green scale. Red blisters. Large and deep pits under salt mounds, but only at one level. (Differential aeration?)
12		*		O$_2$	-40 up slowly	390		Large green mounds. Pits under salt mounds not very deep. Probably no tinning left. Similar to NaClO$_4$ 12.
105				O$_2$	+20 up slowly			Some loss of tinning, but little attack on copper.
108			*	O$_2$	-150/+65			Green layer. Part of tin coat can be removed by scratching, but no extensive attack of copper.
110				O$_2$	-10 ± 10			Tin layer has been attacked considerably. Some Cu attack. No obvious pit initiation.
114				O$_2$	+30 ± 20			Little attack. One spot could be pit initiation.
116	*			O$_2$	-10 ± 10		-0.14	Some attack of tin coat. Otherwise excellent.
119	*		*	O$_2$	-90 ± 5		+6.4	Brittle surface layer that can be broken off easily. Red crystals underneath, but no pits.

was detected almost exclusively on specimens tested with AC. Even for the tests in the milder N$_2$ atmosphere, corrosion and pitting could be found. It must be kept in mind that AC in N$_2$ atmosphere was often much larger than under oxygen, and this may have enhanced its effect. On the other hand, in O$_2$, a smaller current did not prevent enhancement of the attack and pit formation.

Since the potential of CPE was more positive than that of the CCN wire, as shown in Figure 1, it was expected that coupling between CPE and wire would shift the potential toward more positive values and that an anodic short circuit current would flow in the electrolyte from the wire to the CPE. This expectation was largely fulfilled. In nitrogen, the electrode potentials of the wires

coupled to CPE were almost without exception 20 to 100 mV more positive than the corresponding wires tested without coupling. In oxygen, the situation was less clear, but wires coupled to CPE tended to be more positive.

As far as the direction of the short circuit was concerned, a few exceptions were found where a cathodic current (always small) was measured. It is possible that the reversal was caused by transport of some of the corrosion products to the CPE, providing an anodic reaction there. This explanation is suggested by the fact that some Cu corrosion products were found on the CPE, and also since in the corresponding tests in agar gel, where such transport could not occur, the short circuit current was anodic on the wire.

TABLE 4 — Solution: $NaClO_4$ + NaCl

Exper. No.	CPE	AC	Agar	Gas	DC mV	AC $\Omega \cdot cm^2$	Short Circuit Current Density $\mu A/cm^2$	Visual Observation
1		•		N_2	-230 ± 10	40		Cu_2O layer. Some pits underneath.
2		•		N_2	-190 ± 10	30		Some fairly deep pits under the Cu_2O layer.
5	•	•		N_2	-100 ± 10	14	+3.2	Brushing removes salt scale and tin coat, showing grooved and attacked Cu wire.
102				N_2	-170/-120			Some tin coat can be removed by scratching. No pits.
104				N_2	-100 ± 20			Most tin coat can be removed by scratching, but no pits.
111	•			N_2	-120 ± 20		+1.4	Tin coat can be brushed away easily.
113	•			N_2	-120 ± 20		+1.4	The tin coat crumbles away revealing attack underneath.
6	•	•		O_2	0 ± 10	460	+0.2	Black-green layer with protrusions. Etching reveals some attack, but no pitting.
9		•	•	O_2	-50 ± 20	120		Heavy attack at one level. Red and green crystals. Pits underneath. Good condition at top.
12		•		O_2	-20/+60	420		Green mounds, red inside. Pits.
105				O_2	+10 ± 10			Some green salt. Good condition.
108			•	O_2	-150/+70			Top part good. Bottom part can be removed by scratching. Cu_2O and attack under tin coat but uniform. Pit initiation uncertain.
110				O_2	+10 ± 10			Green layer. Tin coat can be removed by scratching, but little attack of copper.
116	•			O_2	+50 ± 10		0.05	Green layer. Tin coat can be removed by scratching. No pits.
119	•		•	O_2	-80 ± 10		+4.4	Brittle layer. Copper corroded underneath.
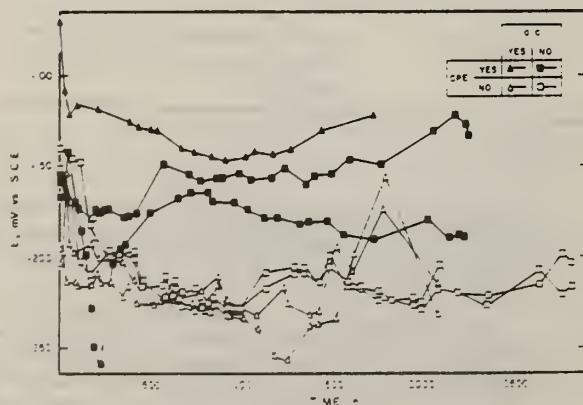
FIGURE 2 — Electrode potential vs time for tinned CCN wire in 2% Na_2SO_4 + 1% NaCl. O_2 atmosphere.

Coupling to CPE increased somewhat the rate of attack on the wires: in the absence of oxygen, attack occurred under the "tin" coating so that often the coating could be removed by gentle scratching or even by brushing with a soft brush. Cases where there was attack under the tin coating were associated with relatively high short circuit current densities, that is larger than 1 $\mu A/cm^2$ and up to 6 $\mu A/cm^2$ in one instance. In general, however, this attack was not associated with pit formation.

The short circuit current density was influenced by both the availability of oxygen, which shifted the potential in a positive direction, and by the formation of a resistive layer on the wire as indicated by the AC resistance. The two factors work against each other, but the second seems to be more important. Therefore, short circuit currents in N_2 atmosphere were often larger than in O_2 in spite of the fact that the potential was more than 100 mV higher in the latter condition.

Potentiodynamic Scans

Potentiodynamic scans afford a useful way to examine quickly the main features of the current-potential behavior of an electrode.
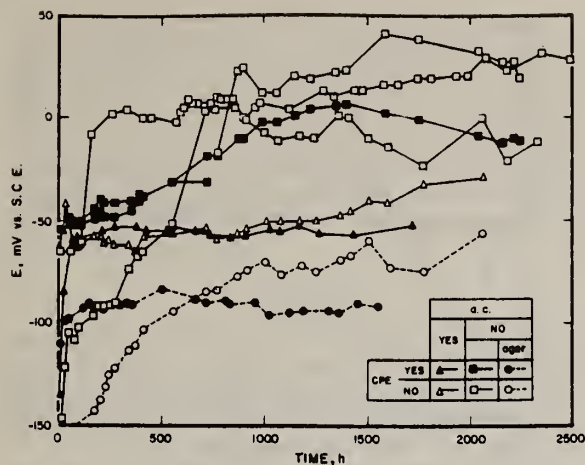
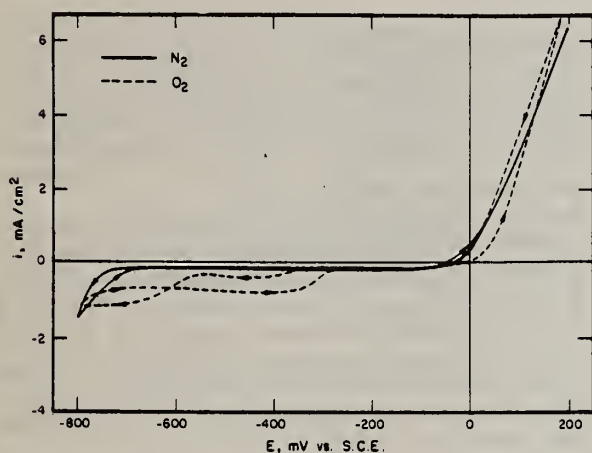FIGURE 3 – Electrode potential vs time for tinned CCN wire in 2% Na_2SO_4 + 1% NaCl. N_2 atmosphere.

FIGURE 6 – Potentiodynamic scans for Cu in 2% Na_2SO_4 + 1% NaCl. Scan rate 4 mV/s.

FIGURE 4 – Potentiodynamic scans for Cu in 2% Na_2SO_4. Scan rate 4 mV/s.

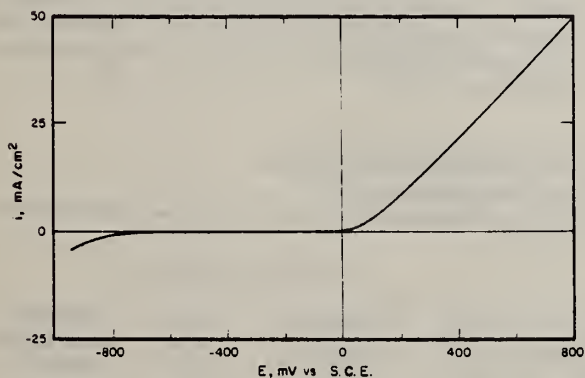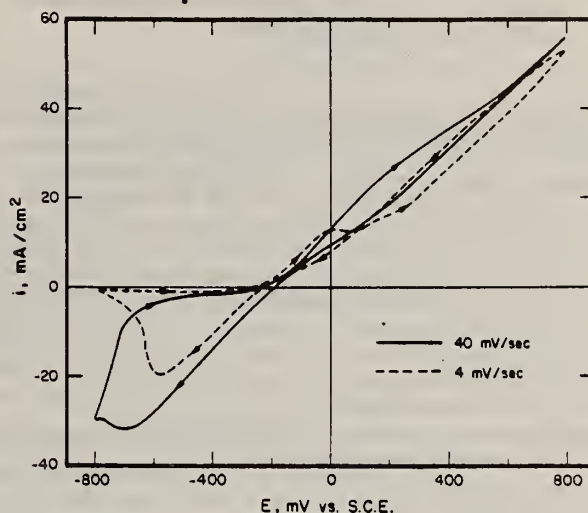FIGURE 7 – Potentiodynamic scans for Cu in 2% Na_2SO_4 + 1% NaCl. Inert atmosphere.

FIGURE 5 – Potentiodynamic scan for Cu in 0.42M $NaClO_4$. Inert atmosphere. Scan rate 4 mV/s.

For this reason, scans on CCN wire were taken in Na_2SO_4, both in the presence and in the absence of NaCl. The results showed a number of peaks, with a very large one in NaCl at about -150 mV vs SCE. However, there was loss of the tin coating during the measurements, and in order to clarify the contribution of copper

and of the tin coating to the electrochemical behavior, potentiodynamic scans were taken both on pure copper and on a sample of the (Pb/Sn) "tinning" alloy used by the manufacturer of the cable.

The results obtained on pure copper are shown in Figures 4 through 7. In the absence of chlorides, no formation of a passive, protecting film was detected, whether in Na_2SO_4 or in $NaClO_4$. Figure 4 shows the scans in sulfate in oxygen and in nitrogen over the range of greatest interest (from -800 to +200 mV vs SCE). Measurements up to +800 mV showed a monotonic increase (*i.e.*, never decreasing) in the anodic current. The curve was very similar to that shown in Figure 5 for a perchlorate solution. From these data, and from visual observation of the solution in the cell, it is quite clear that the Cu^{++} ion produced anodically was precipitated as hydroxide away from the electrode surface and did not form a protective layer on the metal surface. As a consequence, no cathodic reduction took place, in the absence of oxygen, until hydrogen evolved during the cathodic sweep.

In the presence of chlorides, a precipitate formed during anodic attack, which was sufficiently adherent to produce a cathodic peak during the negative sweep. However, the precipitate was ineffective in protecting the metal, and although it caused some poorly reproducible peaks and inflections on the anodic branch, it failed to limit the anodic current density which reached 60 mA/cm² at +800 mV (Figure 7). A comparison of Figures 6 and 7 showed that the

FIGURE 8 — Potentiodynamic scans for 90% Pb-10% Sn alloy in 2% Na_2SO_4. Scan rate 4 mV/s.

FIGURE 9 — Potentiodynamic scans for 90% Pb-10% Sn alloy in 2% Na_2SO_4 + 1% NaCl. Scan rate 4 mV/s. Oxygen atmosphere.

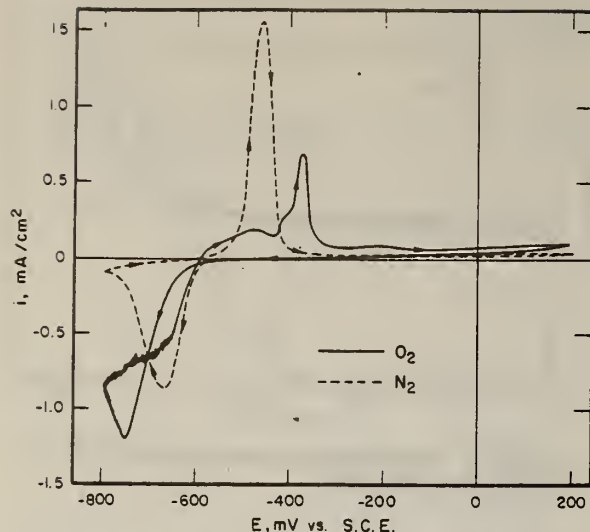position of the cathodic peak was shifted toward more negative values by extending the anodic range as well as by increasing the scan rate. The anodic branch, on the contrary, was little affected by changes in scan rate indicating that the behavior was not transient.

The electrochemical behavior of the 90 Pb-10 Sn alloy, both in the presence and absence of chlorides, is shown in Figures 8 and 9. Scans were carried out varying both range and rate in chloride containing solutions. The results confirmed that the more negative cathodic peaks corresponded to the anodic peak and was caused by the irreversible reduction of a $PbSO_4$ film. The more positive cathodic peaks were absent if the scan did not exceed -200 mV and corresponds to anodic oxidation occurring between -200 and +200 mV, which probably results in the formation of lead chloride. The metal exhibited passive behavior up to 800 mV vs SCE.

The results indicate that some of the features seen from the potentiodynamic scans on tinned wire are indeed due to the "tin" coating. However, the alloy used in these experiments did not correspond to the composition of the tin coating as discussed in the next section.

Chemical Analysis of the Surface

In order to determine the extent of removal of the tin coating during corrosion tests, some specimens were analyzed in a scanning electron microscope.

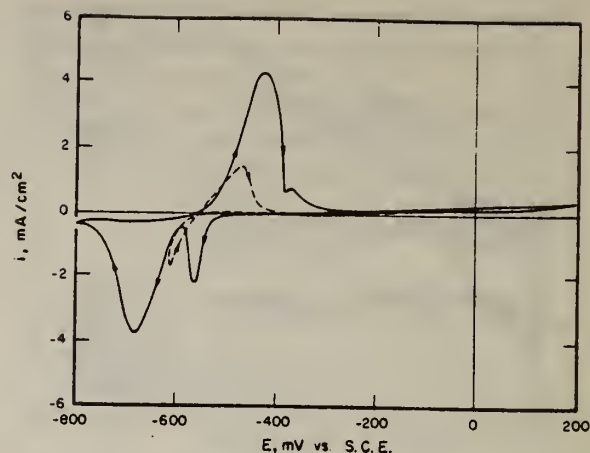In the course of these analyses, information on the composition of the original tin coating was obtained. From a comparison of the spectra obtained on an untouched CCN wire, the 90% Pb-10% Sn alloy used in the tinning bath, and on a 40% Pb-60% Sn alloy, it was concluded that on the tinned wire, the Sn/Pb ratio is larger than in either Pb-Sn alloy tested. The tinning layer consisted mainly of Sn, with probably only 20 to 30% Pb. This is not surprising, since Sn forms intermetallic compounds with Cu, and it is taken up preferentially during the tinning process.

Spectra taken after the corrosion tests showed total loss of the tin coating for many specimens exposed to oxygenated sulfate solutions, and some loss of Pb when the corrosion tests were carried out in inert atmosphere. In chloride solutions, the formation of $PbCl_2$ was indicated by the presence of a small Cl peak. On a sample exposed to oxygenated chloride solution gelled with agar, the Sn had disappeared but both Pb and Cl were detected. In this case, because of the lack of convective motion in solution, insoluble $PbCl_2$ was left on the surface in spite of the total disappearance of the tin coating.

Steady State Current Potential Measurements

Potentiostatic measurements on a number of CCN wires in various solutions gelled with 1% agar were taken at long time intervals, to estimate the corrosion current by intersecting the anodic and cathodic Tafel lines. The open circuit potentials as well as the calculated corrosion current densities at various time intervals are reported in Table 5.

TABLE 5 — Open Circuit Potentials and Corrosion Current Densities
for Tinned CCN Wire in Agar Gel. Potentials vs SCE

| Solution Composition: | | 2% Na_2SO_4 | | | | 2% Na_2SO_4 + 1% NaCl | | | |
| Atmosphere: | | O_2 | | N_2 | | O_2 | | N_2 | |
Time, Hours	AC	Open Circuit mV	Corrosion Current Density $\mu A/cm^2$	Open Circuit mV	Corrosion Current Density $\mu A/cm^2$	Open Circuit mV	Corrosion Current Density $\mu A/cm^2$	Open Circuit mV	Corrosion Current Density $\mu A/cm^2$
460	No	+5	1	-45	0.1	-155	0.8	-175	0.4
1150	No	-25	0.5	-95	0.1	-95	1.5	-175	0.6
1900	No	+15	0.6	-125	0.08	-135	1.5	-185	0.3
4300	No	+35	0.5	-145	0.1	-65	5	-175	0.9
5000	No	+45	0.7	-145	0.07	-65	7	-175	0.9
6700	No	+25	0.5	-155	0.03	-95	0.7	-185	0.5
1600	Yes	+25	0.4	-125	0.3	-65	2	-220	0.2
2400	Yes	—	—	-155	0.2	-45	2	-240	0.3
4200	Yes	+15	0.3	-155	0.06	-5	0.6	-200	0.3

The results obtained from the steady state potentiostatic data are in general agreement with the corrosion tests, as far as the open circuit potentials are concerned. The corrosion rates deduced from the polarization values are larger in the presence of oxygen, particularly in chloride containing solutions, as expected. However, no clear effect of superimposed AC was found. Since these tests are continuing and the wires have not been inspected visually, it is impossible at writing to correlate the current-potential data with the extent of pitting on the wires.

Discussion

The main purpose of this work was to obtain information useful for planning and interpretation of field tests. At the same time, the results have given a number of interesting indications concerning the possible causes of corrosion of buried CCN cables and the interplay of the factors that can initiate pitting on the copper wires.

The corrosion tests for long exposure times showed that a superimposed AC was a powerful cause of pitting. However, in some cases extensive corrosion was found on specimens not subjected to AC, indicating that this is not absolutely necessary to cause corrosion, but that its presence increases considerably the rate of attack.

The presence of a reducible species such as oxygen was expected to enhance corrosive attack, and this was verified experimentally to a certain extent. However, the effect of the attack was to form a layer of corrosion products that slowed further corrosion considerably. Which of the two opposing consequences of the availability of oxygen will predominate in a certain instance may depend on subtle differences in the environment, and are difficult to predict.

The presence or absence of a protective scale influences the amount of AC leakage, and probably explains why extensive pitting was found in tests where oxygen was kept low by a nitrogen blanket. In these conditions, no protective scale was found, and extensive pitting occurred in many cases. Analogous conclusions can be drawn from those tests in agar gel where oxygen could not readily reach the bottom part of the specimen, and the attack there was quite severe. These tests also point to differential aeration as a possible cause of failure in the field. The presence of chloride ions also enhances corrosive attack, since they tend to reduce the resistance of the protective layer.

Since it has been pointed out[5] that sulfates, or perhaps other sulfur containing materials, might play an important role in the corrosion of CCN wire in the field, corrosion tests employing $NaClO_4$ instead of Na_2SO_4 as the main electrolyte were carried out. From the results reported here, it appears that no special role is played by sulfates. Although the effect was quite minor, the $NaClO_4$ solution was a slightly more corrosive environment than Na_2SO_4. This may have been because perchlorates of the heavy metals (including Pb) are more soluble than the corresponding sulfates.

The crude measurements of electrode impedance obtained by monitoring the AC voltage and current have given some interesting clues concerning the susceptibility of the CCN wire to attack. This suggests that AC impedance measurements can be a useful diagnostic tool.

References

1. Zastrow, O. W. Materials Performance, Vol. 13, No. 8, p. 31 (1974).
2. Schick, G. Corrosion of Concentric Neutrals of Buried Power Distribution Cables, NACE National Conference, 1975, Toronto, unpublished paper No. 128.
3. Compton, K. G. Materials Performance, Vol. 14, No. 8, p. 14 (1975).
4. Kroon, D. H. Materials Performance, Vol. 15, No. 8, p. 13 (1976).
5. Latanision, R. Private communication (1977).
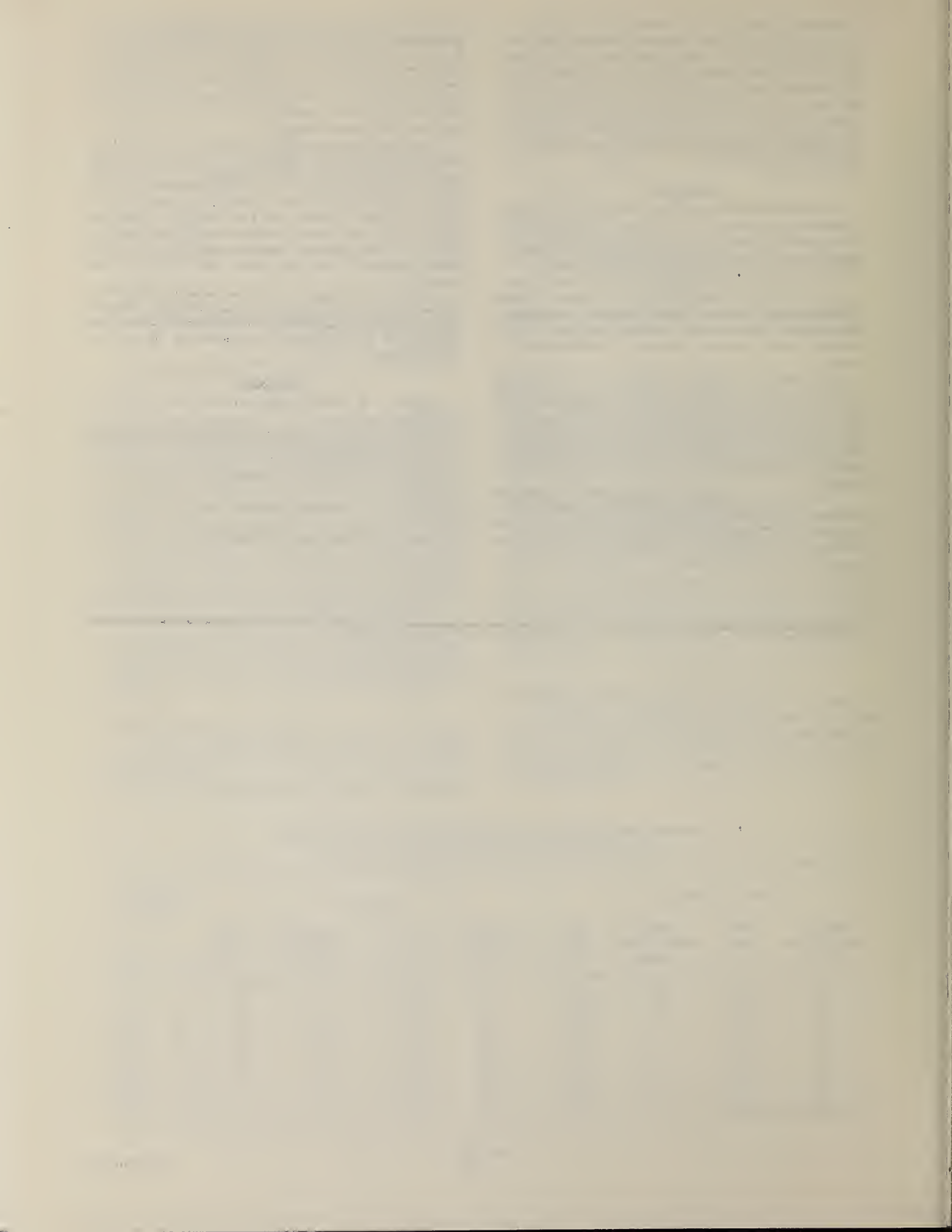
AC Induced Corrosion. The Effect of an Alternating Voltage on Electrodes Under Charge-Transfer Control[*]

U. BERTOCCI [*]

Abstract

The equation relating current to voltage for an electrode under charge-transfer control has been solved for a sinusoidal modulation of the electrode potential. The rectified Faradaic component has been obtained, so as to derive its value as a function of the Tafel parameter and of the amplitude of the modulating voltage, as well as of average electrode potential. The case where one electrode reaction is under diffusion control also has been treated. The amplitude and phase characteristics of the harmonic components have been derived, and their use for determining the kinetic properties of the electrode have been discussed. The capacitative current generated by the alternating voltage also has been investigated, and the conditions under which it can be separated from the Faradaic current have been given. The implications of these results on the corrosion due to AC leakage have been examined.

In recent times, there has been renewed interest in the effect of alternating current (AC) on the corrosion of metals. The interest is due to the fact that serious cases of corrosion of underground power cables have been reported,[1] and there have been claims that such corrosion is caused, or at least greatly enhanced, by AC leakage from the cable to the ground.[2]

For the study of such an effect, a number of workers have carried out current-potential measurements with a superimposed sinusoidal modulation, and indications of a high corrosion current density under these conditions have been reported.[3,4]

The effect of AC on corrosion was examined many years ago.[5] The experiments showed only minor effects that progressively decreased with increasing frequency of the AC. The conclusion at the time was that little harm was to be expected from AC of the frequency used for power transmission.

As far as the analysis of the effect of a modulating sinusoidal current or potential on electrodes is concerned, an extensive literature exists, under names such as redoxokinetic effect,[6] Faradaic rectification,[7] and Faradaic distortion.[8] The results of this analysis have been applied, for instance, to the development of AC polarography.[9]

The present treatment, therefore, is not a novel one. However, while previous workers were mainly concerned with the effects of the modulation on transport in solution, starting with the classical work of Warburg[10] and Krüger,[11] the emphasis here is on systems such as those frequently encountered in corrosion practice or research, although the results can be applied also to electrodes in equilibrium with the surrounding solution.

Statement and Analysis of the Problem

The model to be treated here is that of an electrode whose kinetic behavior is determined only by charge transfer so that the relationship between current (i) and potential (E) can be written in the form:

$$i = i_c + i_f = i_c + \sum_n k_n^+ \exp(A_n E) - \sum_m k_m^- \exp(-B_m E) \qquad (1)$$

The summation should be extended so as to include all anodic and cathodic reactions that might become significantly large in the range of potentials of interest. Here analysis is restricted mainly to the case where only one anodic and one cathodic reaction are

important. Then

$$i = i_c + i_f = i_o[\exp(A\eta) - \exp(-B\eta)] + i_c \quad (2)$$

where i_c is the capacitative current, given by the derivative of the electrode charge $Q = CE$

$$i_c = C\frac{d\eta}{dt} + E\frac{dC}{dt} \quad (3)$$

i_o represents either the exchange current density (if an equilibrium situation is considered) or the corrosion current density. A and B are related to the anodic and cathodic Tafel slopes b_a and b_c by the usual relationships $A = (\ln 10)/b_a$, $B = (\ln 10)/b_c$. The voltage (η) is the difference between the actual electrode potential and the potential at which no DC is going through the electrode in the absence of an alternating modulation.

We now want to examine the current output of the electrode if a voltage signal of the form

$$\eta = \eta_o + V\sin\omega t \quad (4)$$

is applied to the electrode by means of a potentiostat.

Introducing Equation (4) into Equation (2), the Faradaic current becomes:

$$i_f = i_o[\exp(AV\sin\omega t)\exp(A\eta_o) - \exp(-BV\sin\omega t)\exp(-B\eta_o)] \quad (5)$$

Since one can make the substitution[1,2]

$$\exp(z\sin x) = I_o(z) + 2\sum_o^\infty (-1)^k I_{2k+1}(z)\sin\{(2k+1)x\}$$

$$+ 2\sum_1^\infty (-1)^k I_{2k}(z)\cos(2kx) \quad (6)$$

where $I_n(z)$ is the modified Bessel function of order n, whose value can be calculated by means of the expression

$$I_n(z) = (\frac{z}{2})^n \sum_o^\infty \frac{(\frac{z}{2})^{2k}}{k!(n+k)!} \quad (7)$$

the DC component of the Faradaic current as well as its harmonic components can be obtained.

When time averages are considered, only the DC term is not zero, and represents a current which can affect the electrode. Combining Equations (5), (6), and (7), and considering only the DC component,

$$(i_f)_{dc} = i_o\left[\sum_o^\infty \frac{(AV)^{2k}}{2^{2k}(k!)^2}\exp(A\eta_o) - \sum_o^\infty \frac{(BV)^{2k}}{2^{2k}(k!)^2}\exp(-B\eta_o)\right] \quad (8)$$

Equation (8) shows that both the anodic and cathodic DC partial currents have been multiplied by a factor that depends on the kinetics of the reaction (through A and B) and the amplitude V of the modulation. In particular, if the average potential (η_o) is kept at zero (the open circuit voltage), a DC current may be measured, as

$$(i_f)_{dc}, \eta_o = o = i_o\sum_o^\infty \frac{V^{2k}}{2^{2k}(k!)^2}[A^{2k} - B^{2k}] \quad (9)$$

which will be zero if A = B, that is if the anodic and cathodic Tafel slopes are the same, or it may be either positive or negative, if the activation energy of the anodic reaction is, respectively, smaller or larger than the cathodic one.

This result shows also that if a Tafel plot (potential vs logarithm of the current) is obtained under sinusoidal modulation of the voltage, the Tafel slopes will be independent of V, but their locations will be shifted horizontally by amounts given by the terms
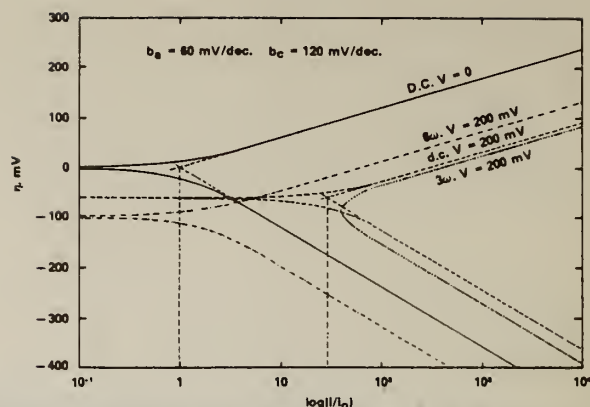

FIGURE 1 — Effect of a sinusoidal amplitude of 200 mV applied to an electrode with anodic Tafel slope (b_a) 60 mV/decade and cathodic slope (b_c) 120 mV/decade.

in A and B of Equation (9). Figure 1 shows the effect if a sinusoidal amplitude (V = 200 mV) is applied to an electrode whose anodic Tafel slope (b_a) is 60 mV/decade, and the cathodic slope (b_c) is 120 mV/decade. The figure also illustrates the fact that the intersection of the two new slopes occurs at a value of η_o different from zero, and that the value of the corrosion current (or the exchange current density, if the plot refers to an electrode in equilibrium) obtained from the intersection is larger. This value of i_o, obtained under sinusoidal voltage modulation, will be designated as i_{corr} or as i_o.

The shift in the potential at which no DC is flowing, which has been observed experimentally,[3] is a qualitative indication of what would happen if the circuit were constructed so that no DC could circulate, as for instance, if a capacitor were inserted in the current circuit. The correspondence between voltage modulation, as treated here, and current modulation has to be considered only qualitative, because while in this case the nonlinear characteristics of the electrode reaction causes harmonic distortion in the current, in the galvanostatic case, the harmonic distortion would appear in the voltage signal.

In the preceding paragraphs, the DC component of the Faradaic current has been assumed to be also the DC component of the total current, that is, it was assumed that no rectification occurred for the capacitative current. The next section will discuss the limits of validity of this assumption.

Capacitative Current

The value of double layer capacitance is in general a function of potential and can vary quite significantly when adsorption processes take place at the electrode. If only voltage modulations of periods large compared with the relaxation times of adsorption reactions are considered, then the double layer capacitance is only a function of the electrode potential (η) but not of its derivatives. It is then

$$C = C_o + \sum_k a_k\eta^k \quad (10)$$

In this case, when Equation (10) is introduced into Equation (3), and since

$$\frac{dC}{dt} = \frac{dC}{d\eta}\frac{d\eta}{dt}$$

The capacitative current is given by

$$i_c = (C_o + \sum_k a_k\eta^k + \sum_k ka_k\eta^{k-1})\omega V\cos\omega t$$

which can be rearranged into

$$i_c = (C_o' + \sum_k a_k'\eta^k)\omega V\cos\omega t \quad (11)$$

In Equation (11), each term of the summation is of the form

b_c / b_a mV/dec	V mV	30 mV/dec i_{corr}/i_o	30 mV/dec η_o mV	40 mV/dec i_{corr}/i_o	40 mV/dec η_o mV	60 mV/dec i_{corr}/i_o	60 mV/dec η_o mV	120 mV/dec i_{corr}/i_o	120 mV/dec η_o mV	∞ i_{corr}/i_o	∞ η_o mV
30	10	1.15	0	1.11	-0.5	1.07	-1.0	1.04	-1.4	1	-1.9
	30	2.84	0	2.26	-3.0	1.74	-6.4	1.31	-10.0	1	-13.6
	100	.316	0	115	-13.2	31.2	-30.1	5.84	-52.0	1	-75.0
	300	$8.4 \cdot 10^8$	0	$2.4 \cdot 10^7$	-41.8	$4.9 \cdot 10^5$	-96.9	1477	-173	1	-268
40	10			1.08	0	1.06	-0.5	1.03	-0.9	1	-1.4
	30			1.90	0	1.55	-3.5	1.25	-7.3	1	-11.1
	100			53.8	0	19.4	-17.7	4.82	-41.9	1	-69.3
	300			$3.1 \cdot 10^6$	0	$1.1 \cdot 10^5$	-57.8	832	-143	1	-259
60	10					1.04	0	1.02	-0.5	1	-1.0
	30					1.36	0	1.17	-3.9	1	-8.0
	100					9.83	0	3.57	-26.4	1	-59.5
	300					11892	0	325	-93.8	1	-245
120	10							1.01	0	1	-0.5
	30							1.08	0	1	-4.2
	100							2.16	0	1	-40.0
	300							53.9	0	1	-208

$\sin^k \omega t \cdot \cos \omega t$, whose integral is proportional to $\sin^{(k+1)} \omega t$, and therefore, the time average is zero. In other words, no rectification is produced by the double layer capacitance as long as it is a function that can be expanded in powers of η.

It is also interesting to look at the phase relationships between the harmonic components of the capacitative current and the modulating voltage assuming that Equation (10) holds. It can be shown that all even harmonics (that is components with frequency 2ω, 4ω, etc.) are sine functions and therefore bear a zero or a $\pm\pi$ relationship to the modulating voltage as given by Equation (4), while all odd harmonics (ω, 3ω, 5ω, etc.) are cosine functions, and therefore out of phase by $\pm\pi/2$ with the modulating voltage.

Diffusion Limited Electrode Reactions

Although the present treatment does not apply if the modulating voltage causes changes in the concentrations of the reactants at the electrode, it can be used if one of the electrode reactions is under limiting diffusion conditions. This is often the case in corroding systems when the cathodic reaction is the reduction of oxygen reaching the electrode. When this is the case, the corresponding Tafel slope is infinity, and the coefficient A or B is zero. If for instance, the cathodic reaction is under diffusion control (B = 0), the second summation in Equation (8) is equal to 1 and Equation (9) is accordingly simplified, the DC being only a function of A. The condition at which the DC is zero will be reached by lowering the potential (η_o), the more so the larger the modulating amplitude V is, until the anodic partial current, as expressed by the first term in Equation (8) is equal to i_o, the corrosion current that can be sustained under diffusion control. If the electrode is allowed to remain at this average potential, no enhanced corrosion should be experienced.

In order to give an idea of the effect of the modulation on corrosion current (or apparent exchange current density, if this analysis is applied to an electrode in equilibrium) and on the shift in the potential for which the net DC is zero as a function of A, B, and V, Table 1 has been prepared. One should note that interchanging A with B does not change i_{corr} nor the absolute value of η_o. Only its sign is reversed.

The values show that even relatively small sinusoidal amplitudes cause very large increases in i_{corr}, particularly if the Tafel slopes are small. This is not surprising, since the electrode potential oscillates in a range 2V around the average value η_o, bringing it to values where the current, if only change-transfer limited, would be quite large.

Frequency Analysis

The increasing availability of instrumentation that can perform signal analysis, allowing one to transform a signal from the time to the frequency domain as well as to obtain information on phase relationships, makes it interesting to explore what can be obtained from examination of Equation (5) when Equations (6) and (7) have been substituted into it. The result is a representation of the Faradaic current as a Fourier series.

The first observation is that all odd harmonics (ω, 3ω, 5ω, etc.) are sine functions in phase with the modulating signal, while the even harmonics are $\pm\pi/2$ out of phase. Remembering the phase behavior of the capacitative current (i_c) as discussed in a preceding section, it appears that, within the limits of validity of the present model, it is always possible to distinguish between capacitative and Faradaic components.

The amplitude of the odd and of the even harmonics of the Faradaic current, expressed in terms of i_o, the corrosion (or exchange) current density in the absence of a modulating voltage, are the following: odd term of frequency $(2k-1)\omega$

$$\frac{i_{(2k-1)}}{i_o} = -(-1)^k \sum_{k}^{\infty} \frac{V^{2n-1}}{2^{2(n-1)}(n-k)!\,(n-1+k)!}\left[A^{2n-1}\exp(A\eta_o) + B^{2n-1}\exp(-B\eta_o)\right]; \tag{12}$$

even term of frequency $2k\omega$

$$\frac{i_{2k}}{i_o} = (-1)^k \sum_{k}^{\infty} \frac{V^{2n}}{2^{2n-1}(n+k)!\,(n-k)!}\left[A^{2n}\exp(A\eta_o) - B^{2n}\exp(-B\eta_o)\right] \tag{13}$$

As Equations (12) and (13) show, the symmetry or lack of it of the electrode reactions as contained in the values of A and B, is reflected in the frequency spectrum of the current. In particular, if

η, mV	V mV	DC	ω	2ω	3ω	4ω	5ω	6ω	7ω	15ω
	20	52.7	52.6	41.4	26.8	9.80	-9.07	-29.5	-51.2	-258
	50	62.9	67.0	61.9	54.2	44.5	33.2	20.4	6.32	-138
+100	100	84.6	89.8	87.4	83.4	78.0	71.4	63.6	54.8	-44.1
	200	131	137	136	134	131	128	124	119	58.8
	300·	180	186	185	183	182	179	177	173	131
	500	277	283	283	282	281	280	278	276	250
	20	50.3	41.8	21.4	-2.60	-29.8	-57.5	-87.6	-118	-450
	50	51.9	50.6	37.8	21.7	3.08	-17.5	-39.6	-62.4	-285
-300	100	56.7	59.4	51.8	41.2	28.3	13.6	-2.63	-19.6	-195
	200	69.8	74.5	70.7	64.7	56.9	47.5	36.8	25.5	-103
	300	84.6	89.8	87.3	83.3	77.8	71.0	63.1	54.8	-48.2
	500	116	121	120	117	114	109	104	99.9	49.1

A = B, all even harmonics disappear at η_o = 0. The presence of peaks for the even harmonics in the spectrum at this potential is an indication of the differences in the anodic and cathodic Tafel slopes.

Since all amplitude components contain the double exponential expression that is characteristic of charge-transfer kinetics, plots of any component amplitude of the current versus η will yield the same Tafel slopes if put in semilogarithmic form. [Examples are given in Figure 1 where the amplitude of the third (3ω) and sixth (6ω) harmonics are also plotted.] This also indicates that all amplitudes increase when the electrode is polarized, so that high harmonics, which are small when η_o is close to 0, might become detectable with larger η_o, even for moderately small values of the modulating amplitude V. For similar reasons, because a larger modulating amplitude pushes the electrode periodically away from η_o = 0, more power is proportionally found in the higher harmonics when V is increased.

Some idea of the effect of varying the modulating amplitude V on the various harmonics at constant anodic and cathodic polarization can be obtained from Table 2. All values are given in decibel referred to i_o in the absence of modulating signal as zero.

Discussion

Limits of Validity of the Model

The very large values of current that can be calculated from moderate modulation voltages, overvoltages, and corrosion (or exchange) current densities, some of which are reported in Tables 1 and 2, immediately point to the limitations in the applicability of this treatment: certainly other factors in these circumstances would limit the current, such as transport in solution. The formation of films of anodic products or other alterations of the electrode surface leading to passivation would also restrict the amount of current to much lower values than those predicted by this model. One can imagine a current-potential plot for the system under investigation, ranging between $[(\eta_o)_{max} + V_{max}]$ and $[(\eta_o)_{min} - V_{max}]$, the maximum and minimum values of the DC potential plus or minus the largest voltage modulation under consideration. If such a plot cannot be described by Equation (2), this treatment is not appropriate, although sometimes its pertinence can be extended with the aid of Equation (1), taking into account other reactions such as oxygen evolution at positive potentials and hydrogen evolution at negative ones. Effects such as slow adsorption or desorption that can cause rectification of the capacitative current can also limit the validity of this treatment.

Effect of Frequency

It may be useful at this point to discuss the influence of the frequency of the modulating voltage upon the current response: as Equations (8), (9), (12), and (13) show, there is no effect on the Faradaic part of the current. This is a consequence of the fact that charge-transfer processes occur in times much shorter than the reciprocal of the frequencies that are in common use in electrochemistry. In experimental work, the upper frequency limit is therefore set by the response of potentiostats and amplifiers and by the geometry of the cell. On the other hand, high frequency current leakage cannot be expected to cause less corrosion than low frequency current leakage if conditions akin to a potentiostatic system exist. In laboratory practice, it might be advantageous to study the effect of changing frequency as a means to detect the influence of slow processes such as transport in solution or chemisorption.

The capacitative current, on the contrary, increases linearly with frequency as indicated by Equation (5). This fact should not, however, affect the DC component nor complicate the frequency analysis of the Faradaic current, as long as phase information is available and within the limits already discussed. The experimentalist should, however, remember that at high frequency, the large capacitative current can very well exceed the maximum output of the potentiostat.

Derivation of Information Concerning the Electrode Kinetics

In the preceding sections, some of the information that can be obtained from examining the various components of the current has been pointed out. This information concerns the symmetry of the electrode reaction, and values of the electrode capacitance (and its dependence on potential) as well as i_o and its dependence on the modulating voltage. We would also like to mention some other points.

Away from η_o = 0, in the so-called Tafel region, Equations (12) and (13) contain only the terms in A or in B. Then, from Equation (7), it can be derived that the ratio between the amplitude of the nth and the (n-1)th harmonic component is approximately equal to A (or B) times V/2n. The Tafel slope can be obtained from a single frequency spectrum. The accuracy increases with the order of the harmonics and with decreasing V, in other words when smaller amplitude peaks are used. A few numerical examples are given here, taking the values from Table 2. On the anodic side, if the ratios between the 4th and the 3rd harmonics for V = 20 mV are used, the slope calculated is 40.7 and for V = 100 mV, the 7th and 6th harmonics yield b_a = 45.3. On the cathodic side, for V = 300 mV and using the 6th and 5th harmonic, b_c is calculated as 141 mV/decade, while for V = 50 mV, the third and fourth harmonics give a value of 121 mV/decade.

More elaborate mathematical schemes can be devised to obtain the kinetic parameters from the frequency and phase spectra, but only extensive experimental testing can show their usefulness. In fact, one can expect difficulty in the recovery of the information if a significant ohmic drop occurs; then the modulation of the electrode voltage would not be a simple sinusoid, and a phase

difference would exist between control voltage and electrode voltage. Another source of complications would be the presence of harmonic content in the modulating signal. If the harmonic content is known, however, attempts can be made to estimate its effect. In fact, in analogy with Equations (4) and (5), if the signal is in the form

$$\eta = \eta_o + \Sigma_k \alpha_k \sin k \, \omega t + \Sigma_k \beta_k \cos k \, \omega t \qquad (14)$$

Equation (5) becomes

$$i = i_o \, [\exp(A\Sigma_k \alpha_k \sin k \, \omega t) \exp(A\Sigma_k \beta_k \cos k \, \omega t) \exp(A\eta_o)$$

$$-\exp(-B\Sigma_k \alpha_k \sin k \, \omega t) \exp(-B\Sigma_k \beta_k \cos k \, \omega t) \exp(-B\eta_o)] \qquad (15)$$

so that the analysis outlined in this treatment can be applied to each term of the summation. Without further elaboration, it must be pointed out that it might be interesting to analyze in detail the consequences of using, instead of a sine function as modulating voltage, either a square wave signal or a triangular scan, since their Fourier representation involves only odd harmonics and, therefore, should allow the separation of the Faradaic and capacitative components.

Consequences in the Field of Corrosion

According to the treatment described above, if the corrosion current is derived from the intersection of the Tafel slope or from the linear polarization method, or by means of some curve fitting procedure,[13] using the values of the DC component of the current under alternating voltage modulation, it will be found that the corrosion current is larger than in the absence of the alternating signal. The only exception is when either the cathodic or the anodic reaction is under diffusion control, but even in this case, the same conclusion could be drawn if the shift in the potential for which $i_{DC} = 0$ is neglected and the current given by one Tafel line at $\eta_o = 0$ is assumed to represent the corrosion current.

The conclusion that AC modulation enhances corrosion is therefore justified, provided that two important points are given proper consideration: one is that the extent of the enhancement depends on the value of the average potential (η_o), since the potential at which the net DC current is zero will vary, in general, with the amplitude V of the modulating voltage, as illustrated in Figure 1. If conditions are such that η_o can shift to the value for which no net DC flows, the enhanement of corrosion will be minimized. In particular, if all cathodic reactions in the potential range down to (η_o -V) are either diffusion-controlled or negligibly small, no enhancement of corrosion will take place. This point is illustrated in Figure 2; if η_o is zero when a modulation of amplitude V = 200 mV is applied, the net DC, marked as i_{DC} on the drawing, is 8.8 times the i_o in the absence of a modulating signal, and the corrosion rate, marked as i_{corr}, is 9.8 times i_o. If, however, η_o shifts to about -120 mV, where $i_{DC} = 0$, the corrosion current is equal to i_o.

The second point to be considered is that the effects described in this work arise from the superposition of an alternating voltage, whose amplitude is independent of frequency. If, on the contrary, an alternating current of constant amplitude is applied, a large fraction of it will be shunted by the double layer capacitance, the more so the higher the frequency, without causing material transport across the electrode interface. This explains some of the conclusions of earlier work in this area.[5] To which extent in a practical situation, the AC leakage can be described as a current or as a voltage has to be decided after careful examination of the system.

The same considerations apply to the manner of carrying out corrosion tests in the laboratory. Control of the electrode potential, rather than superposition of an alternating current to the specimen, simplifies the analysis of the results, but dictates caution in applying
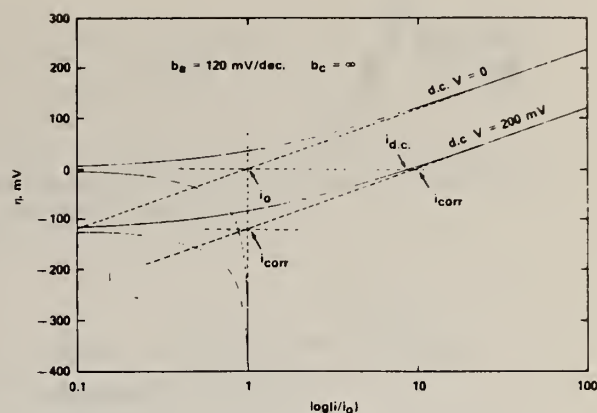

FIGURE 2 — Current-potential curves for an electrode with anodic Tafel slope b_a of 120 mV/decade and cathodic reaction under diffusion control ($b_c = \infty$). DC components of the current in the absence and in the presence of an alternating modulation of 200 mV.

the information obtained to the real cases.

References

1. O. W. Zastrow. Materials Performance, Vol. 13, No. 8, p. 31 (1974); K. G. Compton. Materials Performance, Vol. 14, No. 8, p. 14 (1975); D. H. Kroon. Materials Performance, Vol. 15, No. 8, p. 13 (1976).
2. G. Schick. Paper No. 128, Intern. Corr. Forum, Toronto (1975).
3. J. Kruger, U. Bertocci, E. Escalante, and J. L. Mullen. Annual Report NBSIR 77-1232 (ERDA), April, 1977; D. T. Chin, T. W. Fu, G. F. Kamrowski, and S. Pookote, 1978 NACE Research Conference, Houston (1978); U. Bertocci and J. L. Mullen, submitted for publication; D. J. Nesslage, Paper No. 162, Corrosion/78, NACE (1978).
4. K. G. Compton. INCRA Research Report Project 265 (1977).
5. B. McCollum and G. H. Ahlborn. Tech. Pap. BS T72 (1916).
6. K. S. G. Doss and H. P. Agrawal. Proc. Indian Acad. Sci., Vol. 34A, p. 263 (1951); Vol. 35A, p. 45 (1952).
7. K. B. Oldham. Trans. Faraday Soc., Vol. 53, p. 80 (1957); G. Barker, R. Faircloth, and A. Gardner. Nature, Vol. 181, p. 247 (1958); G. Barker. Anal. Chim. Acta, Vol. 18, p. 118 (1958); P. Delahay, M. Senda, and C. H. Weis. J. Phys. Chem., Vol. 64, p. 960 (1960); I. Imai and P. Delahay, ibid., Vol. 66, p. 1108, 1683 (1962).
8. H. H. Bauer. Austral. J. Chem., Vol. 17, p. 591, 715 (1964).
9. B. Breyer and H. H. Bauer. Alternating Current Polarography and Tensammetry. Interscience, New York (1963); P. Delahay. New Instrumental Methods in Electrochemistry, Interscience, New York (1954); D. E. Smith. Electroanalytical Chemistry, A. J. Bard, ed., Vol. 1, Ch. 1, M. Dekker, New York (1966); T. McCord and D. E. Smith. Anal. Chem., Vol. 41, p. 116 (1969).
10. E. Warburg. Ann. Phys. U. Chem., Vol. 67, p. 493 (1899).
11. F. Krüger. Z. Phys. Chem., Vol. 45, p. 1 (1903).
12. Handbook of Mathematical Functions, M. Abramowitz and I. A. Stegun, eds., p. 376, NBS Publication 55 (1965).
13. F. Mansfeld. Advances in Corrosion Science and Technology, Vol. VI, M. G. Fontana and R. W. Staehle, eds., Plenum Press, New York (1976).
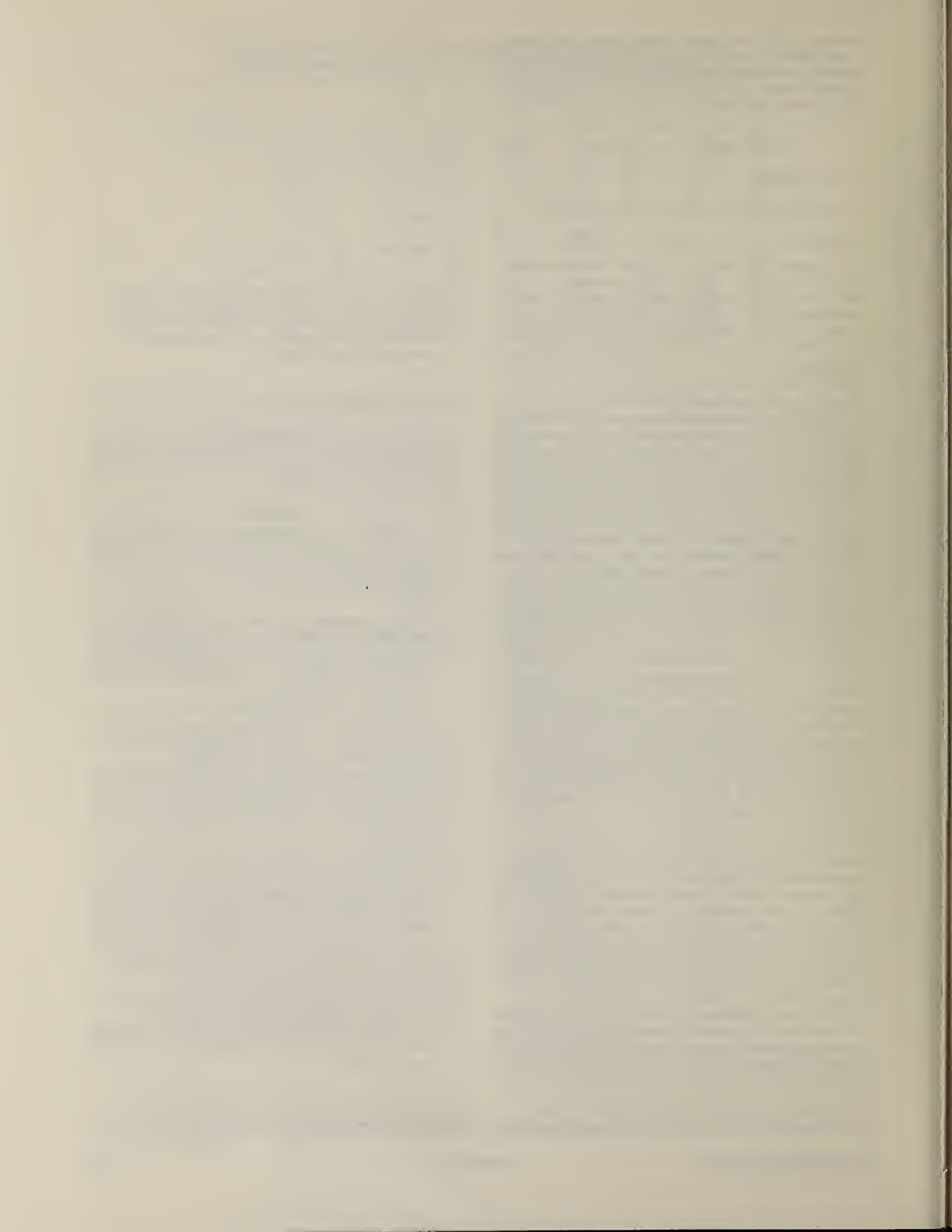
CORROSION/79

Corrosion Induced by an Alternating Voltage. A Comparison Between
Theoretical Predictions and Experimental Results

U. Bertocci and J. L. Mullen
Chemical Stability & Corrosion Division
Center for Material Science
National Bureau of Standards
Washington, D. C. 20234

1. Purpose of the Work

In a large number of practical situations metallic structures are
subjected to alternating voltages which cause currents to flow into ionic
conductors in contact with them, the most common of which is soil. These
currents might flow because of failure of insulation, but there are also
cases where the metals are exposed without protection. There is, therefore,
a substantial interest in understanding what happens in these situations,
so as to be able to predict when and to which extent corrosion can be
caused by the effect of alternating currents. [1]

As a part of research carried out at NBS concerning the corrosion
of copper concentric neutral cables, a mathematical analysis of the
effect of an alternating voltage on electrodes under charge-transfer
control has been developed [2]. It is the purpose of this paper to
present briefly the principal points of this analysis and to compare
its predictions with experimental results.

2. Mathematical Analysis

a. Faradaic Current

We will present here in a simplified form some of the results of the analysis which has been given in detail elsewhere [2]. For an electrode under charge-transfer control, the partial anodic or cathodic current can be expressed as

$$i_{dc}^* = I_o \exp (AE) \qquad (1)$$

where I_o and A are positive for anodic processes and negative for cathodic ones. E is the electrode potential, taken with respect to some convenient reference point. As it is well known, (1) can be used to express the total current in the so-called Tafel region, that is when the partial current of opposite sign is very small. If the voltage is sinusoidally modulated, so that

$$E = E_o + V\sin \omega t \qquad (2)$$

The expression for the faradaic current can be obtained and by harmonic analysis the current can be separated into a constant (or d.c. as customarily called) component and into the various harmonics (of frequency ω, 2ω, . . . $n\omega$) of the modulating signal.

It can be shown that each of these components can be expressed in the form

$$i_{f,n} = I_o \exp (AE_o) \cdot F_n (A,V) \qquad (3)$$

that is as a product of the constant current i_{dc}^* in the absence of a modulating signal, times a term which depends only on the coefficient A (which determines the Tafel slope) and on the amplitude V of the modulating signal. The index n indicates the order of the harmonics, with zero designating the d.c. term.

A second piece of information is derived from the analysis, concerning phase relationships. It can be shown that the components of the faradaic current of odd order (ω, 3ω, 5ω, . . .) bear alternately

a 0 or $\pm \pi$ phase relationship with the modulating signal, while even $(2\omega, 4\omega, 6\omega, \ldots)$ components are shifted in phase by $\pm \pi/_2$ with respect to the modulating signal.

From equation (3) it can be immediately deduced that current components depend on the constant component E_o of the voltage in the same way as (1), giving parallel lines in a semilogarithmic, or Tafel, plot. This is illustrated in Fig. 1, where both anodic and cathodic reactions are taken into account. Also, since the factors F_n do not depend on the frequency of the signal, the amplitude of all the current components should be independent of the frequency. It can also be shown that F_o, the factor for the d.c. component of the faradaic current is always greater than 1, showing that a sinusoidal modulation of the voltage produces a rectified current that will enhance the rate of the electrode reaction.

As it is well known, the coefficient A is related to the Tafel slope by the equation $A = \dfrac{\ln 10}{b}$. Therefore, since the factors F_n depend on A, if the anodic and cathodic reactions are associated with different Tafel slopes, their intersection, which determines the open circuit potential, that is the potential at which no d.c. current flows, will be shifted by the application of a sinusoidal modulation. This fact is also illustrated in Fig. 1. Here the anodic Tafel slope is smaller than the cathodic one, and the open circuit potential is shifted in a negative direction.

b. Capacitative Current

For the analysis of the effect of an alternating voltage on an electrode it is necessary to consider the capacitative current i_c as well, since the electrode-solution interface constitutes a circuit with a capacitance and resistance in parallel. Therefore the total current is

$$i = i_f + i_c \qquad (4)$$

The electrode capacitance in general varies with potential and it is strongly affected by adsorption phenomena, some of which can be rather slow, so that relaxation times can be large compared with variations in electrode potential.

However, in many instances the capacitance is only a function of potential, and as a matter of fact, its variation can be relatively minor within certain potential ranges. The analysis has shown that if the electrode capacitance is only a function of potential, a sinusoidal modulation as in (2) does not cause any d.c. component of i_c. Moreover, it can be shown that its odd harmonic components (ω, 3ω, 5ω, . . .) are shifted by $\pm\pi/2$ with respect to the modulating signal, while the even components are shifted by 0 or π.

Comparison of these phase-shifts with those of the faradaic current shows that when the hypotheses employed in this analysis are applicable, it is possible to separate the faradaic and capacitative components of the current, provided that phase information is available.

3. <u>Experimental Aspects</u>

    a. Introduction

The experiments studying the effect of a modulating voltage on the correct response of an electrode have three main purposes:

    1) Verification of the correctness of the theoretical predictions

    2) Investigation of the usefulness of different types of measurements for gathering information of diagnostic character concerning a particular corrosion system.

    3) Examination of the behavior of electrodes beyond the limits of validity of the present model.

In this paper we report the results of experiments which concern point 1) and only in part address point 2). This work is still in progress. We intend in the future to collect information related to point

3) in the hope to widen our understanding of the effect of alternating voltage to larger classes of electrode systems, and to contribute the experimental basis for a more encompassing theoretical model.

b. Experimental Methods

With the exception of some preliminary runs, the experiments aimed at testing the validity of the theoretical model have been carried out on the hydrogen evolution reaction. The electrode material was OFHC copper and the solution composition was 0.5 M Na_2SO_4 + 0.1 M H_2SO_4. The reason for the choice was that of employing a system which could be considered under charge-transfer control over a potential range as wide as possible. By minimizing other cathodic reactions, in particular oxygen reduction by bubbling Ar in the cell, and favoring transport in solution by means of vigorous stirring, it was possible to obtain a straight Tafel plot with a slope of 120 mV/decade over a potential range larger than 300 mV.

As further test of the applicability of the hypothesis used in the mathematical analysis to the electrode system under study, the electrode impedance was measured by applying a very small (<2mV) modulating signal, about in the middle of the potential range where a straight Tafel slope was obtained. The results are given in Fig. 2, where the imaginary component Z" of the electrode impedance (for unit surface area) is plotted versus the real component Z'. The plot is approximately a semicircle, indicating that there is no detectable contribution of transport to the electrode kinetics. From the plot the ohmic drop error is found to be about $6\Omega \cdot cm^2$, while the charge-transfer resistance is $450\Omega \cdot cm^2$ and the electrode capacitance of the order of $30\mu F/cm^2$.

The circuit employed for the measurements is given in Fig. 3. Two voltages, a constant or slowly varying one (E_o of equation (2)) and a pure sinewave (of amplitude V), where higher harmonics had been minimized by filtering, were added and applied to the control voltage input of the potentiostat. The resulting current was then decomposed

242/5

using a low pass filter to obtain the constant (or d.c.) term. A phase-sensitive lock-in amplifier gave the amplitude of the current both at the frequency ω of the modulation, and at twice that frequency, each one divided in the component in phase with the modulating signal and the component at 90 degrees.

Inputs and outputs of the circuit, with the symbols used here are given in Table I.

In a few instances the current signal was fed to a 200 channels spectrum analyzer. In this way the amplitude of higher order harmonics could be obtained. However, all phase information was lost and only the absolute value of the current density of angular frequency $n\omega$

$$i_{n\omega} = \sqrt{(i'_{n\omega})^2 + (i''_{n\omega})^2}$$

was obtained.

4. Results and Discussion

Current-potential measurements in the absence and in the presence of a modulating sinusoidal voltage were carried out. Fig. 4 shows the Tafel plot of i_{dc} in both conditions, as well as i'_ω, i''_ω and $i''_{2\omega}$. In the figure are also drawn the lines calculated from the mathematical model. They have a slope of 120 mV/decade. As shown, the d.c. component runs parallel to the value without modulation and it is increased by a factor which is in good agreement with that given by (3). A similar behavior is shown by i'_ω and i''_ω which, as discussed before are both components of the faradaic current. The major difference is that the potential range where the slope is close to 120mV/decade tends to decrease with the order of the harmonics. The component 90 degrees out of phase i''_ω, on the contrary, is largely independent of potential, indicating that the electrode capacitance remains nearly constant in the range studied. In agreement with this conclusion the term $i'_{2\omega}$ was found to be negliglibly

242/6

small, suggesting that all higher harmonics of the current are al-
most exclusively faradaic.

As an additional test, the current signal was examined with a
spectrum analyzer for a value of E_o of -506mV vs. N.H.E. and a modulation
at 25 Hz of 35.4 mV r.m.s. The output values recorded, during the
spectrum analysis, as well as those obtained from the spectrum analyzer
are reported for comparison in Table II, which also gives theoretical
and experimental ratio between the various current components and the current
density in the absence of modulation. The spectrum is given in Fig. 5,
together with the spectrum obtained substituting a pure resistor for the
cell, and passing a current of the order of 100μA rms at 25 Hz. The
spectral purity was excellent: the amplitude of the 50 Hz harmonics
was below the detection limits (about 10^{-7}A) and could be measured at
about $4 \cdot 10^{-8}$A only after filtering out the large 25 Hz signal. As Fig. 5
shows, the only spurious signal detected on the resistor was a 60 Hz
peak of $5 \cdot 10^{-7}$A. The small peak at about 20 Hz which can be seen on the
side of the 25 Hz peak of the electrode current is caused by the mag-
netic stirrer and could be eliminated by shutting it off.

Another Tafel plot, for a modulation of 88.3 mV rms. (V = 125 mV)
at 100 Hz, is shown in Fig. 6. The behavior of the d.c. component is
close to the theoretical prediction over a range of about 300 mV, but sign-
ificant distortions can be seen in the other frequency components.

This is not surprising, since the peak-to-peak amplitude was 250 mV
and, therefore, almost everywhere the oscillations of the electrode
potential exceeded the linear Tafel region. As expected for a fre-
quency higher than that used to take the data of Fig. 4, the capacita-
tive component i''_ω was larger. The significant deviation of i'_ω, which
is constant above -350 mV, is due to the effect of the ohmic drop error.
When the faradaic resistance becomes large (as shown by the value of i^*_{dc}
and i_{dc}) the circuit becomes equivalent to a resistance and capacitance

in series, causing the observed phase shift in the current. The results observed for i'_ω and i''_ω above -350 mV can be accounted for by an ohmic drop resistance of 6.5 $\Omega \cdot cm^2$ and an electrode capacitance of 50 $\mu F/cm^2$.

Comparisions between the predictions about the amplitude of the faradaic components and the experimental values are summarized in Fig. 7. On it the experimental ratios between i_{dc}, i'_ω and $i''_{2\omega}$ with respect to i^*_{dc}, as well as the theoretical lines are given. The agreement is very good for amplitudes V up to about 200 mV. Beyond that the current density caused by the modulation was less than predicted, because the electrode potential was being driven outside the linear Tafel range.

The effect of the frequency of the modulating signal has also been examined. Fig. 8 shows the ratio between the dc current i_{dc} and i^*_{dc}. The measurements were carried out at the same potential ($E_o = -456$ mV vs. N.H.E.) and at the same modulating amplitude (V = 100 mV), at frequencies ranging from 25 Hz to 3kHz. The results agree satisfactorily with the prediction of independence of the current response on the frequency of the modulating voltages. The deviations from the theoretical values at frequencies larger than 500 Hz are due to a large extent to the ohmic drop error, which tends to become the largest element of the circuit. Attempts are being made to further reduce the IR drop by changing the cell geometry and by testing positive feedback systems. These are however difficult to apply to the present work, because of the stringent need to avoid introducing spurious phase shifts.

The experimental results presented here show conclusively that the mathematical analysis previously presented [2] predicts accurately the current response to a sinusoidal voltage of an electrode under charge-transfer control, and can be used, therefore, as a basis for the understanding of the effect of a.c. on corrosion. It also shows that frequency analysis holds promise to be an important tool for the

study of electrodes undergoing corrosion. There is, however, a need to extend the experimental work as well as the theoretical analysis to encompass other kinds of kinetic control.

This work has been performed as part of contract E(49-1)3800 with the Department of Energy, whose financial support is gratefully acknowledged.

References

[1] B. McCollum, G. H. Ahlborn, Tech. Pap. BST72 (1916)

K. G. Compton, INCRA Research Report Project 265 (1977)

D. T. Chin, T. W. Fu, G. F. Kamrowski, S. Pookote, 1978 NACE Research Conference, Houston (1978)

D. J. Nesslage, Paper N. 762, Corrosion 78, NACE (1978)

[2] U. Bertocci, Corrosion, in press.

Table I

Input and Output Quantities

Input Quantities		
E_o	V	$\omega = 2\pi\nu$
d.c. component of electrode potential	Amplitude of modulating voltage	Angular frequency of modulating voltage

Output Quantities			
constant (d.c.) components		In phase with modulating voltage	$\pm\pi/2$ with respect to modulating voltage
i^*_{dc} current density for V = o	i_{dc} current density for V > o	i'_ω current density at frequency ω $i'_{3\omega}$ current density at frequency 3ω	i''_ω current density at frequency ω $i''_{2\omega}$ current density at frequency 2ω

Table II

Values obtained from circuit in Fig. 2 and from spectrum analyzer. E_o = -506 mV vs. N.H.E., V = 35.4 mV r.m.s. at 25 Hz. Current density values in $\mu A/cm^2$ r.m.s.

	i^*_{dc}	i_{dc}	i'_ω	i''_ω	$/i_\omega/$	$i'_{2\omega}$	$i''_{2\omega}$	$/i_{2\omega}/$	$/i_{3\omega}/$
Circuit	186	238	152	161	221	0.1	32	32	
Spectrum Analyzer					215			31	7.3

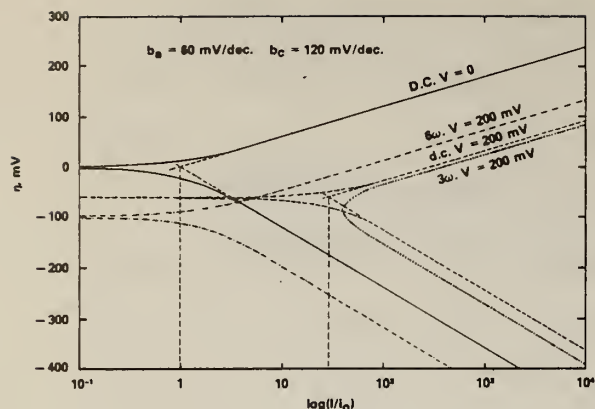| Ratios	i_{dc}/i^*_{dc}	i'_ω/i^*_{dc}	$i''_{2\omega}/i^*_{dc}$	$i'_{3\omega}/i^*_{dc}$
Theoretical	1.24	0.76	0.176	0.0276
Found	1.28	0.82	0.17	0.039

Fig. 1. Example of calculated curves. Electrode with anodic Tafel slope of 60 mV/decade and cathodic slope of 120 mV/decade. Solid line: d.c. current in the absence of alternating modulation. Dashed line: d.c. current in the presence of alternating modulation, amplitude 200 mV. Dotted line: faradaic component at frequency 3ω. Dot-dashed line: faradaic component at frequency 6ω.
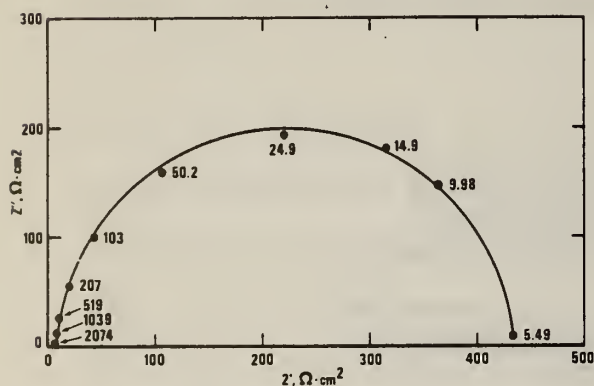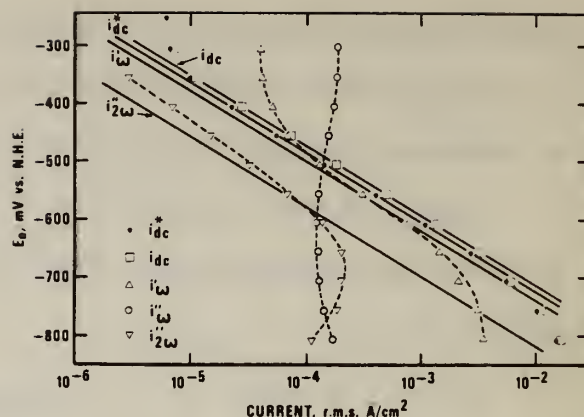

Fig. 4. R.m.s. current density vs. electrode potential for copper in $H_2SO_4 + Na_2SO_4$ with and without voltage modulation (V = 50 mV, ν = 25 Hz). Solid lines are calculated values.
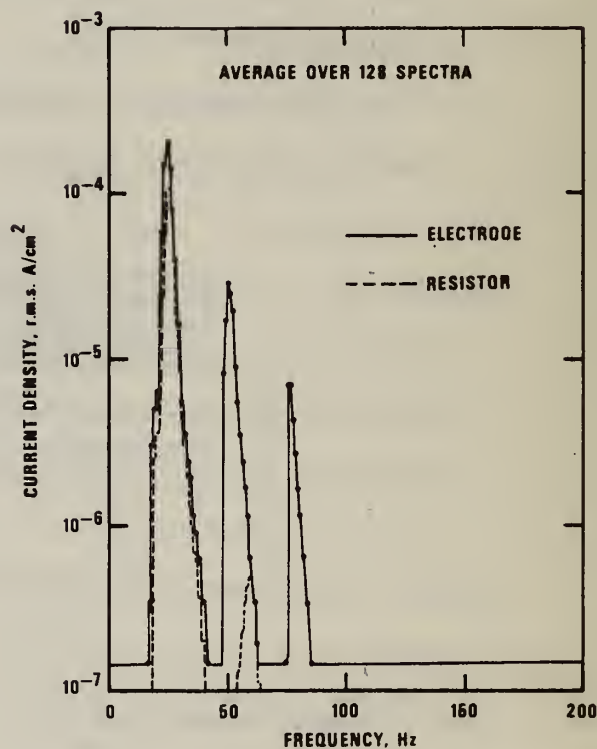

Fig. 2. Imaginary Z" vs. real component Z' of the electrode impedance. $Cu/H_2SO_4 + Na_2SO_4$. E_o = -506 mV vs. N.H.E. Frequency as parameter.

Fig. 5. Solid line: spectrum of current density for a Cu electrode in $H_2SO_4 + Na_2SO_4$. E_o = -506 mV vs. N.H.E., V = 50 mV, ν = 25 Hz. Scale is log (r.m.s. A/cm^2) vs. Hz. Average over 128 spectra. Dotted line: spectrum of current through resistor. Scale is log (r.m.s. A) vs. Hz. Average over 128 spectra.
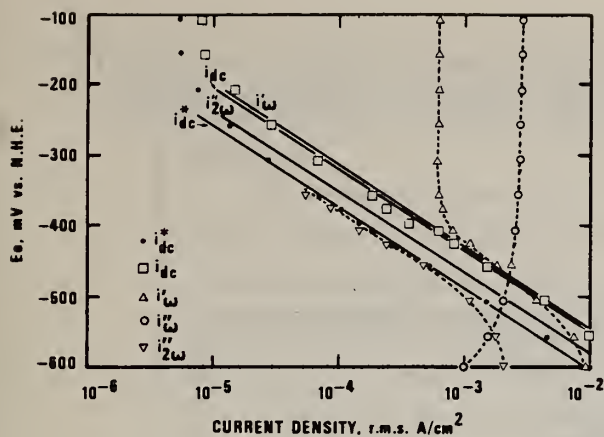

Fig. 3. Block diagram of the circuit used for the measurements.

Fig. 6. R.m.s. current density vs. electrode potential for Cu in H_2SO_4 + Na_2SO_4, with and without voltage modulation (V = 125 mV, = 100 Hz). Solid lines are calculated values.

Fig. 7. Ratio between various components of the faradaic current and d.c. current in the absence of modulation, as a function of the amplitude of modulation. $Cu/H_2SO_4 + Na_2SO_4$. E_o = -506 mV vs. N.H.E. = 103.3 Hz.
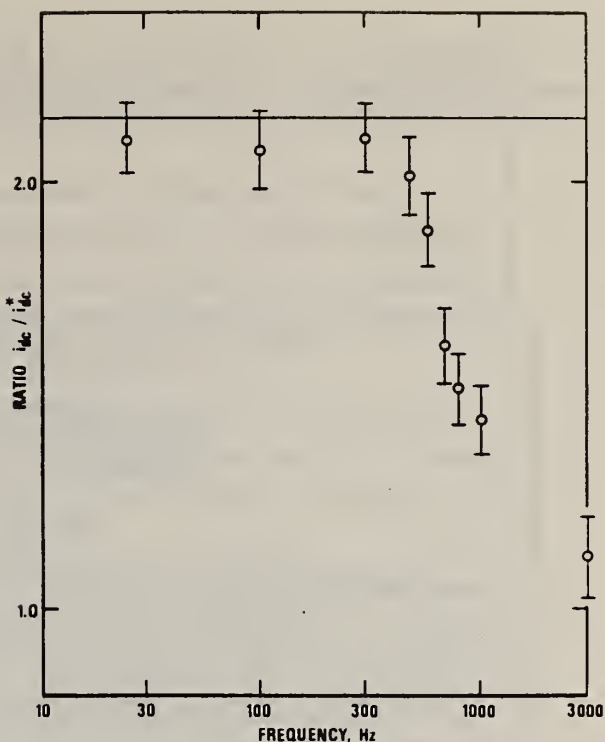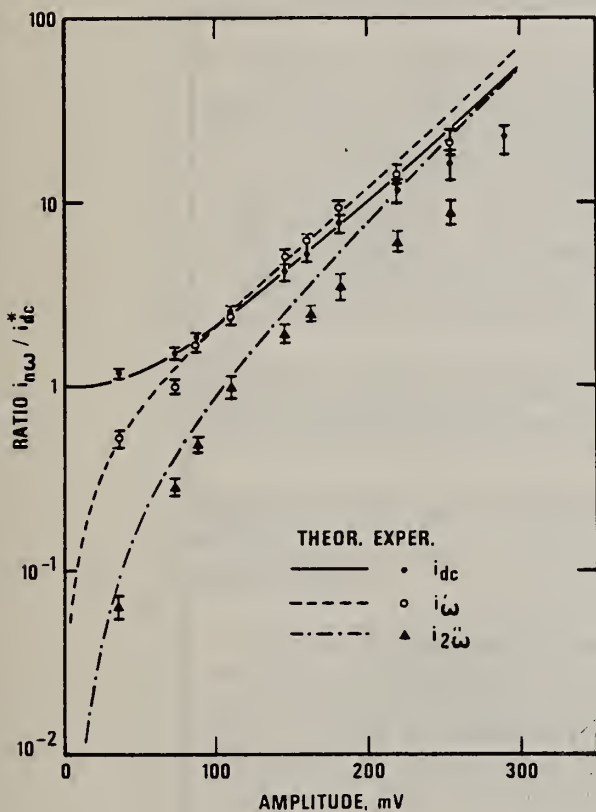

Fig. 8. Ratio between d.c. current in the absence and in the presence of modulation, as a function of frequency. $Cu/H_2SO_4 + Na_2SO_4$. E = -456 mV vs. N.H.E., V = 100 mV. Solid line indicates theoretical value.

Detection and Analysis of Electrochemical Noise
for Corrosion Studies

U. Bertocci
National Bureau of Standards
Institute for Materials Research
Washington, D.C. 20234

ABSTRACT

This paper describes the work done at the U.S. National Bureau of Standards for the study of the fluctuations in current and potential of electrochemical systems, which are commonly referred to as electrochemical noise.

Since control of the electrode potential is desirable in corrosion studies and since commercial potentiostats tend to generate considerable noise that can often inter- fere with the measurements, a battery-operated potentiostat was developed, with a special amplifier for the detection of the current fluctuation. The results of the testing of such an instrument are reported. It was found that the instability of the control voltage generates a signal of the order of $5 \cdot 10^{-8}$ V/$\sqrt{}$Hz, while the amplifying system contributes a noise current of $3 \cdot 10^{-11}$ A/$\sqrt{}$Hz.

Two different experimental arrangements for the analysis and detection of electro- chemical noise are described. With one of them, noise lower than that generated by the instrumentation can be measured.

The equipment described has been used for investigating a number of electrochemical reactions. One of them was the electrodeposition of nickel. In this case, the noise detected apparently was related to the change-transfer process.

Two systems of interest to corrosion science have been investigated, iron and aluminum, both in neutral solution. It is shown that anodic polarization above the pitting potential increases the noise generated by a Fe electrode. In the case of Al, addition of small amounts of chlorides, that are known to cause pitting, was found to enhance the noise current by two orders of magnitude.

INTRODUCTION

The measurement and analysis of the fluctuations in current and potential of electrodes, which are generally called electrochemical noise, are receiving increasing attention as a means for the study of electrode kinetics [1], but are also being applied to the field of corrosion, where the method holds promise to be an useful tool for the detection of localized corrosion [2].

In the area of electrode kinetics one of the advantages is that there is no need to apply an external signal to the system under study. On the other hand the development of mathematical models for the interpretation of the results is still at an early stage and the difficulties are considerable [1], [3].

In the field of corrosion, early work [4] had shown that a very simple experimental arrangement was sufficient to show the correlation between the reduction in corrosion rate caused by an inhibitor and the decrease of the amplitude of the electrochemical noise. With a more modern and complex instrumentation there is reason to believe that the method can be quite powerful and susceptible of application outside the laboratory for the monitoring of corrosion in underground cables and pipes, metallic structures and chemical plants.

At the present time there is a need, however, for accurate laboratory measurements in order to gather information about the range of applicability of electrochemical noise studies, and to collect a data base for the theoretical understanding of the physico-chemical processes involved.

The purpose of this communication is to describe the work done so far at NBS for the development of instrumentation, and to present some experimental results obtained.

INSTRUMENTATION

Two methods are being used in our laboratory for the analysis of the noise generated by an electrode so as to obtain information about its frequency characteristics. The first consists in processing the noise current at constant voltage or the noise voltage at constant current by means of a spectrum analyzer. Since the signals to be studied are often very small, suitable amplification is necessary. The basic

block diagram for this kind of measurements in the case of potentiostatic configuration is shown in Fig. 1. For a galvanostatic configuration, a constant current power supply is substituted for the potentiostat.

Since for corrosion studies it is desirable that the potential of the electrode be controlled, and since the analysis of noise often requires the processing of signals of very small amplitude, it was concluded that a low-noise potentiostat with characteristics better than those of commercial instrument was necessary. Fig. 2, for example, shows the voltage noise that a commercial potentiostat generates when connected to a purely resistive load, in the range between 0.25 and 50 Hz. Although for most purposes the characteristic exhibited by such a potentiostat are excellent, the noise level seldom exceeding 3μV, this is still too high in many instances for noise studies. Also, since the instrument is a.c. powered, large peaks, about two orders of magnitude greater than those shown in Fig. 2, can be found at 60 Hz and at its harmonics.

The potentiostat developed and built at NBS is battery-powered, and in its first version has a maximum output of 5 mA. By careful selection of its components, the noise level generated by the instrument is considerably lower than that shown previously.

Fig. 3 shows the noise voltage found across a resistive load up to 200 Hz. The figure shows that some increase in noise occurs when the maximum current 5 mA is passing. The two peaks at 60 and 180 Hz are due to a.c. pick-up, and can be further reduced by additional electromagnetic shielding. In the figure it is also shown the spectrum obtained when the potentiostat is switched off, which corresponds to the noise generated inside the amplifying circuit. The noise introduced by the potentiostat is less than 10 times the background.

The potentiostat, as schematically indicated in Fig. 1, has built-in a special amplifier for the detection of the fluctuations of the current running through the electrochemical cell under study. The frequency range is between 10 mHz and 1 kHz, which should cover most of the fluctuations of interest in electrochemical systems.

Several spectra of the noise current obtained through this amplifier for resistive loads of various values are shown in Fig. 4. The results can be summarized and described

in the following way: the noise current I_N generated by the potentiostat is the sum of a current I_{CV} caused by the instability of the control voltage and of a current I_A generated inside the a.c. amplifier.

$$I_N = I_{CV} + I_A \qquad (1)$$

As shown in Fig. 4 the noise current, which is largely independent of frequency except at the very low frequencies where flicker noise predominates, is inversely proportional to the value of the load resistance R, that is

$$I_{CV} = V_{CV}/R \qquad (2)$$

where V_{CV} is the noise voltage in the control voltage generator. This instability is about $5 \cdot 10^{-8}$ V/√Hz, as can be deduced directly from the spectrum of Fig. 3. When the resistance R is larger than a few ½Ω, the noise current given by (2) becomes negligibly small when compared with the intrinsic noise I_A of the amplifier, which is of the order of $3 \cdot 10^{-11}$ A/√Hz.

The figures shown and the numbers reported here give an idea of the limits of detection of electrochemical noise which are set by the instrumentation developed. The experimental results, which will be discussed in the next section, indicate that this instrumentation is adequate for a number of electrochemical systems. A graphic example of the capabilities of the instrument is given in Fig. 5. Here a 5μV signal at 500 Hz was added to the control voltage so as to generate a current of 10^{-8}A in a 500 Ω resistor. The spectrum shows how clearly such a small current signal stands above the background noise.

For noise amplitudes smaller than the background generated by the amplifiers, it is necessary to separate the different sources. One such scheme is being employed in our laboratory. This scheme, which is indicated in Fig. 6, should be able, at least in principle, to measure noise levels lower than the noise of the instruments used to detect it. It consists of two identical amplifying and filtering channels, which are connected to two reference electrodes. The output of the two channels is then fed to a multplying and averaging amplifier. Since the noise of the two amplifying systems, including that produced by the reference electrodes, is uncorrelated, its time-average should be zero, while the signal produced by the working electrode is present in both channels and will

appear as a positive value (since it is squared) at the output. The main drawback of the system is its slowness, since one measurement at each frequency requires the resetting of the active filters and adequate time must be allowed for averaging the output. This time can be quite considerable for low frequency measurements. The system, nevertheless, has been used in some instances. An example of its calibration is shown in Fig. 7. Here the noise voltage from a 10 kΩ resistor was measured. Below 10 Hz the noise could be detected although it was smaller, up to about a factor of 10, than the instrumental noise. The large peak shown is due to 60 Hz pick up and has no significance.

EXPERIMENTAL

We will describe here the results obtained on various electrode systems, which have been examined to gain familarity with the capabilities of the instrumentation. Some of these systems are of interest in the corrosion field.

An electrochemical reaction examined was the deposition of Ni from the Watts bath, whose noise has been already studied [5]. The measurements have been carried out both potentiostatically and galvanostatically. In Fig. 8 the spectra under galvanostatic conditions show a slight decrease in voltage noise during cathodic deposition as compared with open circuit. The potentiostatic results of Fig. 9 show that the current noise is the higher the higher is the deposition current density. These results are in agreement with the conclusion that the change-transfer resistance is the principal source of noise and that it decreases when the electrode is cathodically polarized. No evidence of electrocrystallization noise could be obtained from these results.

Among the electrode systems of interest in corrosion science the Fe electrode in a neutral borate solution with a small amount of chloride added has been examined. The voltage noise under galvanostatic conditions was much larger when the electrode was polarized anodically. As shown by the spectra in Fig. 10, the noise levels increased by more than a factor of ten when the electrode was above the pitting potential. Correspondingly, observation of the voltage signal as a function of time revealed sudden bursts of oscillations which were probably related to the formation of pits. Fig. 11 compares the relatively small voltage instabilities at open circuit with the much larger fluctuations above the pitting potential.

Another system examined was that of aluminum in a neutral solution, studying the effect of small additions of NaCl, which is known to cause pitting. Fig. 12 shows the spectra obtained under potentiostatic conditions, in the absence of NaCl. Anodic polarization up to 1.3V vs SCE has only a minor effect on the results. By comparison, the spectrum obtained under cathodic polarization is also shown. The high noise level in this case is believed to be related to the evolution of hydrogen bubbles.

When NaCl was added, although the noise spectrum at the corrosion potential was practically the same as that without chlorides, a small anodic polarization was sufficient to increase the noise current by more than two orders of magnitude, as shown in Fig. 13. This high noise level coincided with the formation of pits over the surface. The noise spectrum was found to consist in many cases of fairly well defined peaks, as shown, for example in Fig. 14. Whether or not these peaks are specific of these conditions and can be used to infer the onset of pitting cannot be answered at the moment, and will require a much more extensive study.

CONCLUSIONS

In this paper, instrumentation suitable for the study of electrochemical noise, particularly for systems of interest in corrosion, has been described. This instrumentation has a low level of intrinsic noise allowing the detection of relatively small signals.

The results obtained on some electrodes indicate that noise levels can vary quite strongly as a function of the corrosion conditions, pointing to noise analysis as a new and promising tool in corrosion science.

REFERENCES

[1] V.A. Tyagai, Elektrokhimiya, 3, 1331 (1967).
C. Blanc, C. Gabrielli, M. Keddam, Electrochim. Acta, 20 687 (1975).
C. Blanc, I. Epelboin, C. Gabrielli, M. Keddam, J. Electroanal. Chem. 62, 59 (1975).

[2] G. Okamoto, T. Sugita, S. Nishiyama, K. Tachibana, Boshoku Gijutsu, 23, 439, 445 (1974).

[3] G. Blanc, C. Gabrielli, M. Keddam, C.R. Acad. Sci. Paris, C, 283, 107 (1976).
G. Blanc, J. Epelboin, C. Gabrielli, M. Keddam, J. Electroanal. Chem. 15, 97 (1977).

[4] W. P. Iverson, J. Electrochem. Soc. 115, 617 (1968).

[5] C. Gabrielli, M. Ksouri, R. Wiart, J. Electroanal. Chem. 86, 233 (1978).
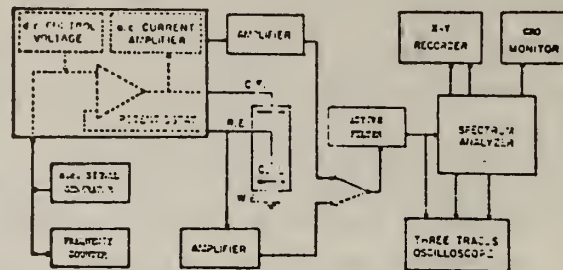C. Blanc, C. Gabrielli, M. Ksouri, R. Wiart, Electrochim. Acta, 23, 337 (1978).

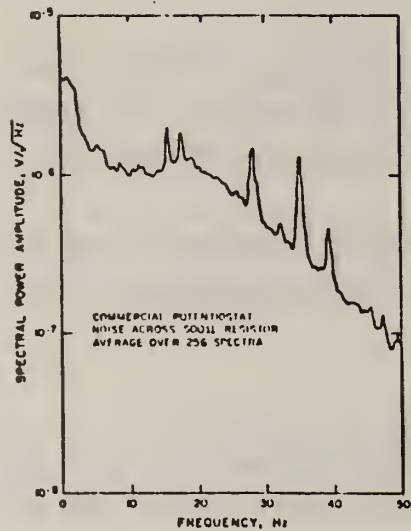Fi.. 1. Schematic diagram of circuit for potentiostatic noise studies.
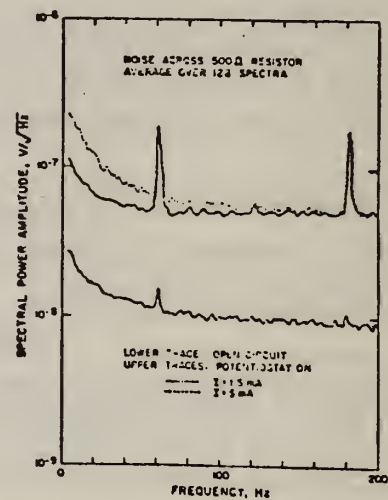

COMMERCIAL POTENTIOSTAT
NOISE ACROSS 500Ω RESISTOR
AVERAGE OVER 256 SPECTRA

SPECTRAL POWER AMPLITUDE, V²/Hz

FREQUENCY, Hz

NOISE ACROSS 500Ω RESISTOR
AVERAGE OVER 128 SPECTRA

LOWER TRACE OPEN CIRCUIT
UPPER TRACES. POTENTIOSTAT ON
——— I = 15 mA
———— I = 5 mA

SPECTRAL POWER AMPLITUDE, V²/Hz

FREQUENCY, Hz

Fig. 2. Noise spectrum of commercial
         potentiostat.

Fig. 3. Noise voltage across
         resistor.

2016
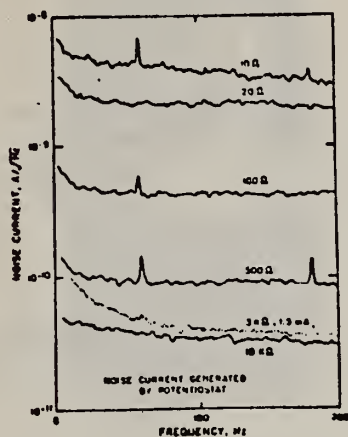
Fig. 4. Effect of load resistance on noise current.
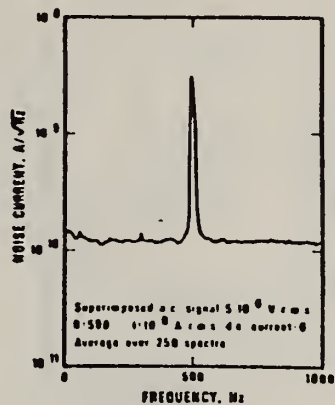
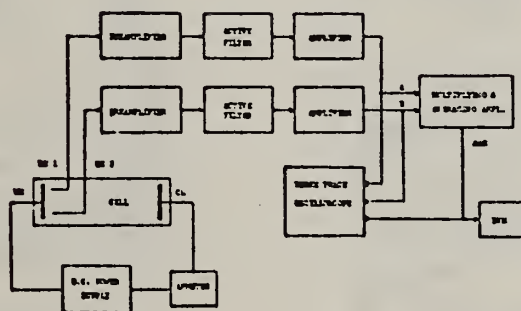Fig. 5. Small amplitude current signal superimposed to noise background.

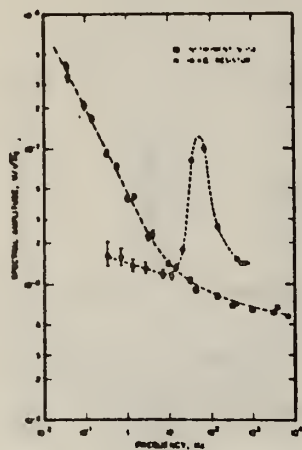Fig. 6. Schematic diagram of circuit for measuring low noise signals.

Fig. 7. Noise generated by the
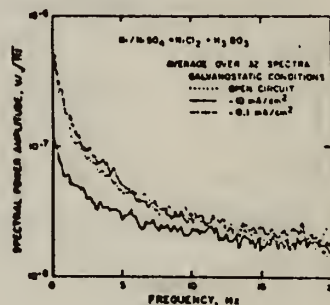instrumentation and by
a 10 k Ω resistor.

Fig. 8. Noise spectra for electrodeposition
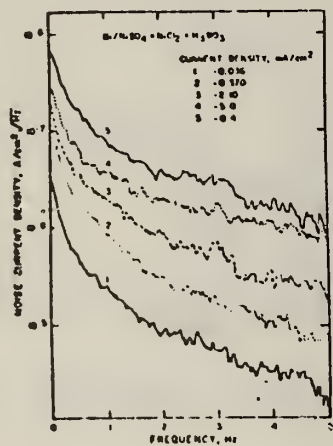of nickel. Potentiostatic conditions

Fig. 9. Noise spectra for electro-
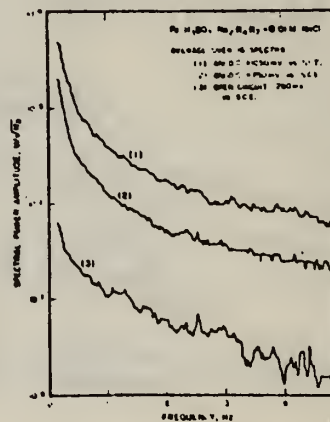deposition of nickel.
Potentiostatic conditions

Fig. 10. Noise spectra for the corrosion
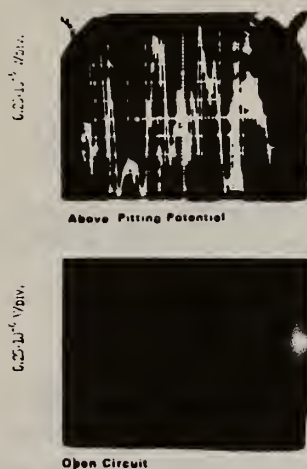of Fe in neutral borate solution

Fe/H₃BO₃-Na₂B₄O₇+0.01 m NaCl

Above Pitting Potential

Open Circuit

Fig. 11. Oscillographic record of
electrode potential of Fe in
1:1 H_3BO_3 – $Na_2B_4O_7$ + 0.01 M
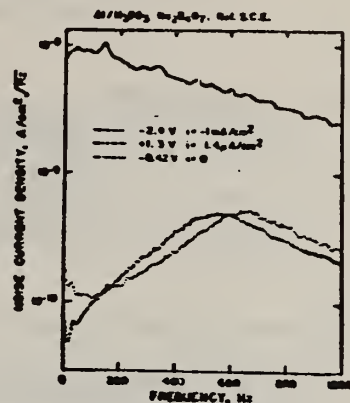NaCl above and below the pitting
potential.

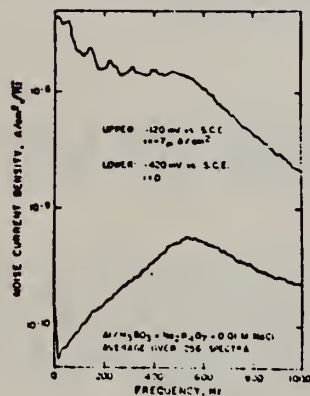Fig. 12. Noise spectrum of Al in
H_3BO_3–$Na_2B_4O_7$.
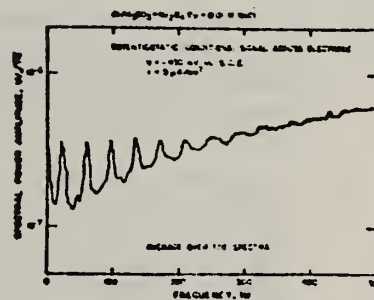

Fig. 13. Effect of NaCl on noise
spectrum of Al.

Fig. 14. Peaks in noise voltage of
Al in Boric - Borate + NaCl.

DISCUSSION

Q: Hideo Kitagawa

What kinds of noises from corrosion measure in the practical dirty surfaces, solution with impurities, etc.)

A: U. Bertocci - We hope to be able to use the technique under a variety of conditions. The noise measured should be characteristic of the corrosion process in any environment being examined.

Q: Tatsuo Ishikawa - Sapporo, Japan

1) When Al in boric acid borate solution is cathodically polarized at -2.4V, what is occuring on the Al surface that causes a high level of noise?

2) If you have, I would like to know the data for stainless steel in H_2SO_4 + Cl^- system. If not, what results could you expect to the noise spectrum of this system?

A: U. Bertocci

1) Probably hydrogen evolution.

2) Electrochemical noise on stainless steel has been studied by Okamoto and coworkers [Boshoku Gijutsu, 23, 439, 445 (1974)].

Q: M. Froment - Paris, France

You have found in the case of anodic polarization of aluminum different behaviors according to the presence or absence of chloride. It is possible to observe a sharp maximum of the level of noise at 500 Hz. Have you a electrochemical model to explain the result?

A: U. Bertocci - The apparent peak at about 600 Hz is an artifact of the instrumentation. In the version used for these studies the a.c. noise in the control voltage of the potentiostat was being filtered out above about 500 Hz. As a consequence, the current response which was increasing with frequency because of the impedance rolloff due to the double layer capacitance, started decreasing beyond ~600 Hz, thus creating the appearance of a peak. We have since extended the frequency range where control voltage noise is about constant to about 5 kHz.

Applications of a Low-Noise Potentiostat
in Electrochemical Measurements

Ugo Bertocci
Chemical Stability and Corrosion Division
National Bureau of Standards
Washington, D.C. 20234

Abstract

Measurements on two electrochemical systems, copper in copper sulfate and aluminum in boric acid: sodium tetraborate buffer with and without chloride added, have been carried out employing a low-noise potentiostat developed and built at NBS by recording the amplitude spectrum of the fluctuations in the current density. In the case of copper, the current spectra resulted to be the deterministic response of the electrode to the noise voltage generated by the potentiostat. The electrode characteristics for charge-transfer and for diffusion could be obtained from the impedance plots derived from the measurements when the level of the applied signal was of the order of 10^{-7} V. In the case of aluminum, the deterministic response observed in the absence of pitting was overcome by random fluctuations in the current in conditions leading to pitting. It is shown that the onset of pit formation can be detected from noise measurements. The significance of the information obtained in electrochemical noise measurements is briefly discussed.

Applications of a Low-Noise Potentiostat in Electrochemical Measurements

Ugo Bertocci
Chemical Stability and Corrosion Division
National Bureau of Standards
Washington, D.C.   20234

INTRODUCTION

The study of random fluctuations in current and potential of electrodes, usually known as electrochemical noise, is receiving increasing attention, and interesting applications are being envisaged in the field of corrosion [1]. In these studies, it is often necessary to detect and measure very low amplitude signals, and it is therefore very important to reduce the noise generated by the measuring instruments. Since in most electrochemical studies it is desirable to control the electrode potential, a low-noise potentiostat is a particularly useful device [2].

Elsewhere [3], the circuit and performance of a potentiostat designed and built at NBS have been described. The purpose of this communication is to report on measurements carried out on some electrochemical cells, taking advantage of the characteristics of such a potentiostat. These measurements are not restricted to the detection of noise, but concerns also the observation of the current response to very small voltage signals.

EXPERIMENTAL PROCEDURES

The measurements were carried out with the apparatus shown schematically in Fig. 1. All the instruments inside the dot-dashed enclosure are battery operated, and the enclosure represents electro-magnetic shielding as well as some protection from mechanical vibrations. The potentiostat provides a low-noise dc control voltage and for the measurement of the dc current. A built-in ac amplifier is employed for the detection of the fluctuations in the current in the frequency range approximately between 0.1 Hz and 2 kHz. The cell is provided with two reference electrodes, a low impedance one, which is used as a sensor for the potentiostat and for the measurement of the voltage noise, and a second one, often a SCE, employed for the monitoring of the dc electrode potential. The values of the dc voltage and current are recorded on a two-channel recorder.

An additional voltage signal can be added to the dc control voltage. In this work, the superimposed voltage consisted of a constant amplitude, swept frequency signal, varying linearly over a factor of ten. The repetition rate was slightly less then the time of acquisition of a spectrum by the spectrum analyzer.

The frequency analysis of the output signal, either the current or the electrode potential depending on the position of the switch shown in Fig. 1 was carried out by a spectrum analyzer with a frequency

resolution of 1/200 of the range. In the 50 Hz range, for example, the spectrum consisted in 200 values at intervals of 0.25 Hz. The acquisition time for one spectrum is equal to one period at the lowest frequency, that is 4 seconds for the range mentioned above.

The input waveform to the spectrum analyzer as well as the instantaneous and average spectra were observed continuously on the oscilloscope. Average spectra were then recorded on a X-Y recorder, either on a linear or on a logarithmic frequency scale.

The time involved in acquiring the average spectra in the low frequency ranges can be considerable. In the 5 Hz range, each spectrum requires 40 seconds, so that for an average over 64 spectra, the acquisition time is of the order of 40 minutes.

EXPERIMENTAL RESULTS

The results presented here concern two quite different electrode systems, one having low and the other high resistance to the faradaic current.

As a low impedance system, the reaction between Cu metal and a 0.5 M $CuSO_4$ + 0.1 M H_2SO_4 solution was examined. Figs. 2 and 3 show the voltage and current spectra, respectively. The reference electrode was also copper, and the data were taken in conditions of zero dc current. The spectra were taken also when a swept frequency signal was added to the dc control voltage. The amplitude of the signal as shown in Fig. 2 was about 10 to 100 times the background noise but never larger than about 2 μV. Fig. 3 shows the current response with and without the superimposed voltage signal.

The impedance of the electrode /Z/ can be obtained as the ratio of voltage to the current at every frequency, and the results are shown in Fig. 4. These ratios were calculated after subtracting from each value the instrumental noise, which had been previously measured [3]. The points in Fig. 4 obtained with and without the superimposed voltage signal are very close. This is because the electrode impedance is rather small, and therefore the instrumental noise in the current density is small compared with the recorded value of the current. The increased signal-to-noise ratio obtained by a larger voltage signal has little effect on the accuracy of the results.

The results have been fitted to an equivalent circut (shown in the inset in Fig. 4). The line drawn in Fig. 4 shows /Z/ as calculated from this circuit, using the following values: ohmic drop resistance R_Ω=5 Ω, charge-transfer resistance R_{ct} = 15 Ω, equivalent to an exchange current j_o for the rate-determining step [4] $Cu^{++} + e^- \rightleftharpoons Cu^+$ of 0.42 mA/cm^2; double layer capacitance C = 35 $\mu F/cm^2$.

-2-

Since one of the species involved in the rate-determining step, Cu^+, is present only in low concentrations, a significant Warburg impedance is present at low frequencies. The value of the Warburg impedance

$$W = \frac{RT}{z^2 F^2 (Cu^+) \sqrt{2\omega D_{Cu^+}}}$$

was calculated choosing $D_{Cu^+} = 1.38 \ 10^{-5} cm^2/sec$ and $Cu^+ = 2.9 \cdot 10^{-4}M$. Most of these values are in excellent agreement with the literature; for instance, the exchange current density [5] and the diffusion coefficient of Cu^+ [6]. The Cu^+ concentration that gives the best fit is about 80% larger than that calculated from the reaction

$$Cu^{++} + Cu = 2 \ Cu^+$$
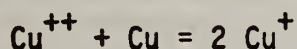
whose equilibrium constant is 7.10^{-4} [6] [7] and taking the activity coefficient of 0.5 M $CuSO_4$ as 0.062 [8]. The value of the Cu^+ concentration affects the magnitude of the Warburg impedance and therefore that of /Z/ only at low frequencies, where the reliability of the experimental points, as shown by the error bars in Fig. 4, is not as good as those at higher frequencies.

The second system examined was 6061 Aluminum in a 1:1 mixture of saturated H_3BO_3 and $Na_2B_4O_7$ with and without addition of 0.05 M NaCl. The current and voltage spectra in the solution not containing chlorides are as given in Fig. 5.

In the chloride-containing solution, which is known to cause pitting if the potential is raised approximately above -700 $\pm$ 50 mV vs SCE [9], the current spectra obtained below and at the pitting potential are reported in Fig. 6 together with the voltage spectrum. During the recording of the spectra, the dc current was about 10 $\mu A/cm^2$ cathodic at -800 mV, while at -650 mV, it became anodic, increasing slowly to about 50 $\mu A/cm^2$.

The impedance plots for this system are given in Fig. 7. Here again the onset of pitting is marked by a fundamental change in the impedance plot up to 1 kHz.

DISCUSSION

The results shown for the $Cu/CuSO_4$ electrode indicate that random fluctuations in electrode characteristics are so low that they do not affect significantly the current response to the broadband noise voltage signal. For this reason, the impedance plot shown in Fig. 4 can be accounted for satisfactorily by the deterministic

response of the circuit drawn, from which reliable values concerning the kinetics of the electrode can be obtained. Therefore, although the intrinsic noise of the control voltage is still too large in this case for the detection of random processes at the electrode, good measurements can be carried out even for signals below 0.1 μV, detecting currents in the nA range.

In the case of aluminum in boric:borate solution, when pitting does not occur, random fluctuations are below the limits of detection, and the electrode response is largely that of a capacitor of about 0.3 μF/cm^2. The data of Fig. 7 seem to indicate a larger capacitance in chloride containing solution, where thinning of the film can occur [10]. Above the pitting potential, the noise current increases more than two orders of magnitude, and the impedance plot in Fig. 7 cannot be explained other than caused by random fluctuations of the electrode current, independently of the voltage signal applied.

The detection of this current noise is a good indication of the beginning of pitting, and the large fluctuations are probably due to hydrogen evolution from the pits [11]. The onset of the large current noise has shown to be reproducible within a range of 10 to 20 mV.

The noise current observed is the sum of several contributions since the fluctuations of the control voltage interact with the random variations of the electrode resistance and capacitance causing intermodulation terms. They are, however, much smaller than the contributions due to the fluctuations of the dc current, which are independent of the control voltage noise. Since the dc current, upon pitting, increases to several μA/cm^2, the noise current observed can be accounted for by oscillations of the order of a few percent of the average dc current.

More difficult it is to estimate the possible contribution of fluctuations in the double layer capacitance; they can be caused by changes in surface area as well as changes in the thickness of the protecting film, a more likely case for Al in neutral solution. The current generated is

$$i_c = (E - E_{zc}) \frac{dC}{dt}$$

where E_{zc} is the potential of zero charge. If the capacitance varies by a fraction k at angular frequency ω, that is

$$C = C_o (1 + k \sin\omega t)$$

The current at that frequency is

$$i_c = (E - E_{zc})\omega C_o k \cos\omega t$$

-4-

The potential of zero charge for Al is at about -0.75 V vs. SCE [12], therefore $|E-E_{zc}|$ can be estimated at being of the order of 0.1 ± 0.2 V. Since $C_0 \simeq 0.3 \ \mu F/cm^2$, for k=1, the rms value of the capacitative noise current would be about $1.3 \cdot 10^{-7}A$ at 1 Hz and 100 times larger at 100 Hz. Since the experimental value of the current decreases with frequency and is about $10^{-8}A$ at 100 Hz, it is safe to conclude that the higher frequency fluctuations of the capacitance are very small, but it is not possible to unambiguously assign the noise observed to variations in the faradaic rather than in the capacitative current.

The results presented show that reduction of the instrumental noise is essential for the study of random fluctuations and that it can be quite useful in all circumstances allowing measurements with very little perturbation of the systems under investigation. The fact that deterministic measurements can be done using the almost white noise in the control voltage [13] has, however, important implications for a proper understanding of the current spectra when "noise" measurements are attempted. Only if the data cannot be explained by assigning constant values to the components of the equivalent circuit, it is appropriate to describe the signal observed as electrochemical noise.
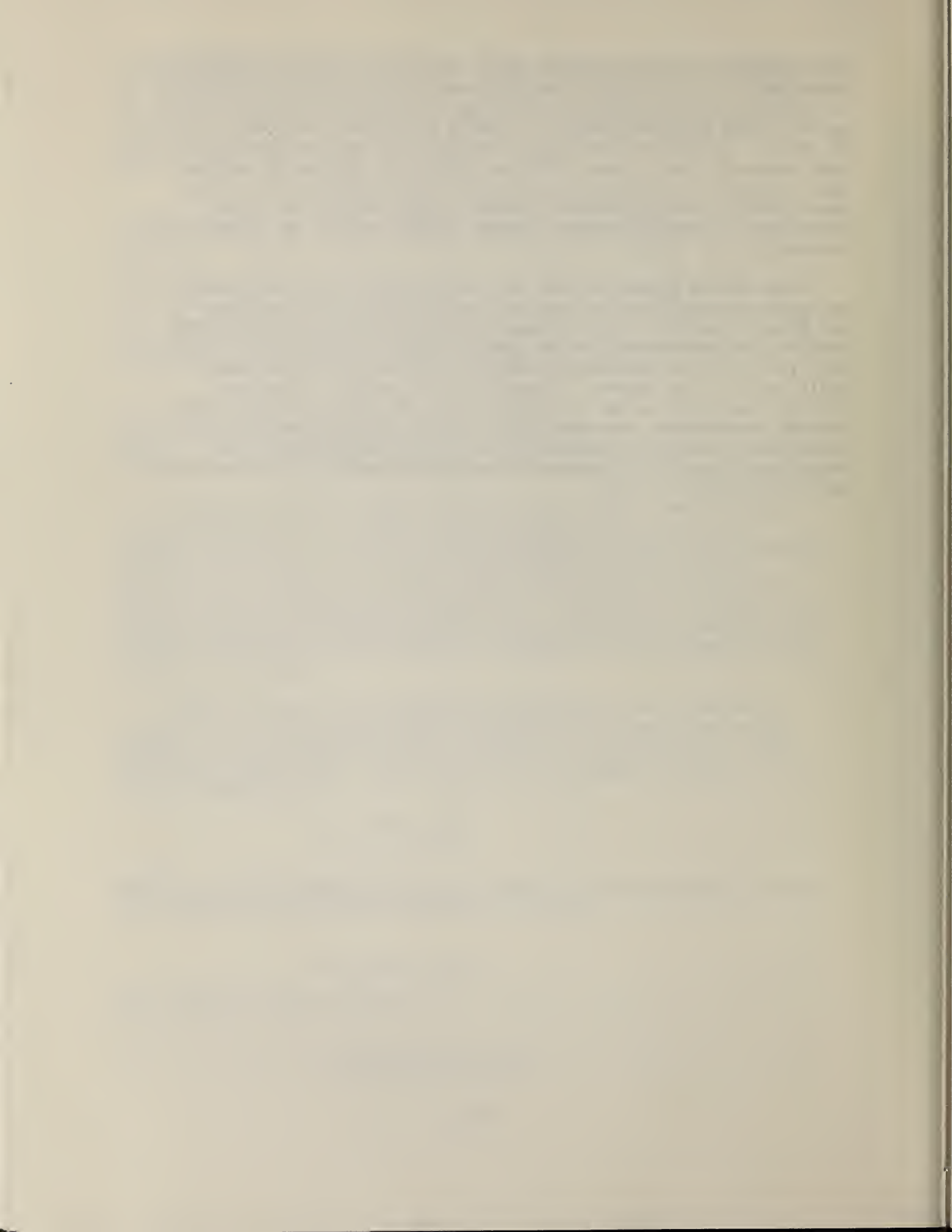
REFERENCES

[1] W. P. Iverson, J. Electrochem. Soc., 115, 617 (1968).

G. Okamoto, T. Sugita, S. Nishiyama, K. Tachibana, Boshoku Gijutsu, 23, 439, 445 (1974).

G. Blanc, I. Epelboin, C. Gabrielli, M. Keddam, J. Electroanal. Chem., 45, 97 (1977).

U. Bertocci, 7th International Congress on Metallic Corrosion, Rio de Janeiro, 1978, in press.

[2] I. Epelboin, C. Gabrielli, M. Keddam, L. Raillon, J. Electroanal. Chem., 91, 155 (1978).

[3] U. Bertocci, R. W. Shideler, NBS J. Res., in press.

[4] E. Mattson, J. O'M. Bockris, Trans. Faraday Soc., 55, 1586 (1959).

[5] A. Damjanovic, T.H.V. Setty, J. O'M. Bockris, J. Electrochem. Soc., 113, 429 (1966).

U. Bertocci, C. Bertocci, B. C. Larson, J. Cryst. Growth, 13/14, 427, (1972).

D. Postl, G. Eichkorn, H. Fischer, Z. Phys. Chem., (NF), 77, 138 (1972).

[6] L. M. Gedansky, E. M. Woolley, L. G. Hepler, J. Chem. Thermod., 2, 561 (1970).

[7] CODATA Bulletin 28, Internat. Council of Scientific Unions (1977).

U. Bertocci, D. R. Turner, in "Encyclopedia of Electrochemistry of the Elements", A. T. Bard, ed., Vol. II, p. 387, M. Dekker, New York (1974).

[8] R. A. Robinson, J. H. Jones, J. A.C.S., 58, 959 (1936).

[9] M. Pourbaix, Corrosion, 26, 431 (1970).

J. R. Galvele, S. M. de DeMicheli, Corr. Sci., 10, 795 (1970).

K. Nisancioglu, H. Holtan, Corr. Sci., 18, 835 (1978).

[10] M. A. Heine, D. S. Keir, M. J. Pryor, J. Electrochem. Soc., 112, 24 (1965).

[11] C. B. Bergeron, R. B. Givens, J. Electrochem. Soc., 124, 1845 (1977): Corrosion Res. Conf., NACE, Atlanta (1979).

[12] S. Trasatti, J. Electroanal. Chem., 33, 351 (1971).

G. Blanc, I. Epelboin, C. Gabrielli, M. Keddam, Electrochim. Acta, 20, 599 (1975).

Figure Captions

Fig. 1.   Experimental circuit for the recording of current and voltage spectra under potentiostatic conditions.

Fig. 2.   Voltage spectra recorded under potentiostatic conditions ($I_{dc}=0$) on Cu in 0.5 M $CuSO_4$ + 0.1 M H_2SO_4.

Fig. 3.   Current spectra recorded under potentiostatic conditions ($I_{dc}=0$) on Cu in 0.5 M $CuSO_4$ + 0.1 M H_2SO_4.

Fig. 4.   Absolute impedance $|Z|$ vs. frequency for Cu in 0.5 M $CuSO_4$ + 0.1 M H_2SO_4 obtained from current and voltage spectra. Solid line calculated for circuit shown.

Fig. 5.   Current and voltage spectra recorded in potentiostatic conditions (E=-330 mV vs. SCE) on Al in H_3BO_3:$Na_2B_4O_7$ solution.

Fig. 6.   Current and voltage spectra recorded under potentiostatic conditions below and at the pitting potential on Al in H_3BO_3:$Na_2B_4O_7$ + 0.05 M NaCl.

Fig. 7.   Absolute impedance $|Z|$ vs. frequency for Al in H_3BO_3:$Na_2B_4O_7$ with and without chloride added.
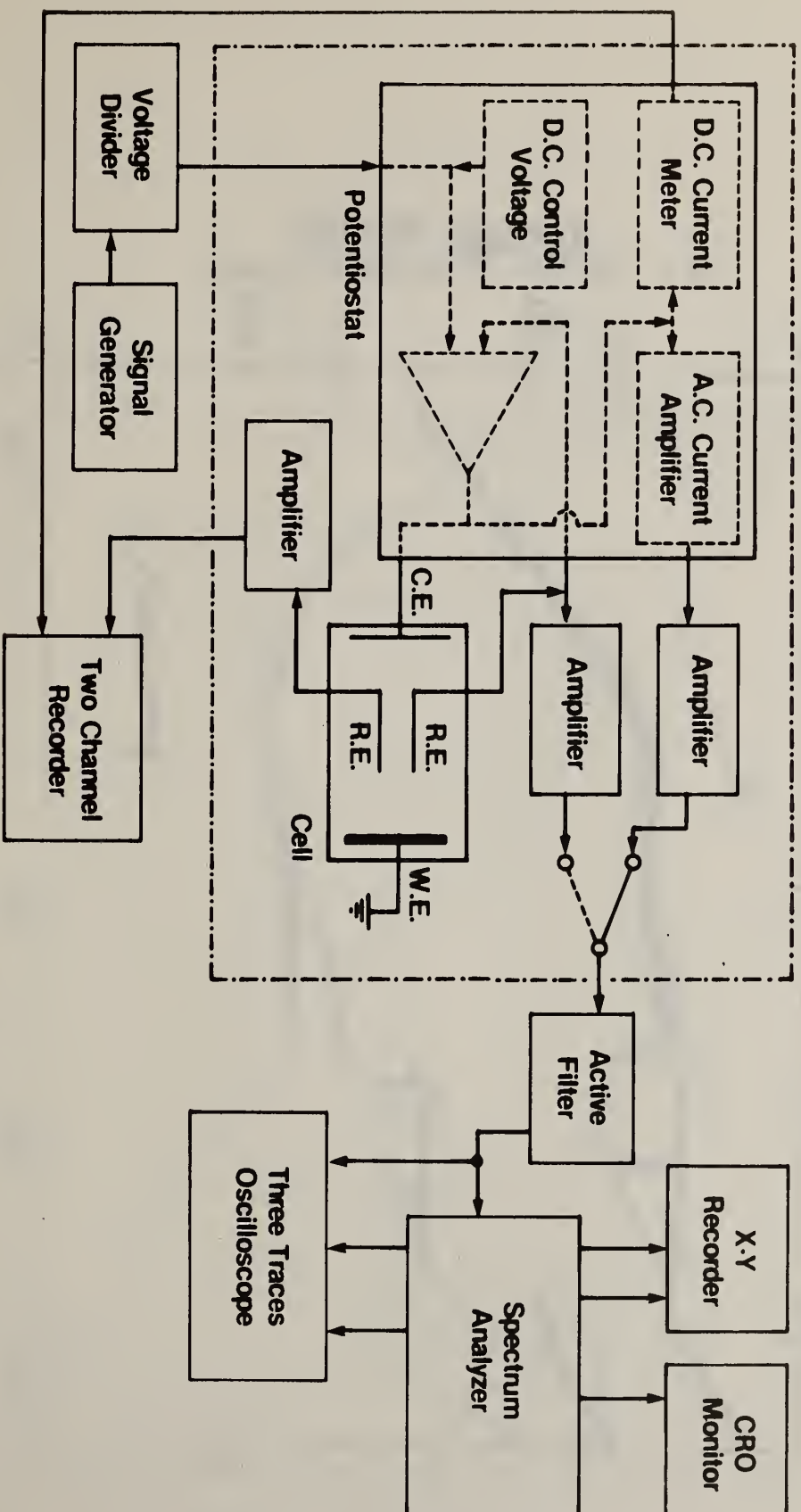
Fig. 1

Fig. 2

Fig. 3

Current Density, A/CM² √Hz

Frequency, Hz

Fig. 4

Frequency, Hz

10^{-1} 1 10 10^2 10^3 10^4

Absolute Impedance |Z|, Ω CM2

4 6 8 10 20 40 60 80 100 200 400

□ No Signal
■ Swept Frequency

R_Ω 5 Ω
R_{ct} 15 Ω
W 171/√ω
C 35 μF

Fig. 5

Fig. 6

Frequency, Hz

Voltage, V/√Hz

Current Density, A/CM²√Hz

Dotted Line: Voltage
Solid Lines: Current Density
Upper: -650 mV vs. SCE
Lower: -800 mV vs. SCE
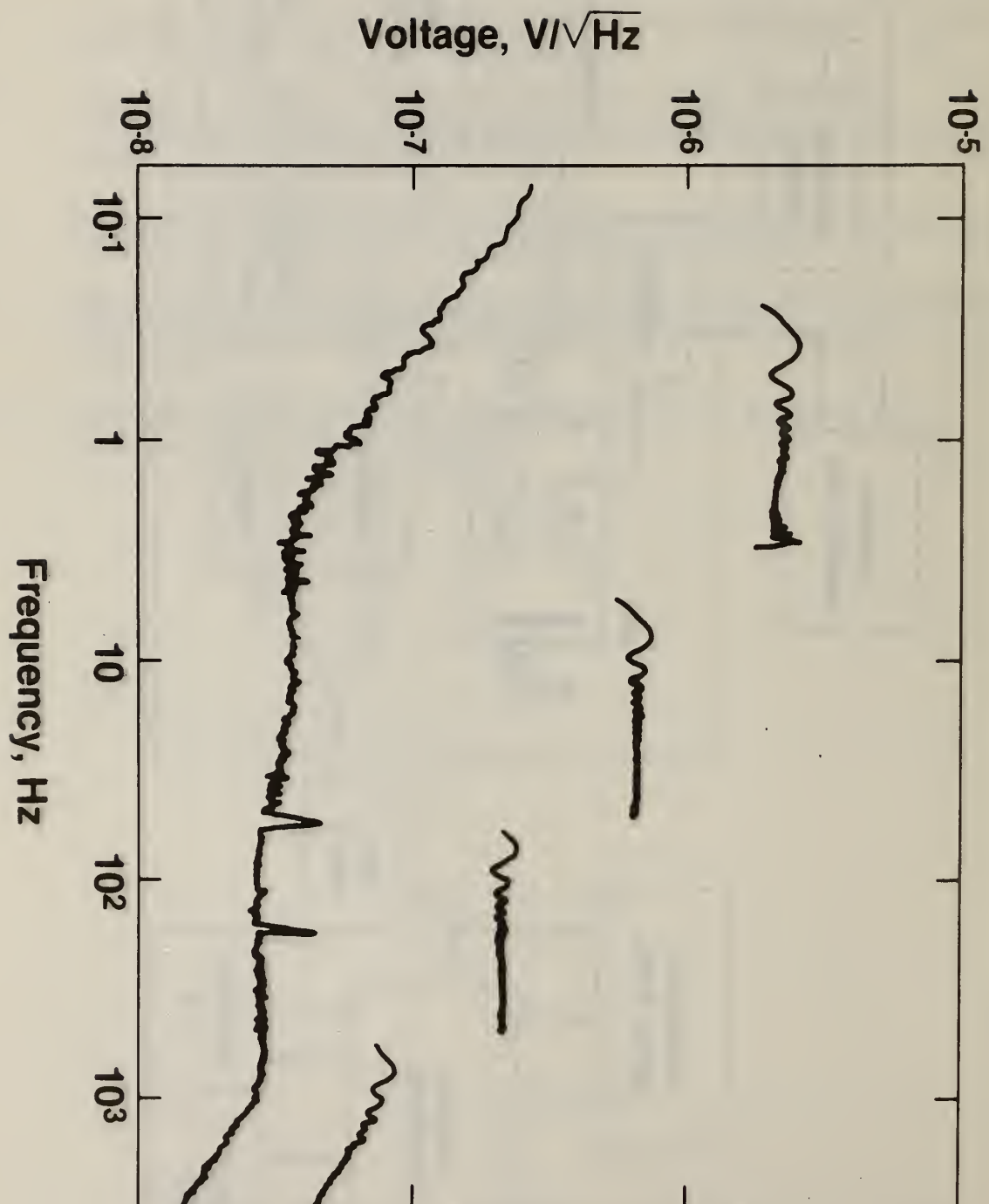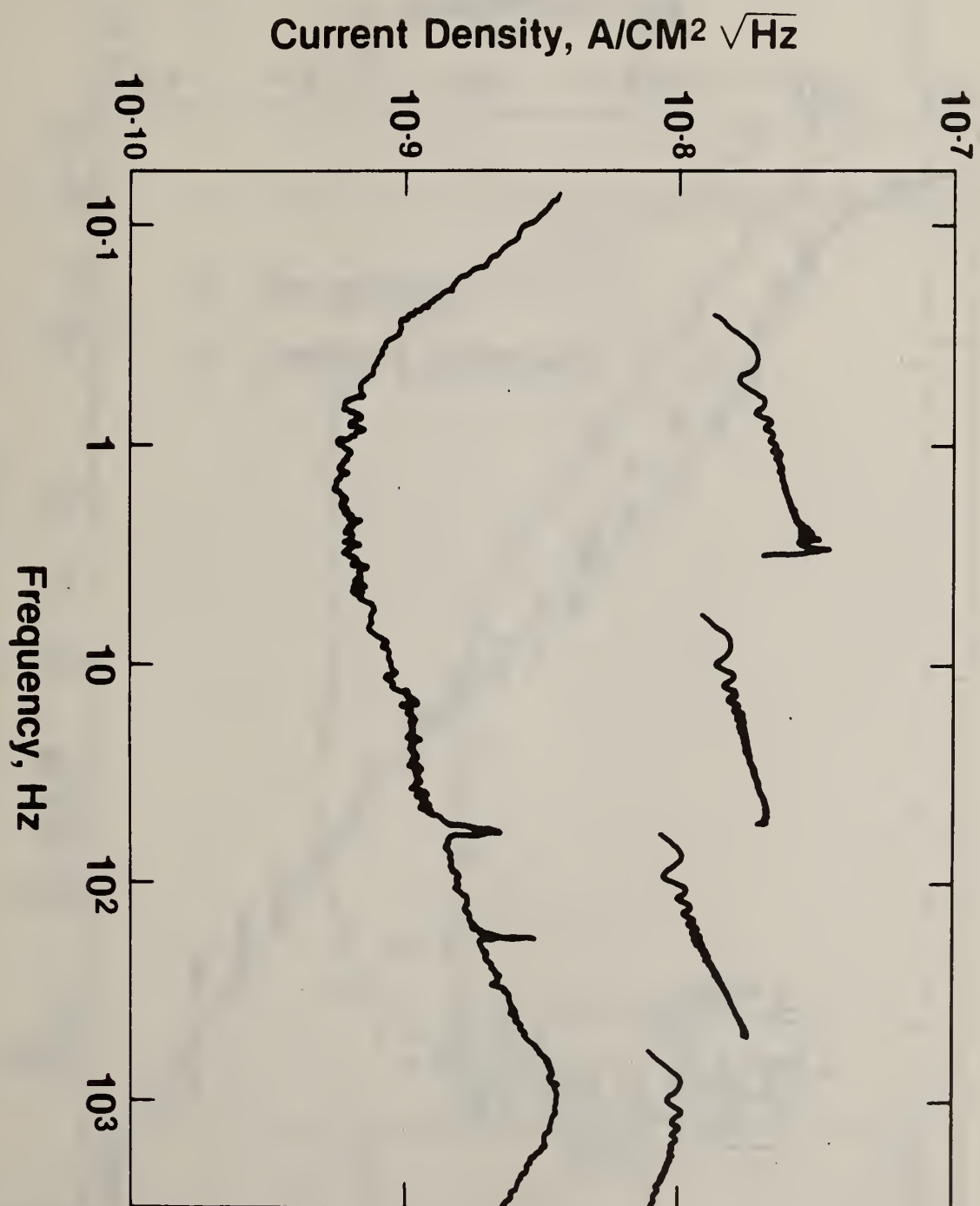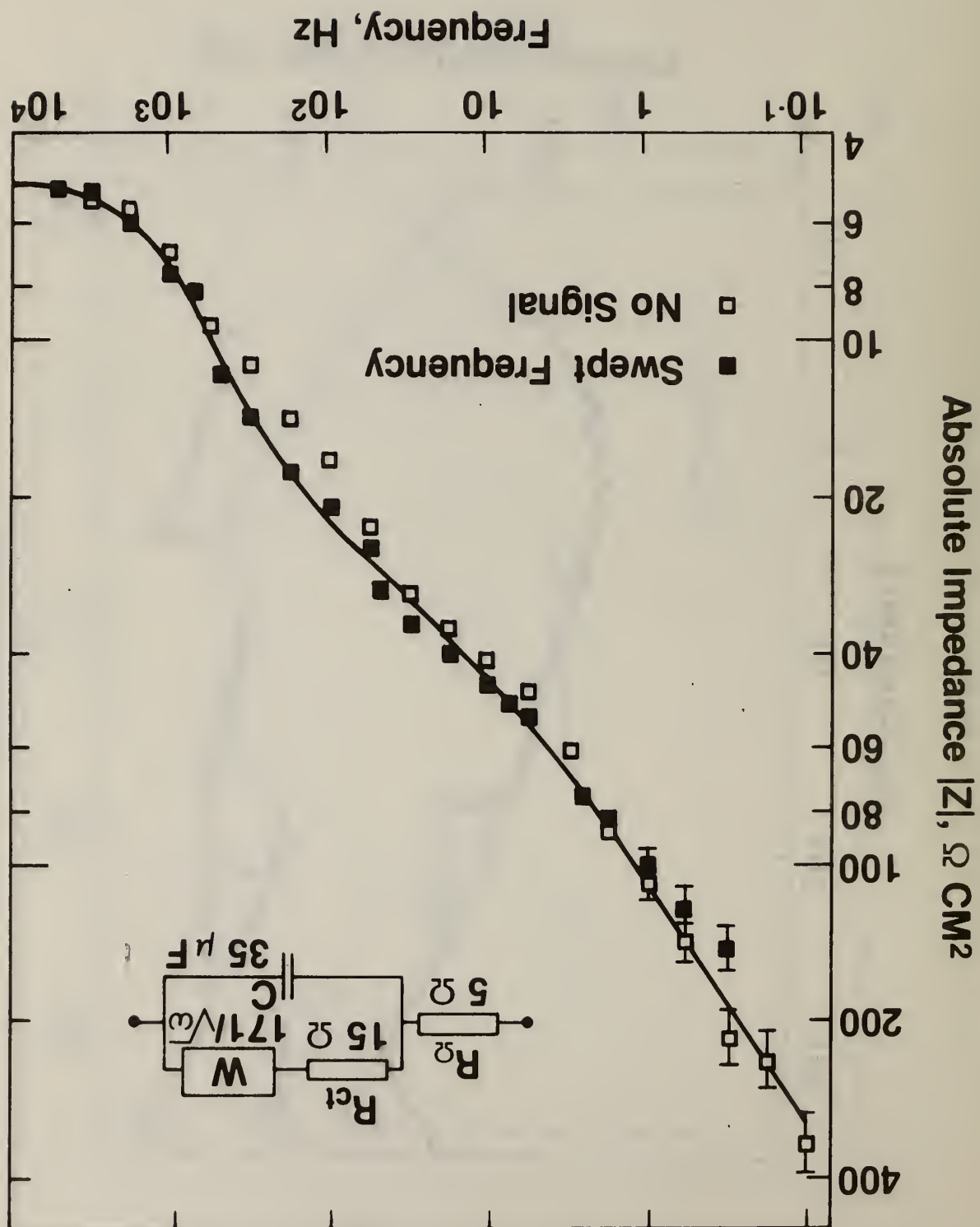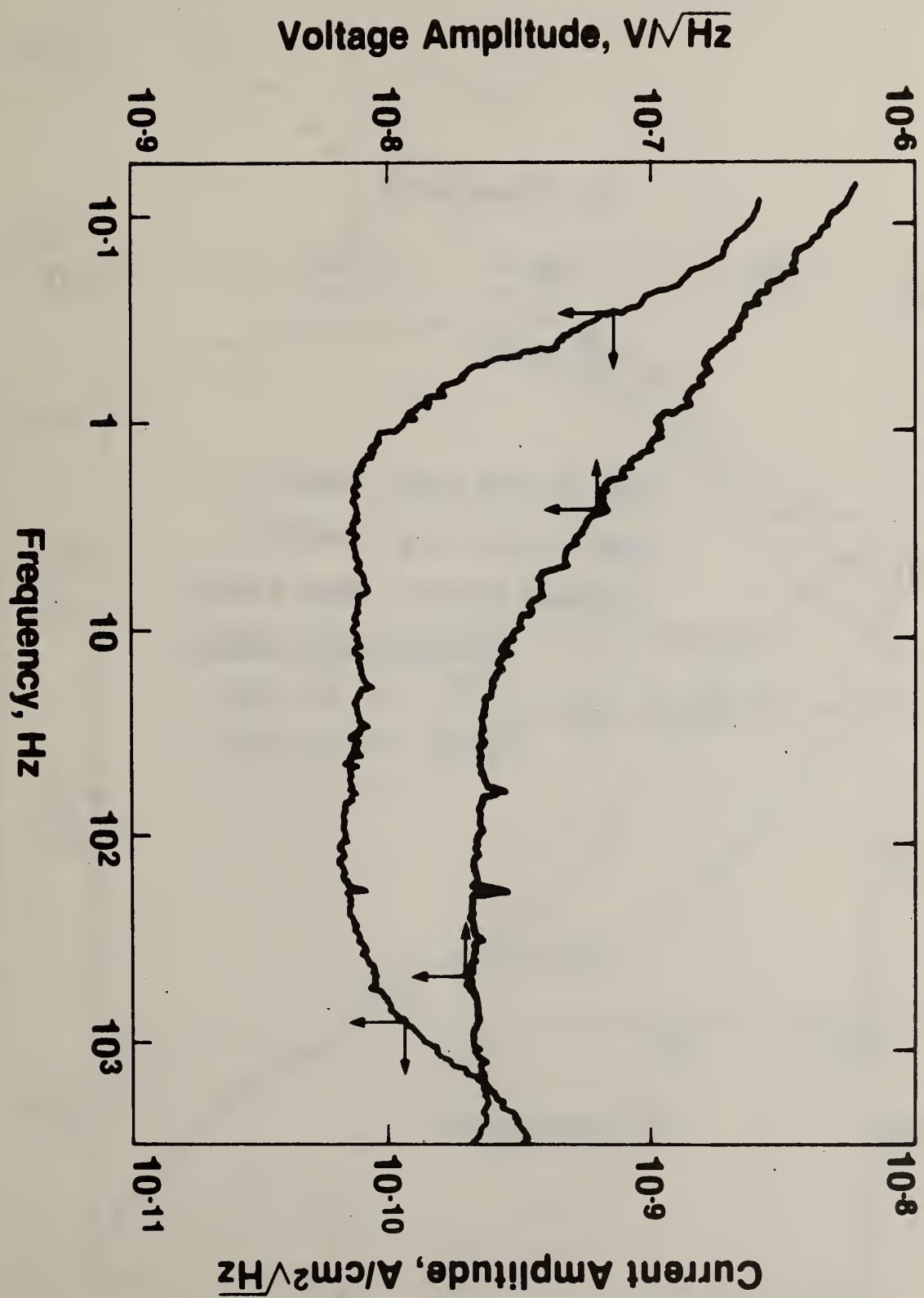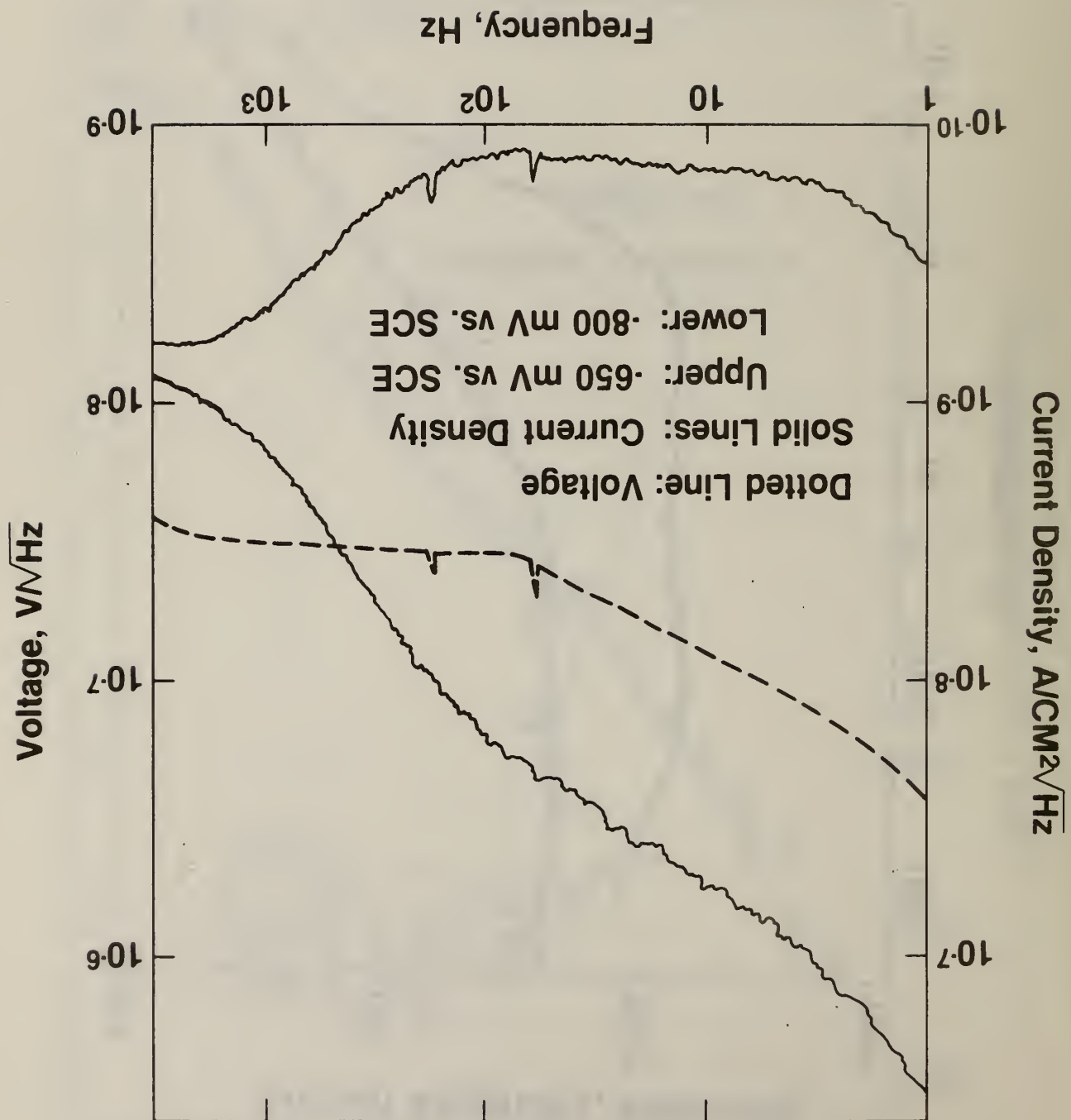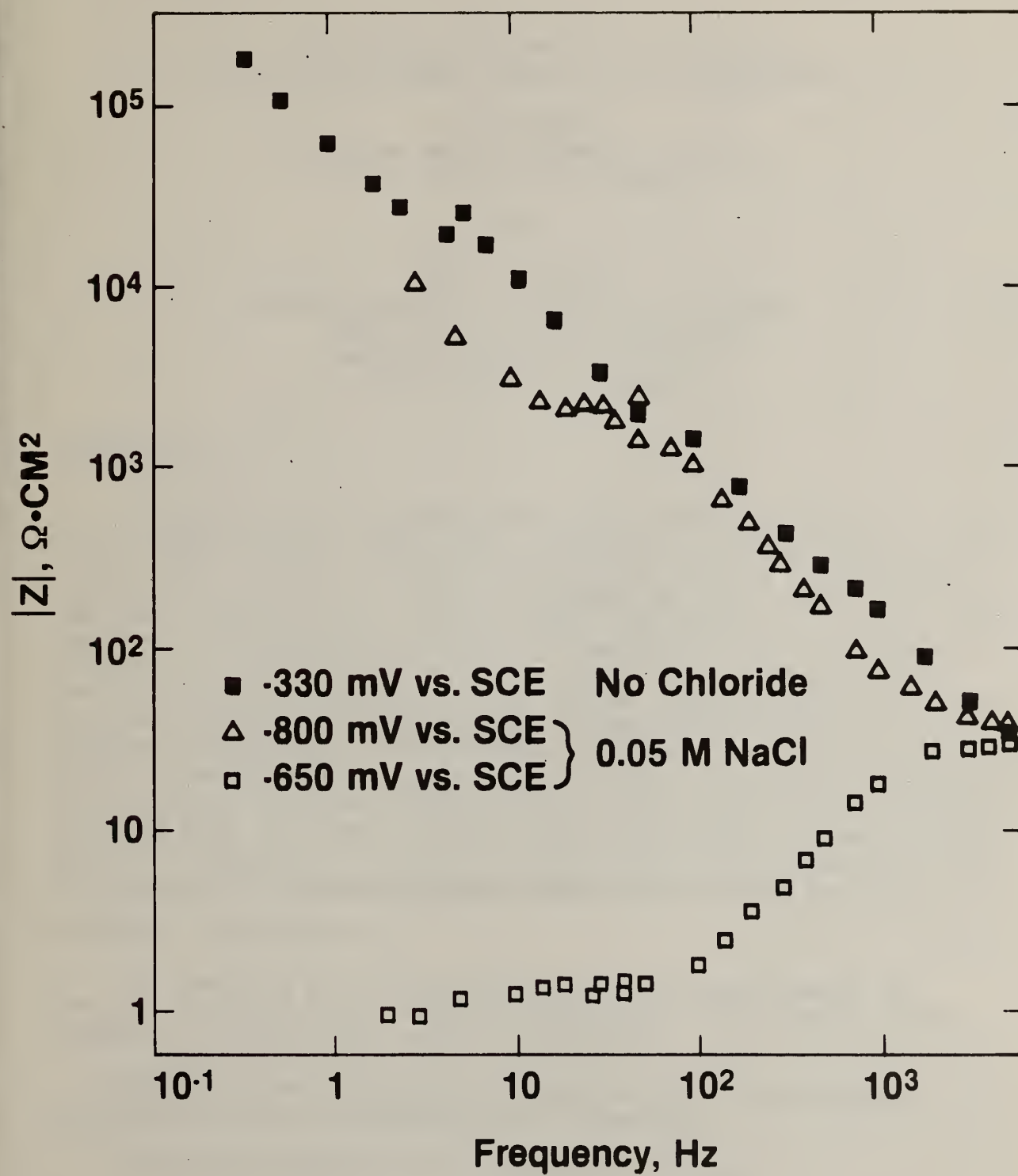
Fig. 7

A Low-Noise Potentiostat for the Study
of Small Amplitude Signals in Electrochemistry

U. Bertocci
Corrosion and Electrodeposition Group
Center for Materials Science

and

R. W. Shideler
Special Analytical Instrumentation Group
Center for Analytical Chemistry
National Bureau of Standards
Washington, D.C. 20234

INTRODUCTION

The ability to detect and measure small amplitude signals in
electrochemistry can be very useful when there is a need to minimize the
input signal in order to perturb as little as possible the electrode/
electrolyte interface as well as to decrease unwanted effects such as
the ohmic drop error, and when the aim of the research is to study the
spontaneous fluctuations in current and potential, which are commonly
referred to as electrochemical noise. This area of endeavor is re-
ceiving increasing attention in the field of electrochemistry [1], and
it is being applied for the detection of corrosion [2]. One of the
problems encountered in these studies is caused by the need of con-
trolling the potential of the electrode without causing an unacceptably
high level of interference from the noise generated by the potentiostat
[3]. In order to improve its performance with respect to commerically
available instruments, a low-noise potentiostat was designed and built,
whose characteristics will be described in the following sections.

INSTRUMENT CHARACTERISTICS

The low-noise potentiostat was designed and developed by the
Special Analytical Instrumentation Group of the Center for Analytical
Chemistry at the National Bureau of Standards.

The design has exceptional low noise and stable low frequency
performance as well as moderately wide bandwidth.

The characteristics of the potentiostat include:

a. Highly stable operation over a wide range of loads with up
to ± 5 mA output.

b. A useful frequency range from DC to greater than 2 kHz.

c. A precision low noise voltage reference source variable from ± 5 V, having a stability of better than 10 µV.

d. A fast recovery, low-noise, ac current signal amplifier with a frequency response of between 5×10^{-2} and $2 \cdot 10^3$ Hz.

Additional features include an external input to allow small signal modulation of the internal voltage reference and the ability to be used as a constant current source or galvanostat. The circuit scheme is shown in Fig. 1.

DESIGN AND CONSTRUCTION CRITERIA

In order to achieve the characteristics desired, the design was chosen so that the working electrode was grounded, facilitating the shielding of stray signals. To reduce capacitative currents across the reference electrode, the lead shield was maintained at the same potential, effecting a guarded input circuit. The high impedance guarded input amplifier is followed by the potentiostat loop amplifier and an output current buffer. (Total noise referred to input is less than 3 µV rms.) The frequency response of the circuit crosses unity gain at approximately six kHz. Immunity to oscillation for all values of cell R and C was secured by tailoring the frequency characteristics of the feedback amplifiers. No provision to compensate for cell parameters at high frequencies is included. A differential amplifier is used to extract the dc current signal from the potentiostat current driver. Signal output is from an ac coupled amplifier having a very low frequency cutoff (5×10^{-2} Hz) and exhibits extremely low noise and prompt over-load recovery. It has three gain settings up to a maximum gain of 1000. For ac components within the frequency range, an ultimate resolution as small as 3 nA (3 mV output) can be measured. A fast recovery circuit brings the amplifier into its linear range within a few seconds for any overload.

Power is supplied by a pair of rechargeable 12 volt gelled lead acid batteries to assure a flat and constant discharge as well as complete freedom from ac pickup. All amplifier circuits make use of high performance operational amplifiers. The amplifier chosen, Precision Monolithics OP-07, is a device having excellent noise and drift performance with long-term drift stability approaching that of chopper stabilized amplifiers.

A double box construction was used to reduce ambient thermal effects and improve immunity to electrical noise. Resistors used were glass metal-film, and all capacitors used in active circuit locations were of polystryrene foil construction. All loose wiring was mechanically secured by using dabs of silicone rubber sealant to reduce vibrations causing microphonics.

PERFORMANCE CHARACTERISTICS

The potentiostat is employed as a part of the circuit shown schematically in Fig. 2. For testing purposes, the cell was substituted with a passive load, which was either a pure resistor or a resistor and a capacitor in-parallel. With the switch in the upper position the fluctuations in the current were analyzed, while with the switch down, the noise voltage applied to the load was recorded. If desired, either a constant or a swept frequency signal of small amplitude was superimposed to the control voltage. All spectra shown in this work were recorded in four sections, over the 5, 50, 500, and 5,000 Hz range. The spectrum analyzer has a frequency resolution of 1/200 of the range, requiring a time of 40, 4, 0.4 and 0.04 s respectively for each spectrum. All recordings are averages over 64 spectra for the lowest range, and 256 or 512 spectra for th higher frequency ranges. All data given are rms values.

Fig. 3 shows the noise current for three values of the load resistance at zero current, as well as at 1 mA of dc current. Fig. 4 shows the noise voltage V_N for any resistive load at I=0 and I=1 mA, as well as the noise of the amplifier with the input shortcircuited. Subtracting this noise from the upper curve (at I=0) gives the dashed line, which represents the noise content V_{CV} of the control voltage of the potentiostat in the frequency range of interest

$$V_{CV} = \sqrt{V_N^2 - V_A^2} \tag{1}$$

This noise is largely independent of frequency above 1 Hz and is about $2.5 \cdot 10^{-8}$ V/$\sqrt{Hz}$. When applied to a resistive load this voltage signal generates the noise current I_N shown in Fig. 3. The noise current I_N observed is the sum of the current I_{CV} generated by the fluctuations in the control voltage and of a noise signal I_A produced by the ac amplifying stage in the potentiostat.

$$I_N = \sqrt{I_{CV}^2 + I_A^2} = \sqrt{\frac{V_{CV}^2}{R^2} + I_A^2} = \sqrt{\frac{V_N^2 - V_A^2}{R^2} + I_A^2} \tag{2}$$

When the resistive load R is sufficiently low (<500 Ω), I_{CV} predominates, as shown by the two upper curves in Fig. 3. When R is large, however, $I_N \sim I_A$, as shown by the lowest curve of Fig. 4. I_A is also largely independent of frequency above 1 Hz and results to be about $3 \cdot 10^{-11}$ A/$\sqrt{Hz}$.

The potentiostat was also tested on a circuit formed by a 10Ω resistor in series with a parallel combination of a 5kΩ resistor and a 5μF capacitor

-3-

(as shown in the inset in Fig. 5). In this case the load impedance is frequency dependent. The voltage and current spectra are given in Fig. 5. Taking the ratio between these values at the same frequency should give the absolute value of the impedance $|Z|$

$$|Z|(\omega) = \frac{V_{CV}(\omega)}{I_{CV}(\omega)} = \sqrt{\frac{V_N^2 - V_A^2}{I_N^2 - I_A^2}} \tag{3}$$

However, as shown before in the case of a resistive load, impedances greater than several hundred ohms are too large to give a current significantly above I_A if one relies only on the control voltage noise. Because of the low intrinsic noise of the potentiostat, the addition of a very low amplitude swept frequency signal to the control voltage was sufficient for obtaining good impedance values. The voltage and current spectra obtained are shown in Fig. 6, and the plot of /Z/ vs. frequency from which the value of the circuit components can be obtained, is shown in Fig. 7. These measurements were obtained applying no more than a few tenths of a mV (in the lowest frequency range) and generating currents less than 100 nA. The possibility of measuring at low amplitudes can be an important advantage when, otherwise, distortions or irreversible changes in the electrochemical system could be produced.

PERFORMANCE AS A GALVANOSTAT

As mentioned before, the instrument can be switched in a configuration where it supplies a constant dc current; up to 5 mA, provided the total load does not exceed 5 V. The ac content of the potential difference between working and reference electrode appears at the output of the ac amplifier.

Recordings taken with a resistor as load are shown in Fig. 8. The noise voltage, in a manner analogous to the potentiostatic case, is the sum of the noise generated by the instability of the control voltage V_{CV}, which in this configuration becomes a noise current through the load, and of the amplifier noise V_A.

$$V_N = \sqrt{\frac{V_{CV}^2}{R_1^2} Z^2(\omega) + V_A^2} \tag{4}$$

R_1 is the internal resistance ($R_1 = 1$ KΩ) on which V_{CV} acts to determine the current, and $Z(\omega)$ is the load impedance, which in this case, is a resistance R. In curve A of Fig. 8, the resistance is zero, and therefore $V_N = V_A$. The noise in the control voltage can then be obtained from (4), and it is close to that obtained in the potentiostat configuration. Curve D shows some increase in noise when a dc current is being drawn.

REFERENCES

[1] V. A. Tyagai, Elektrokhimiya, $\underline{3}$, 1331 (1967).

G. Blanc, C. Gabrielli, M. Keddam, Electrochem. Acta, $\underline{20}$, 687 (1975).

G. Blanc, I. Epelboin, C. Gabrielli, M. Keddam, J. Electroanal. Chem., $\underline{62}$, 59 (1975).

G. C. Barker, J. Electroanal. Chem., $\underline{82}$, 145 (1977).

C. Gabrielli, M. Ksouri, R. Wiart, J. Electroanal. Chem., $\underline{86}$, 233 (1978).

[2] W. P. Iverson, J. Electrochem. Soc., $\underline{115}$, 617 (1968).

G. Okamoto, T. Sugita, S. Nishiyama, K. Tachibana, Boshoku Gijutsu, $\underline{23}$, 439, 445 (1974).

G. Blanc, I Epelboin, C. Gabrielli, M. Keddam, J. Electroanal. Chem., $\underline{45}$, 97 (1977).

U. Bertocci, 7th International Congress on Metallic Corrosion, Rio de Janeiro, 1978, in press.

[3] I. Epelboin, C. Gabrielli, M. Keddam, L. Raillon, J. Electroanal. Chem., $\underline{91}$, 155 (1978).

FIGURE CAPTIONS

Fig. 1.   Schematic circuit of the potentiostat.

Fig. 2.   Experimental arrangement for recording current and voltage spectra.

Fig. 3.   Current spectra recorded in potentiostatic conditions on different resistive loads. Solid lines: $I_{dc} = 0$. Dotted line: $I_{dc} = 1$ mA.

Fig. 4.   Voltage spectra. Upper solid line: potentiostatic conditions, I = 0. Dotted line: same, I = 1 mA. Lower solid line: noise from amplifier with shortcircuited input. Dashed line: Difference between solid lines.

Fig. 5.   Current and voltage spectra recorded under potentiostatic conditions on circuit shown in inset.

Fig. 6.   Current and voltage spectra recorded in potentiostatic conditions on the circuit shown in the inset in Fig. 5. Swept frequency signal superimposed to the dc control voltage.

Fig. 7.   Absolute impedance /Z/ vs. frequency for circuit shown in inset in Fig. 5. Experimental points obtained from spectra in Fig. 6. Solid line: calculated values.

Fig. 8.   Voltage spectra recorded in galvanostatic conditions. Curve A: R = 0, I = 0, Curve B: R = 500 Ω, I = 0, Curve C: R = 1 KΩ, I = 0, Curve D: R = 500 Ω, I = 3 mA.
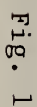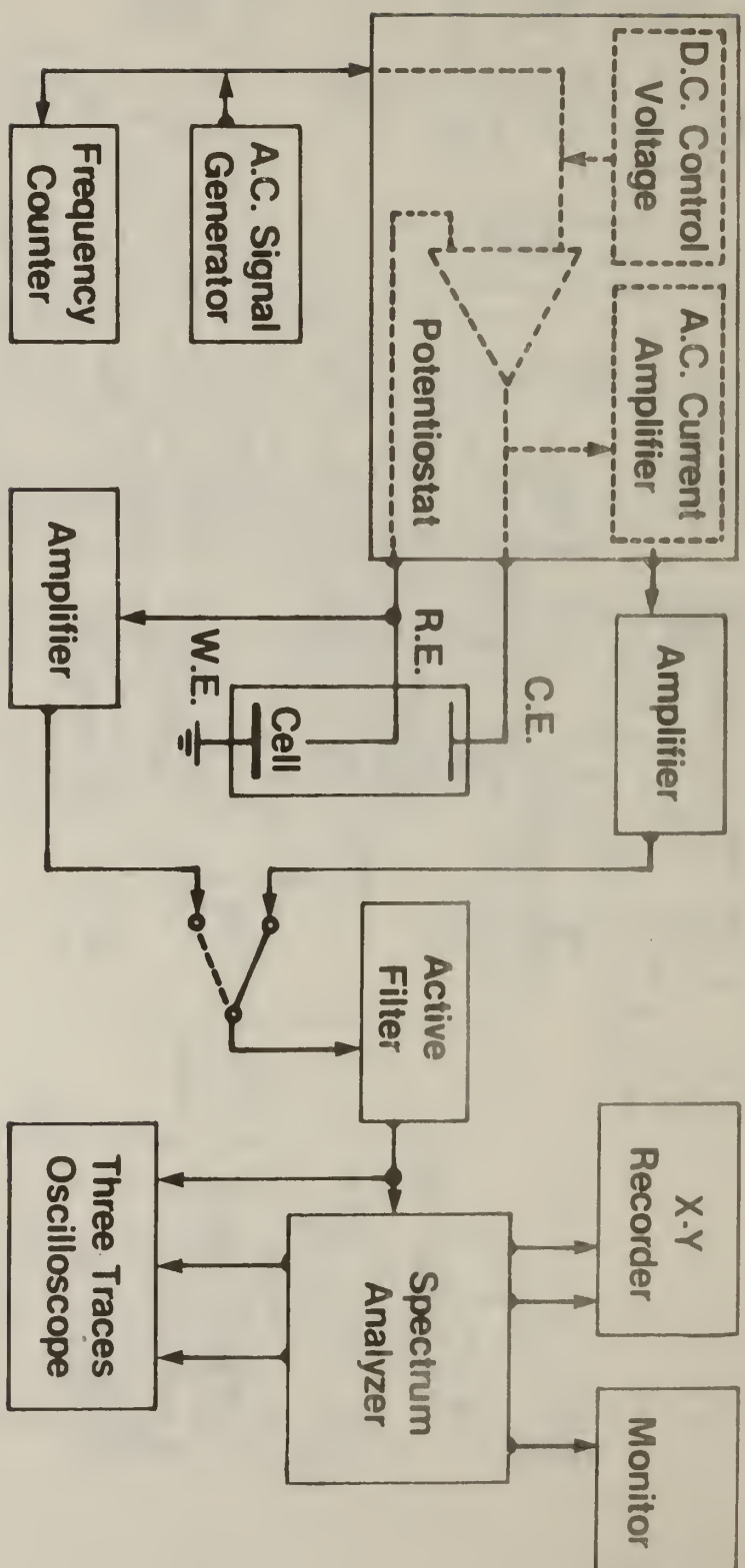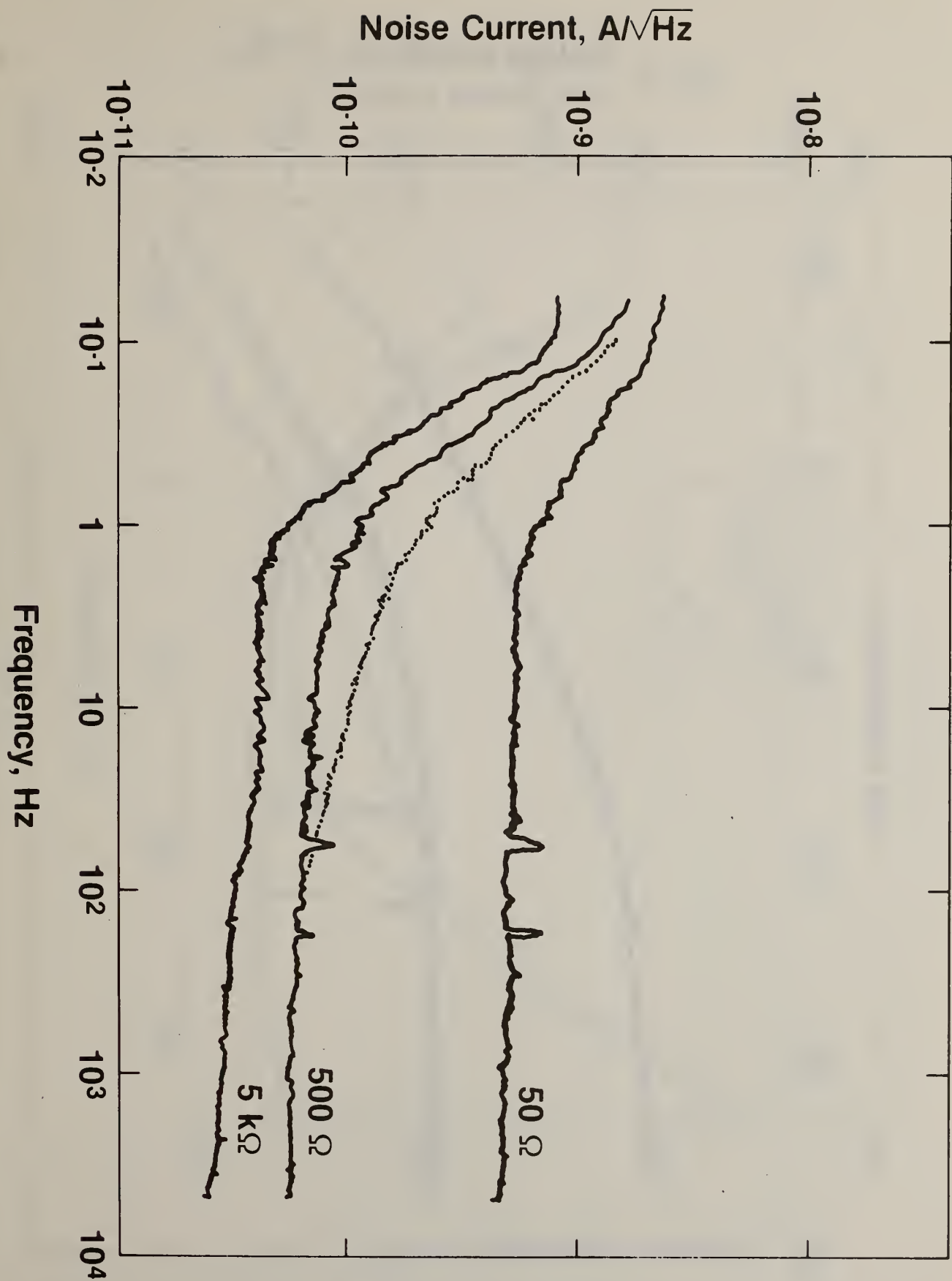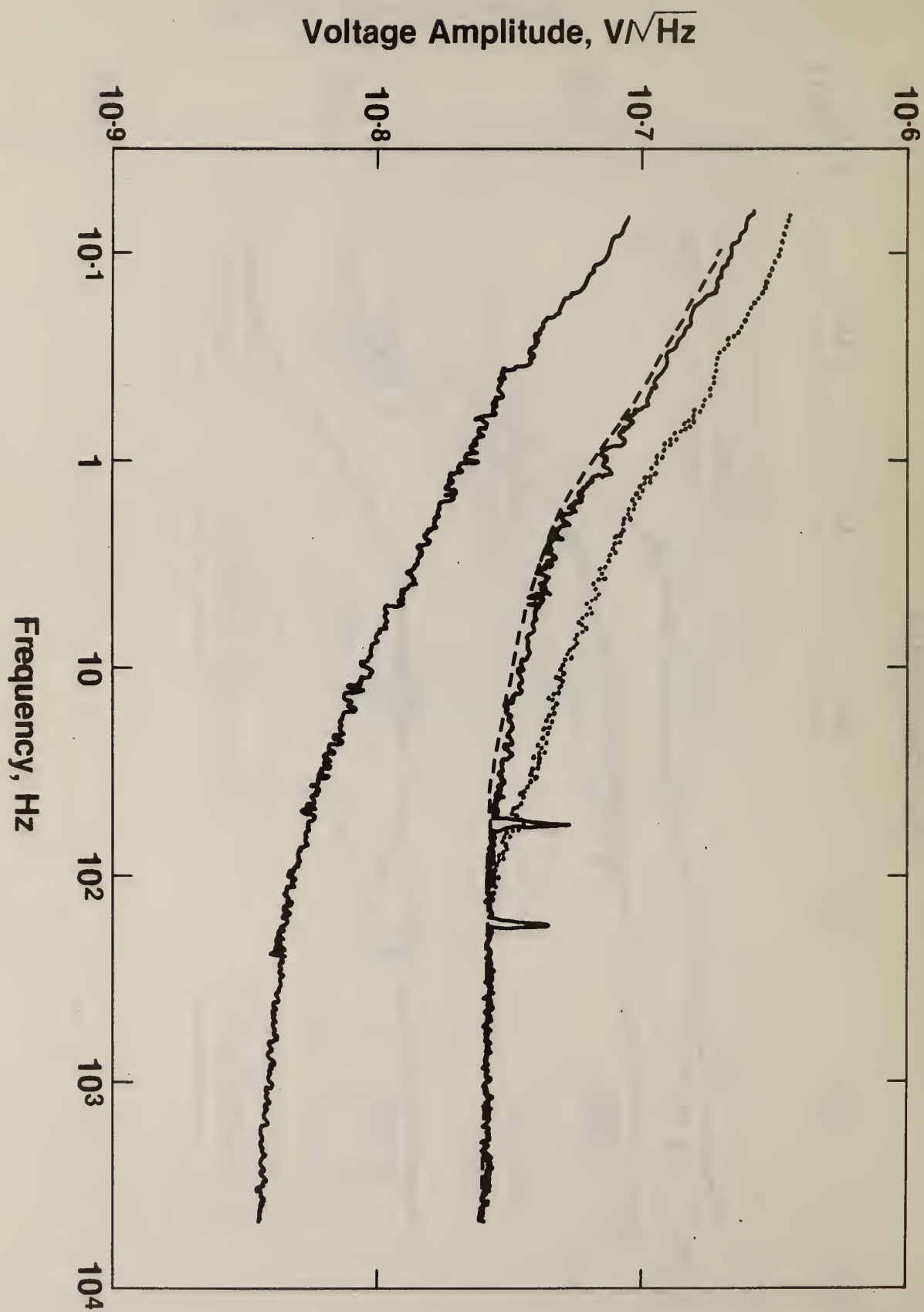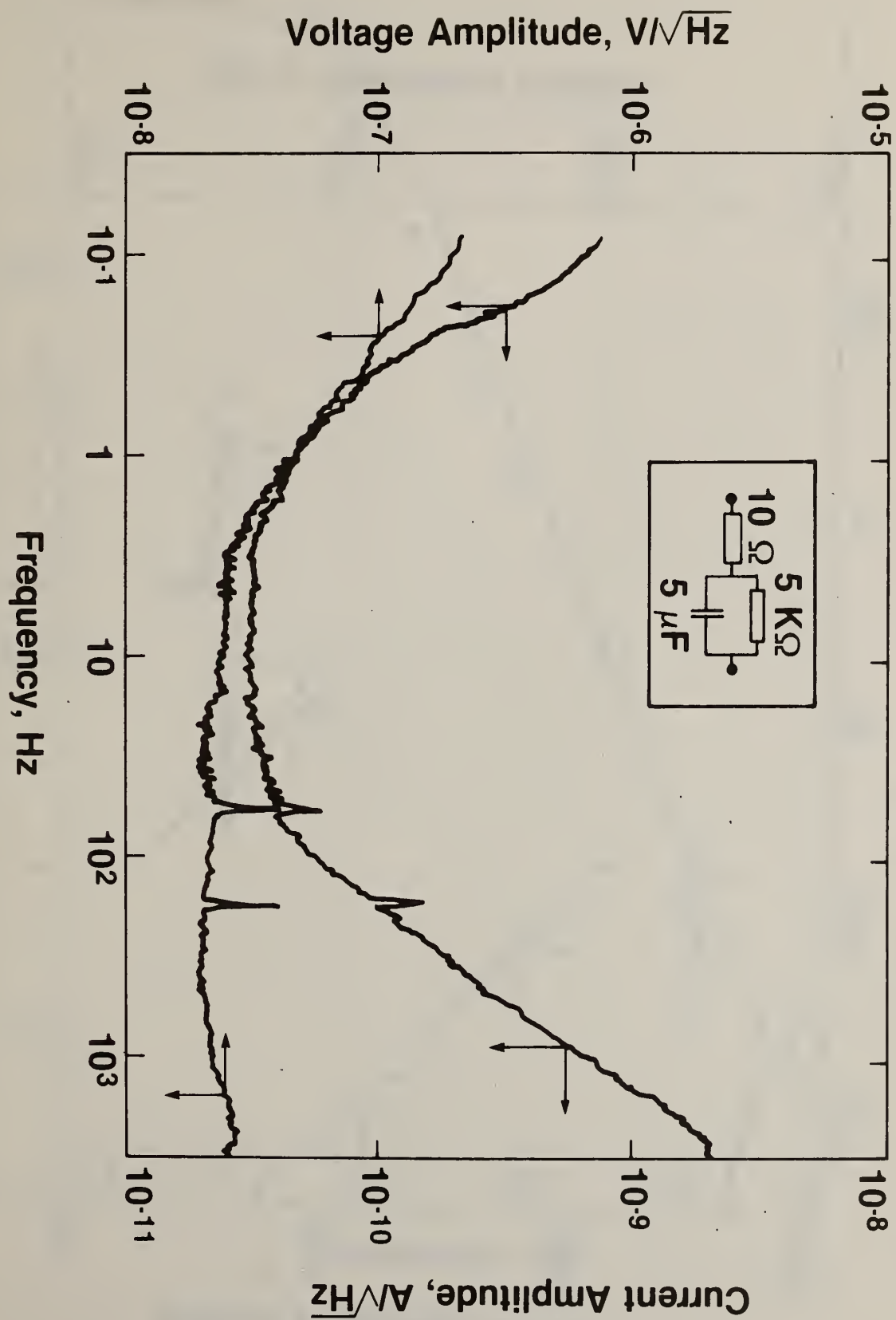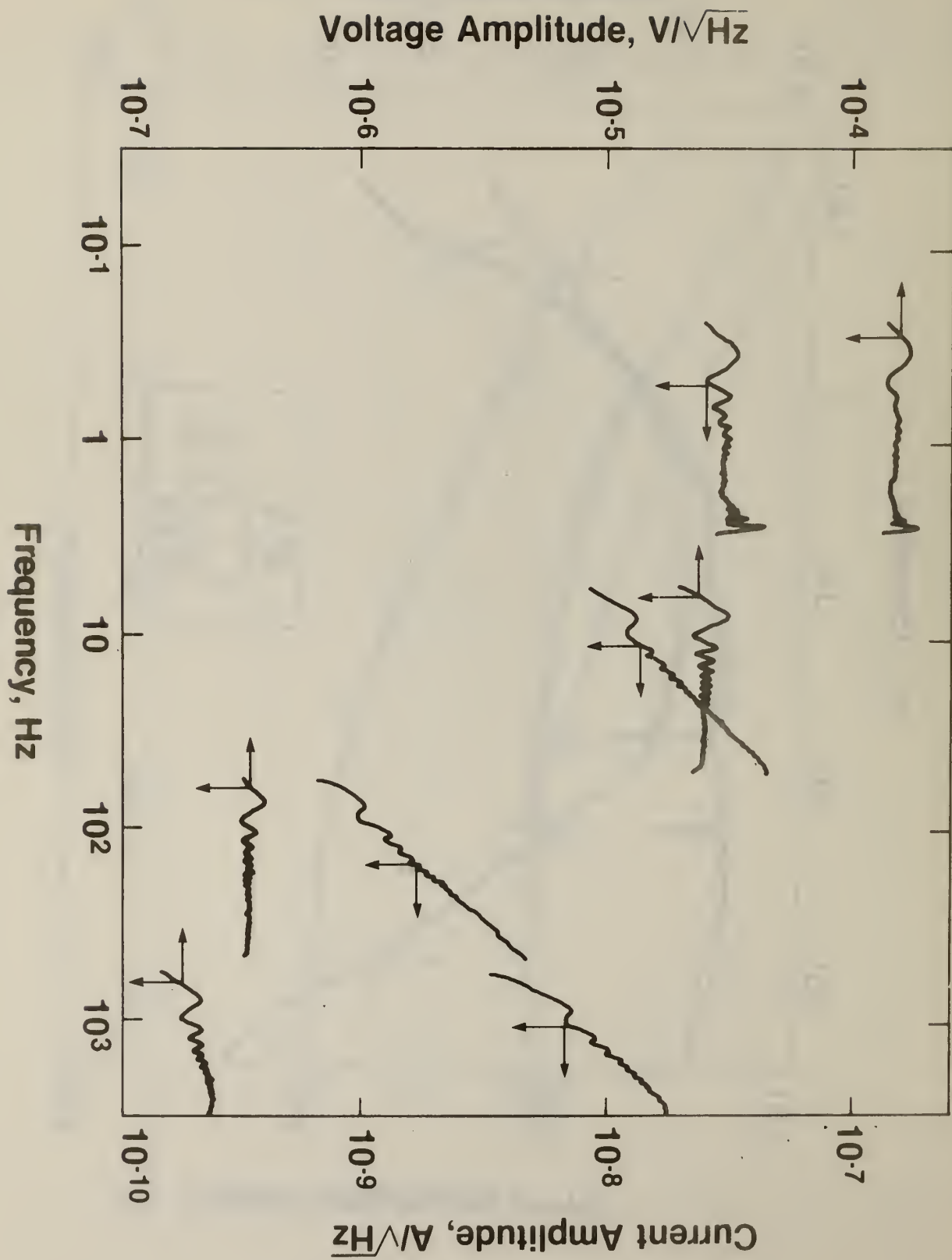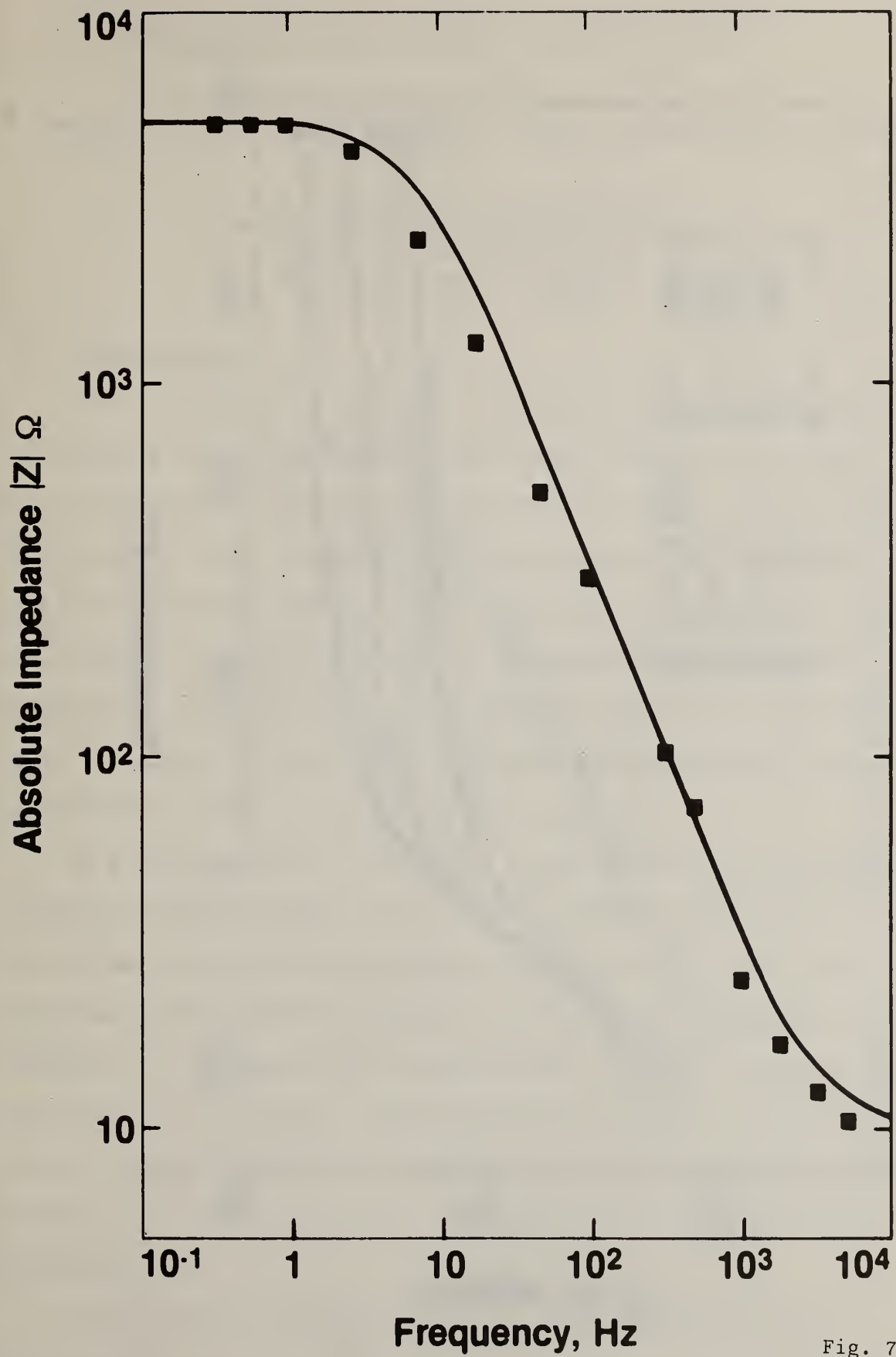
Fig. 1

Fig. 2

Fig. 3

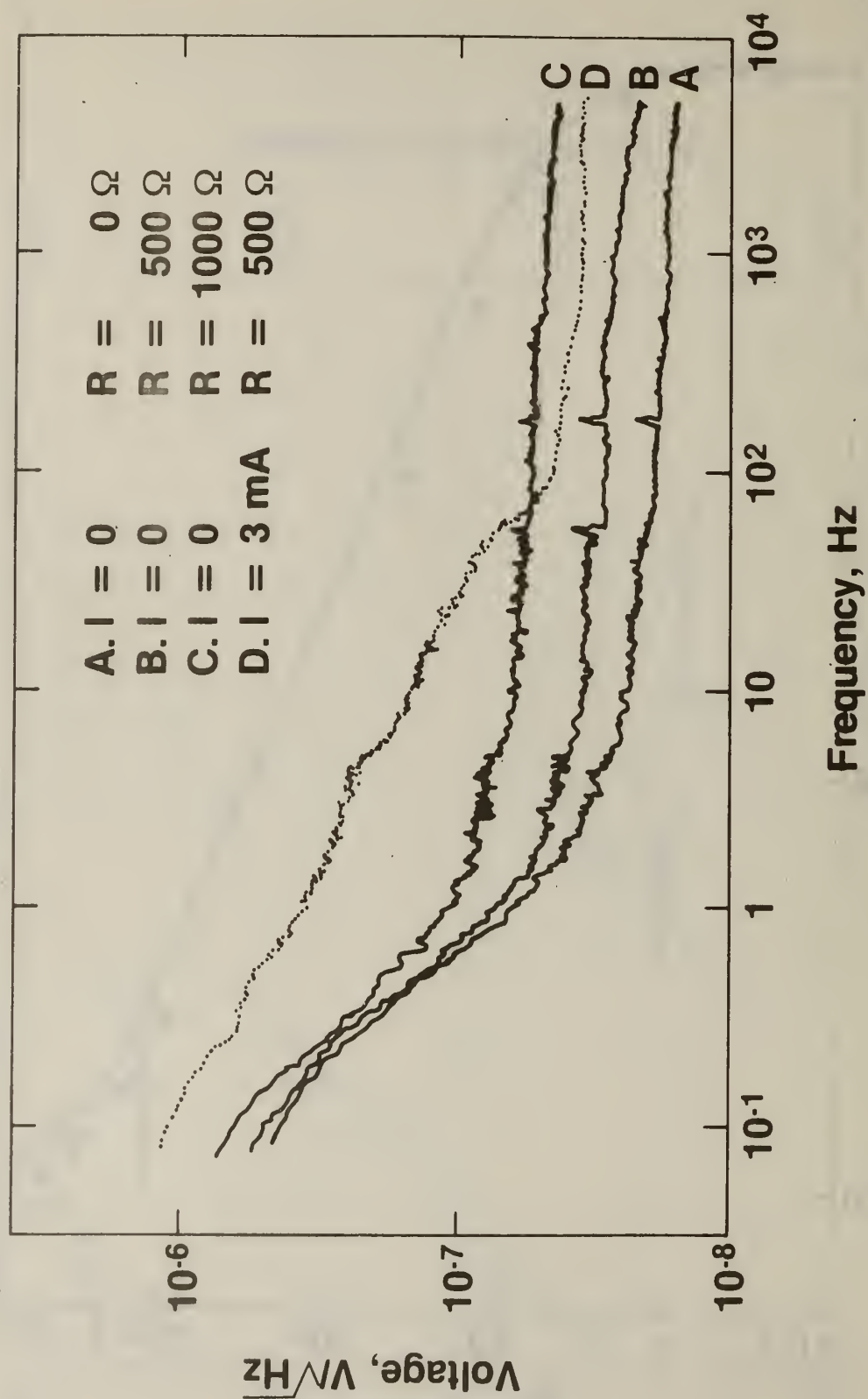Fig. 4

Fig. 5

Fig. 6

Fig. 7

Fig. 8

Corrosion Enhancement Due to Large Voltage Modulations.
Frequency Analysis of the Response of Electrodes Under Charge-Transfer
Control.

U. Bertocci and J. L. Mullen
Chemical Stability & Corrosion Division
Center for Material Science
National Bureau of Standards
Washington, D. C. 20234

1.   Introduction

In a large number of practical situations metallic structures are
subjected to alternating voltages which cause currents to flow into
ionic conductors in contact with them, the most common of which is soil.
These currents might flow because of failure of insulation, but there
are also cases where the metals are exposed without protection. There
is, therefore, a substantial interest in understanding what role an
alternating signal can play in affecting the kinetics of an electrode,
so as to be able to predict when and to what extent corrosion can be
caused by the effect of alternating currents. [1]

As a part of research carried out at NBS concerning the corrosion
of copper concentric neutral cables, the conditions under which ac
enhanced corrosion could be expected were examined, and, as a con-
sequence, a mathematical treatment was developed describing the current
response of an electrode under charge-transfer control to a large sinusoidal
modulation of the voltage. The possibility of measuring separately the
faradaic and the capacitative components of the current was also examined,
leading to the identification of the conditions necessary for such a
separation [2].

The theoretical treatment showed the potential usefulness of
frequency analysis for the recovery of information concerning the
mechanism and rate of the electrode reaction, as well as data concerning
the enhancement of the corrosion process.

In this paper the principal points of the mathematical treatment are briefly reviewed. The effects of ohmic drop error on current measurements are also discussed. Finally frequency analysis techniques are applied to an electrode under charge-transfer control and the experimental results are compared with the theoretical predictions.

2. Mathematical Analysis

a. Faradaic Current

We will present here in a simplified form some of the results of the analysis which has been given in detail elsewhere [2]. For an electrode under charge-transfer control, the partial anodic or cathodic current can be expressed as

$$i_{dc} = I_o \exp{(AE)} \qquad (1)$$

where I_o and A are positive for anodic processes and negative for cathodic ones. E is the electrode potential, taken with respect to some convenient reference value. As is well known, (1) can be used to express the total current in the so-called Tafel region, that is when the partial current of opposite sign is very small.

If the voltage is sinusoidally modulated, so that

$$E = E_o + V\sin{\omega t} \qquad (2)$$

the expression for the faradaic current can be obtained, and by harmonic analysis the current can be separated into a constant (or dc as customarily called) component and into the various harmonics (of angular frequency ω, 2ω, . . . $n\omega$) of the modulating signal.

It can be shown that the amplitude coefficients of each of these components can be expressed in the form

$$i_{f,n} = I_o \exp{(AE_o)} \cdot F_n{(A,V)} \qquad (3)$$

which can be rewritten as

$$i_{f,n} = i_{dc}^* F_n{(A,V)} \qquad (4)$$

-2-

because, in the absence of a modulating signal, (2) becomes $E = E_o$ and therefore

$$i^*_{dc} = I_o \exp (AE_o) \qquad (5)$$

Introduction of (5) into (3) gives (4). The r.m.s. value of each of these sinusoidal components of the faradaic current is

$$(i_{f,n})_{rms} = \sqrt{\frac{(i_{f,n})^2}{2}} \qquad (6)$$

Eq. (4) shows that every frequency component of the faradaic current is proportional to the current in the absence of modulation i^*_{dc} multiplied by a coefficient whose value depends only on the kinetic parameter A (which determines the Tafel slope) and on the amplitude V of the sinusoidal modulation. The index n indicates the order of the harmonics, with zero designating the dc term. An obvious consequence of (4) is that all frequency components of the faradaic current, when plotted against the electrode potential E_o on a semilogarithmic scale, will exhibit the same Tafel slope as i^*_{dc}.

Additional information can be derived from the analysis of the phase relationships among the various current components. It can be shown that the components of the faradaic current of odd order (ω, 3ω, 5ω, . . .) bear alternately a 0 or $\pm \pi$ phase relationship with the modulating signal, while the phase of the even (2ω, 4ω, 6ω, . . .) components is shifted by $\pm\pi/2$ with respect to the modulating signal.

Reflecting the fact that the relaxation times for charge-transfer are extremely short, the factors F_n do not depend on the frequency of the signal, and therefore, the amplitude of all the current components is independent of the frequency. It can also be shown that F_o, the factor for the d.c. component of the faradaic current, is always greater than 1, so that a sinusoidal modulation of the voltage produces a rectified current that increases the rate of the electrode reaction.

As it is well known, the coefficient A is related to the Tafel slope b by the equation $A = \dfrac{\ln 10}{b}$. Therefore, since the factors F_n depend on A, if the anodic and cathodic reactions are associated with different Tafel slopes, their intersection, which determines the potential at which no dc current flows, will be shifted by the application of a sinusoidal modulation.

b.   Capacitative Current

For the analysis of the effect of an alternating voltage on an electrode it is necessary to consider the capacitative current i_c as well, since the electrode-solution interface constitutes a circuit with a capacitance and resistance in parallel. Therefore, the total current is

$$i = i_f + i_c \qquad\qquad (7)$$

The electrode capacitance in general varies with potential and it is strongly affected by adsorption phenomena, some of which can be rather slow, so that relaxation times can be large compared with variations in electrode potential.

However, in many instances the capacitance is only a function of potential, and often its variations can be relatively minor within certain potential ranges. The analysis has shown that if the electrode capacitance is a function of potential only, a sinusoidal modulation as in (2) does not cause any dc component of i_c. Moreover, it can be shown that its odd harmonic components (ω, 3ω, 5ω, . . .) are shifted by $\pm\pi/2$ with respect to the modulating signal, while the even components are shifted by 0 or π.

Comparison of these phase-shifts with those of the faradaic current shows that when the hypotheses employed in this analysis are applicable, it is possible to separate the faradaic and capacitative components of the current, provided that phase information is available.

c.   Ohmic drop effects

The theoretical treatment assumes that no ohmic drop error R_Ω is included into the circuit to which the voltage given by (2) is applied. In practice, however, R_Ω is never zero and this can affect substantially the values measured experimentally, causing a frequency dependence when, according to the theory, none should be found. A careful analysis of the effects of the ohmic drop is therefore necessary in order to examine to what extent it can explain some apparent discrepancies between theoretical predictions and experimental results.

The response of the working electrode to the voltage signal E given by (2) can be described, neglecting the phase relationships between different frequency components, by the equivalent circuit of Fig. 1, to which a new voltage signal $E' = E_0 + V\sum_1^\infty{}_k \sin(k\omega t)$ is applied. Each frequency component of the current is then separated by a tuned filter F before dividing into a faradaic component through a resistor R_n (with n indicating the order of the harmonics) and a capacitative component through a capacitance C_n. The constant, or dc, component obviously has no capacitative counterpart. All current components will flow through the ohmic drop resistor R.

The value of the resistances R_n can be obtained from (3), since R_n is the derivative of E_0 with respect to $i_{f,n}$

$$R_n = \frac{dE_0}{di_{f,n}} = \frac{1}{Ai_{f,n}} = \frac{1}{AI_0 \exp(AE_0)F_n(A,V)} = \frac{R_0^*}{F_n(A,V)} \qquad (7)$$

where R_0^* is the charge-transfer resistance for the electrode at the potential E_0 in the absence of sinusoidal voltage modulation.

The values of C_n depends on how the double layer capacitance varies with potential. Assuming that its variation in the range of potentials investigated is negligible,

$$C_1 = C_{d1} \qquad . \qquad (8)$$

while all other C_n, for $n > 1$, are equal to zero.

Experimental observations on the electrode employed for this work have shown that C_n for $n > 1$ are small and that equation (8) is a good approximation.

Once the values to be assigned to the components in the circuit of Fig. 1 are calculated, it is possible to calculate the in-phase and out-of-phase components of the current at angular frequency $n\omega$. Calling

$$\alpha = 1 + (n\omega C_n R_n)^2 \qquad (9)$$

$$\beta = R_\Omega (1 + [n\omega C_n R_n]^2) + R_n \qquad (10)$$

$$\delta = n\omega C_n R_n^2 \qquad (11)$$

we have

$$(i'_{n\omega})_{rms} = \frac{V}{\sqrt{2}} \frac{\alpha\beta}{\beta^2 + \delta^2} \qquad (12)$$

and

$$(i''_{n\omega})_{rms} = \frac{V}{\sqrt{2}} \frac{\alpha\delta}{\beta^2 + \delta^2} \qquad (13)$$

It is easy to show that if the ohmic drop resistance goes to zero (12) and (13) revert to the theoretical values: $(i_{n\omega})_{rms} = \frac{V}{\sqrt{2} R_n}$ and $(i''_{n\omega})_{rms} = \frac{n\omega C_n V}{\sqrt{2}}$.

It is also interesting to see what is the effect of varying the average electrode potential E_o, upon which, as shown by (7), R_n depends exponentially. At high overvoltages, that is for values of E_o such that the dc current density i^*_{dc} is large and R_n is small with respect to R_Ω, equations (12) and 13) become

$$\lim_{R_n \to o} (i'_{n\omega})_{rms} = \frac{V}{\sqrt{2} R_\Omega} \qquad (14)$$

and

$$\lim_{R_n \to 0} (i''_{n\omega})_{rms} = \lim_{R_n \to 0} \frac{n\omega C_n R_n^2 V}{\sqrt{2} R_\Omega} = 0 \tag{15}$$

The current becomes independent of R_n and is limited only by the ohmic drop resistance. On the other hand, when F_o is shifted to values where the current density is small, R_n becomes larger, so that $(n\omega C_n R_n)^2 \gg 1$. Then

$$\lim_{R_n \to \infty} (i'_{n\omega})_{rms} = \frac{V}{\sqrt{2}} \frac{(n\omega C_n)^2 R_\Omega}{[1+(n\omega C_n R_\Omega)^2]} \tag{16}$$

and

$$\lim_{R_n \to \infty} (i''_{n\omega})_{rms} = \frac{V}{\sqrt{2}} \frac{n\omega C_n}{[1+(n\omega C_n R_\Omega)^2]} \tag{17}$$

These current values are proportional to the admittance of a RC series circuit, where the resistance is the ohmic drop resistance R_Ω.

At both limits the in-phase current, instead of varying with E_o on a Tafel slope, becomes constant, depending only on the ohmic drop R_Ω. One of the effects of an ohmic drop error is that of introducing a phase-shift in the current so that the identity between faradaic current and in-phase component is no longer true. This also introduces an additional dependence of the current components on frequency which can be calculated from (12) and (13) by varying ω at constant E_o.

In the experimental part it will be shown that the effects of the ohmic drop resistance described here account well for the deviations from the theoretical behavior observed.

3. Experimental

    a. Purpose of the experimental work

The distortion of the faradaic current which leads to an increase of the dc current and can cause enhanced corrosion is not dependent on special conditions concerning the electrode surface, such as the presence of a rectifying semiconductor film, but is a consequence only of the non-linearity of the current-voltage characteristics of the electrode, and therefore, should be observed in a large class of electrode-electrolyte systems. The effect is graphically illustrated by the waveforms shown in Fig. 2, which are experimental recordings. The lower trace shows the sinusoidal voltage signal applied to the electrode, while the upper trace is the current response, showing the high degree of distortion which is the cause both of the rectification and of the appearance of harmonics of the modulating frequency.

The particular quantitative mathematical treatment employed here was developed for a specific case of kinetics, charge-transfer control, but should maintain a fair degree of applicability for the prediction of the behavior of electrodes having a more complex kinetics.

The main purpose of this work was that of verifying the validity of the mathematical model as quantitatively as possible. For this reason it was more convenient to choose an electrochemical system that was known to be under charge-transfer control over as wide a range of current densities as possible.

b.   Experimental Methods

The experiments aimed at testing the validity of the theoretical model have been carried out on the hydrogen evolution reaction. The electrode material was OFHC copper and the solution composition was 0.5 M Na_2SO_4 + 0.1 M H_2SO_4. By minimizing other cathodic reactions, in particular oxygen reduction by bubbling Ar in the cell, and favoring transport in solution by means of vigorous stirring, it was possible to

-8-

obtain a straight Tafel plot with a slope of 120 mV/decade over a potential range larger than 300 mV.

As a further test of the applicability to the electrode under study of the hypothesis used in the mathematical analysis the electrode impedance was measured by applying a very small (<2mV) modulating signal, about in the middle of the (dc) potential range where a straight Tafel slope was obtained. The results are given in Fig. 3, where the imaginary component Z" of the electrode impedance (for unit surface area) is plotted versus the real component Z'. The plot is approximately a semicircle, indicating that there is no detectable contribution of transport to the electrode kinetics. From the plot the ohmic drop error is found to be about $6 \Omega cm^2$, while the charge-transfer resistance is more than $400 \Omega \cdot cm^2$.

The circuit employed for the measurements is shown schematically in Fig. 4. Two voltages, a constant one (E_o of equation (2)) and a pure sinewave (of amplitude V), where higher harmonics had been minimized by filtering, were added and applied to the control voltage input of the potentiostat. A phase-sensitive lock-in amplifier measured the amplitude of the current both at frequency ω of the modulation, and at twice that frequency, each one divided into the component in phase and the component in quadrature with the modulating signal. By means of the low pass filters the dc components of the voltage (E_o) and of the current (i_{dc}) could be recorded. With the filters switched off, the total current and voltage signal could be stored in the digital oscilloscope and successively reproduced on the X-Y recorder in the form illustrated in Fig. 2. Inputs and outputs of the measuring system, with the symbols used here are given in Table I.

In a few instances the current signal was fed to a 200 channels spectrum analyzer. In this way the amplitude of higher order harmonics could be obtained. However, all phase information was lost and only the absolute value of the current density of angular frequency $n\omega$

$$/i_{n\omega}/ = \sqrt{(i'_{n\omega})^2 + (i''_{n\omega})^2}$$

was obatined.

Results and Discussion

Current-potential measurements in the absence and in the presence of a modulating sinusoidal voltage were carried out. Fig. 5 shows the Tafel plot of i_{dc} in both conditions, as well as i'_ω, i''_ω and $i''_{2\omega}$. The solid lines represent the theoretical values for the various components of the faradaic current calculated from the experimental values of i^*_{dc} by means of equation (3). The factors $F_n(A,V)$ were calculated according to the formulae given in Ref. [2].

Linear Tafel behavior is shown by the dc current between -350 and -650 mV vs. NHE. When the modulating signal was applied, i_{dc} was larger than i^*_{dc} by a factor in good agreement with the theoretical one. The capacitative component i''_ω is largely independent of potential, indicating that the electrode capacitance remains nearly constant in the range studied. In agreement with this conclusion the term $i'_{2\omega}$ was found to be negliglibly small, suggesting that all higher harmonics of the current are almost exclusively faradaic.

The current signal was also examined with a spectrum analyzer for a value of E_o of -506mV vs. NHE and a modulation at 25 Hz of 35.4 mV r.m.s. The output values recorded during the spectrum analysis, as well as those obtained from the spectrum analyzer are reported for comparison in Table II, which also gives theoretical and experimental ratios between the various current components and the current density i^*_{dc} in the absence of modulation.

-10-

The values reported in Table II confirm that the capacitative currents at 2ω and 3ω are negligibly small, which is equivalent to say that the double layer capcitance varies very little in the electrode potential range (100 mV) covered by the modulation. The ratios are also in excellent agreement with the theory.

The spectrum is shown in Fig. 6, together with the spectrum obtained substituting a pure resistor for the cell, and passing a current of the order of 100μmA rms at 25 Hz. The harmonic distortion is extremely small: the amplitude of the 50 Hz harmonics is below the detection limits (about 10^{-7} A) and could be measured at about $4 \cdot 10^{-8}$A only after filtering out the large 25Hz signal. As Fig. 6 shows, the only spurious signal detected was a 60Hz peak at $5 \cdot 10^{-7}$A. The small peak at about 20 Hz which can be seen on the side of the 25 Hz peak of the electrode current is caused by the magnetic stirrer and could be eliminated by shutting it off.

Another Tafel plot, for a larger modulation of 88.3 mV r.m.s. (V = 125 mV) at 100 Hz, is shown in Fig. 7. The behavior of the dc component is close to the theoretical prediction over a range of about 300 mV, but significant distortions can be seen in the other frequency components.

The main reason for the deviation from the theoretical behavior is the ohmic drop error, as discussed in a preceding section. The deviations can be accounted for quantitatively, as shown in Fig. 8, which reproduces in detail part of Fig. 7, where the dc current density i^*_{dc} in the absence of modulation as well as the experimental values of the ac components of the current at the frequency of modulation ω are shown. The dashed lines represent the theoretical values of i'_ω (from Eq (3)) and of i''_ω (assuming a double layer capacitance of $52\mu/cm^2$).

-11-

in the absence of ohmic drop error. The dot-dashed lines are calculated from (12) and (13) for an ohmic drop resistance of 6Ω, the value obtained from the high frequency end of the semicircle in Fig. 3. As Fig. 8 shows, the experimental values fall quite close to the calculated lines. It should be pointed out that no empirical, adjustable parameters enter these calculations, once the Tafel slope for the current density in the absence of modulation, here shown as a solid line, is drawn through the experimental points.

Comparisions between the predictions about the amplitude of the faradaic components and the experimental values are summarized in Fig. 9. On it the experimental ratios of i_{dc}, i_ω' and $i_{2\omega}''$ to i_{dc}^*, as well as the theoretical lines are given. The agreement is very good for amplitudes V up to about 200 mV. Beyond that the current density caused by the modulation was less than predicted, because the electrode potential was being driven outside the linear Tafel range.

The effect of the frequency of the modulating signal has also been examined. Fig. 10 shows the ratio between the dc current i_{dc} and i_{dc}^*. The measurements were carried out at the same potential (E_0 = -456 mV vs. NHE) and at the same modulating amplitude (V = 100 mV), at frequencies ranging from 25 Hz to 10 kHz. As expected, the deviations caused by the ohmic drop error become quite large when the frequency is increased. The results shown pertain to two different electrodes having different ohmic drop resistance. With R_Ω = 6Ω, significant deviations from the theoretical behavior begin at about 300 Hz, while reducing R_Ω to about 0.8 increases the frequency of the beginning of the deviations by a factor of 10, to around 3 kHz. The effect of the ohmic drop error is even more pronounced on the current components at the modulation frequency.

Fig. 11 shows the values of i'_ω and i''_ω as a function of frequency, together with the lines calculated from (12) and (13), assuming a dc capacitance of $48\mu F$ and $R_\Omega = 0.7\Omega$. The agreement is satisfactory, indicating again that the greatest part of the deviations from the theoretical behavior is due to the ohmic drop error. It should be noted that, in its absence, i'_ω would be independent of frequency.

Conclusions

The experimental results presented here show conclusively that the mathematical analysis previously published [2] predicts accurately the current response to a sinusoidal voltage of an electrode under charge-transfer control, and can be used, therefore, as a basis for the understanding of the effect of ac on corrosion. It also shows that frequency analysis holds promise to be an important tool for the study of electrodes undergoing corrosion. Since the model employed does not involve special properties of the electrode surface in order to produce the effect which has been called faradaic rectification [3], it is to be expected that an increase in the corrosion rate due to ac leakage is a widespread phenomenon, with considerable practical implications.

References

[1] B. McCollum, G. H. Ahlborn, Tech. Pap. BST72 (1916)

K. G. Compton, INCRA Research Report Project 265 (1977)

D. T. Chin, T. W. Fu, G. F. Kamrowski, S. Pookote, 1978 NACE Research Conference, Houston (1978)

D. J. Nesslage, Paper N. 762, Corrosion 78, NACE (1978)

U. Bertocci, J. L. Mullen, Paper No. 242, Corrosion 79, NACE (1979).

[2] U. Bertocci, Corrosion, in press.

[3] B. Breyer, H. H. Bauer, "Alternating Current Polarography and Tensammetry", Interscience, New York (1963)

Table I

Input and Output Quantities

Input Quantities		
E_o	V	$\omega = 2\pi\nu$
d.c. component of electrode potential	Amplitude of modulating voltage	Angular frequency of modulating voltage

Output Quantities			
constant (d.c.) components		In phase with modulating voltage	$\pm\pi/2$ with respect to modulating voltage
i^*_{dc}	i_{dc}	i'_ω	i''_ω
current density for $V = o$	current density for $V > o$	current density at frequency ω	current density at frequency ω
		$i'_{2\omega}$	$i''_{2\omega}$
		current density at frequency 2ω	current density at frequency 2ω

Table II

Values obtained from circuit in Fig. 2 and from spectrum analyzer. $E_O = -506$ mV vs. N.H.E. $V = 35.4$ mV r.m.s. at 25 Hz. Current density values in $\mu A/cm^2$ r.m.s.

	i^*_{dc}	i_{dc}	i'_ω	i''_ω	$/i_\omega/$	$i'_{2\omega}$	$i''_{2\omega}$	$/i_{2\omega}/$	$/i_{3\omega}/$
Circuit	186	238	152	161	221	0.1	32	32	
Spectrum Analyzer					215			31	7.3

Ratios	i_{dc}/i^*_{dc}		i'_ω/i^*_{dc}		$i''_{2\omega}/i^*_{dc}$		$i'_{3\omega}/i^*_{dc}$	
Theoretical	1.24		0.76		0.176		0.0276	
Found	1.28		0.82		0.17		0.039	

Figure Captions·

Fig. 1.   Equivalent circuit of the electrode/electrolyte system under
large sinusoidal voltage modulation.

Fig. 2.   Voltage input signal and current response for Cu in 0.5M Na_2SO_4
+ 0.1M H_2SO_4.

Fig. 3.   Imaginary impedance Z" vs. real impedance Z' for Cu in
0.5M Na_2SO_4 + 0.1M H_2SO_4. E_o = -506 mV vs. NHE.
Frequency as parameter.

Fig. 4.   Schematic diagram of the circuit used for the measurements.

Fig. 5.   R.m.s. current density vs. electrode potential for copper
in 0.1M H_2SO_4 + 0.5M Na_2SO_4 with and without voltage modula-
tion (V = 50 mV, ν = 25 Hz). Solid lines are calculated values.

Fig. 6.   Solid line: Frequency spectrum of current density for a Cu
electrode in 0.1M H_2SO_4 + 0.5M Na_2SO_4. E_o = -506 mV vs.
NHE, V = 50 mV, ν = 25 Hz. Scale is log (r.m.s. A/cm^2)
vs. Hz. Average over 128 spectra. Dotted line: spectrum
of current through resistor. Scale is log (r.m.s. A) vs.
Hz. Average over 128 spectra.

Fig. 7.   R.m.s. current density vs. electrode potential for Cu in
0.1M H_2SO_4 + 0.5M Na_2SO_4, with and without voltage modula-
tion (V = 125 mV, ν = 100 Hz). Solid lines are calculated values.

Fig. 8.   Current density in the absence of modulation i_{dc}^*, and in-phase
(i_ω') and out of phase (i_ω'') components of the current density
at the modulation frequency (ν = 100 Hz). Dashed lines cal-
culated without ohmic drop (Equivalent circuit shown in inset
A). Dash-dot lines calculated with an ohmic drop error of
6Ω (Equivalent circuit shown in inset B).

Fig. 9.   Ratio between various components of the faradaic current and d.c. current in the absence of modulation $i_{dc}^{\star}$, as a function of the amplitude of modulation. $Cu/H_2SO_4 + Na_2SO_4$. $E_0 = -506$ mV vs. NHE_1 = 103.3 Hz.

Fig. 10 Ratio between dc current in the absence and in the presence of modulation, as a function of frequency for two values of the ohmic drop resistance. $Cu/H_2SO_4 + Na_2SO_4$. $E_0 = -456$ mV vs. NHE, $\nu = 100$ mV. Solid line indicates theoretical value.

Fig. 11 In-phase (i_ω') and out-of-phase (i_ω'') components of the current density as a function of the frequency of modulation. Constant amplitude V = 100 mV. Solid lines are calculated for $R_\Omega = 0.7\Omega$ and $C = 48\mu F/cm^2$.
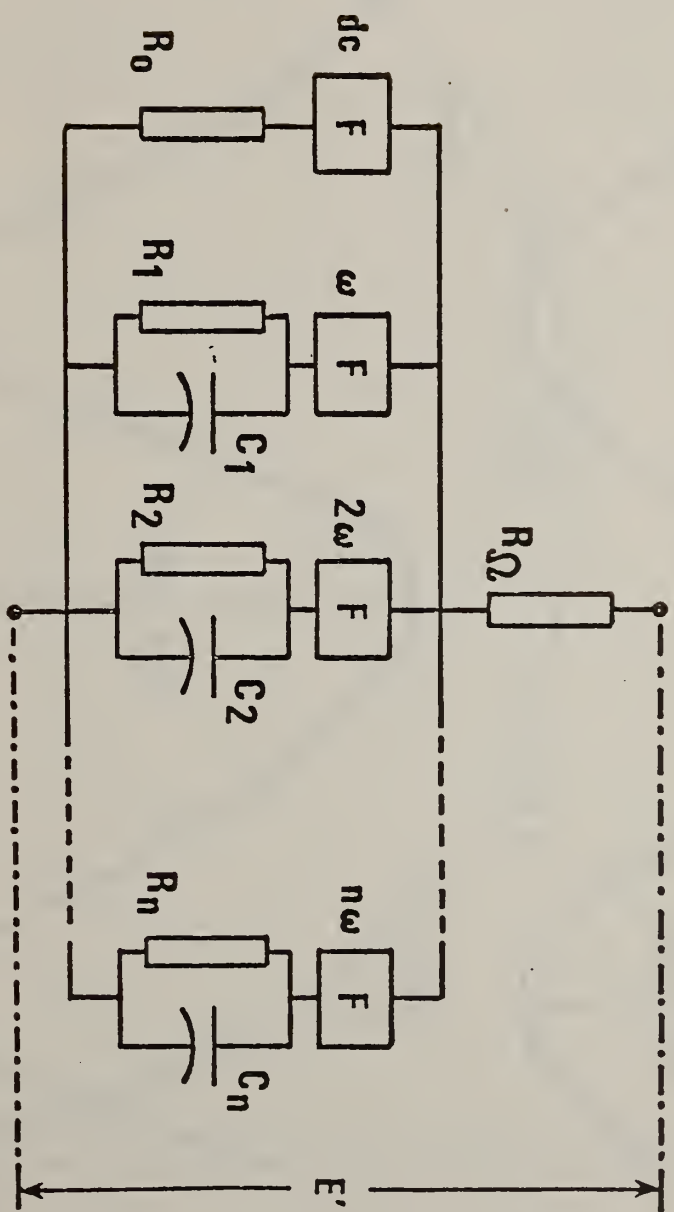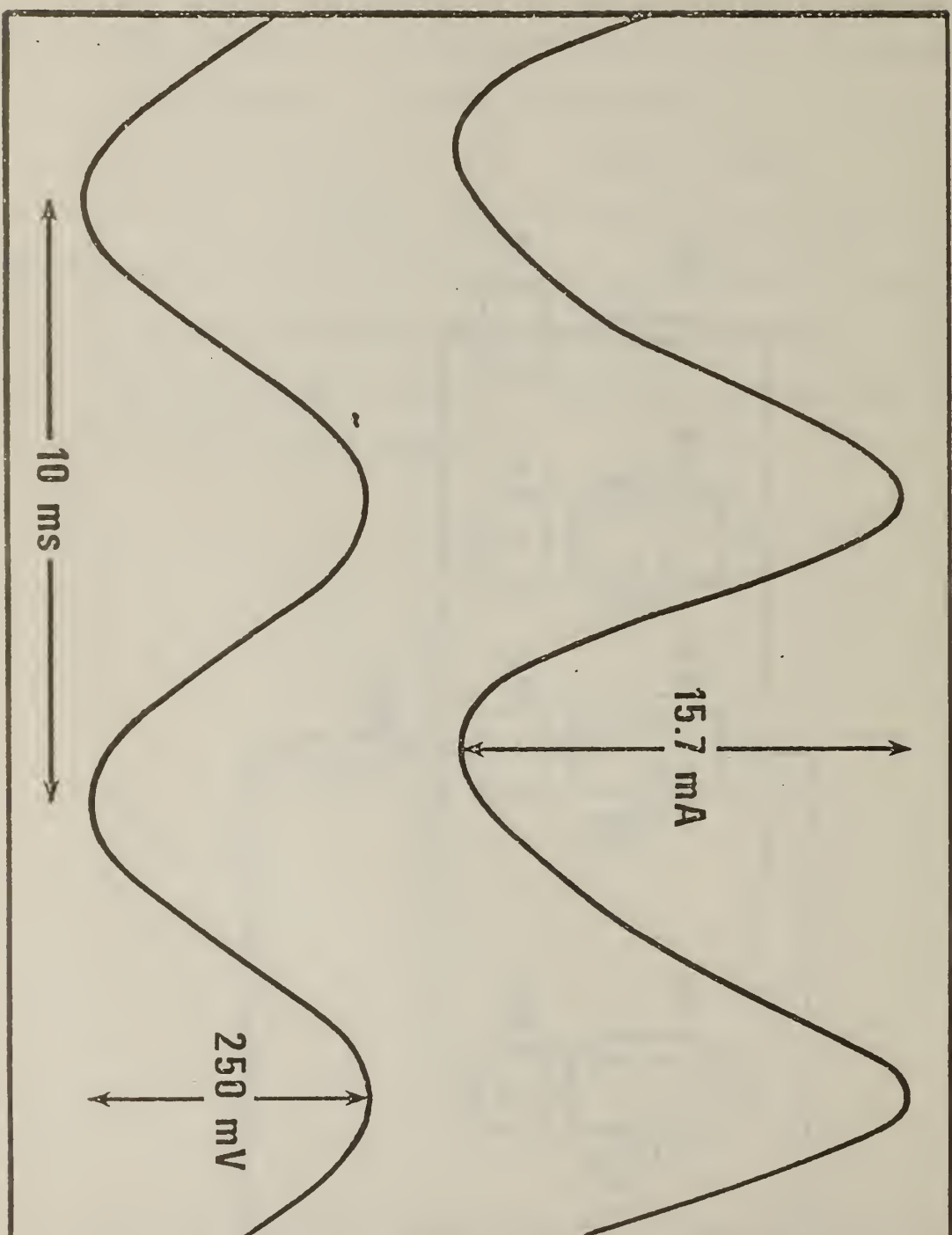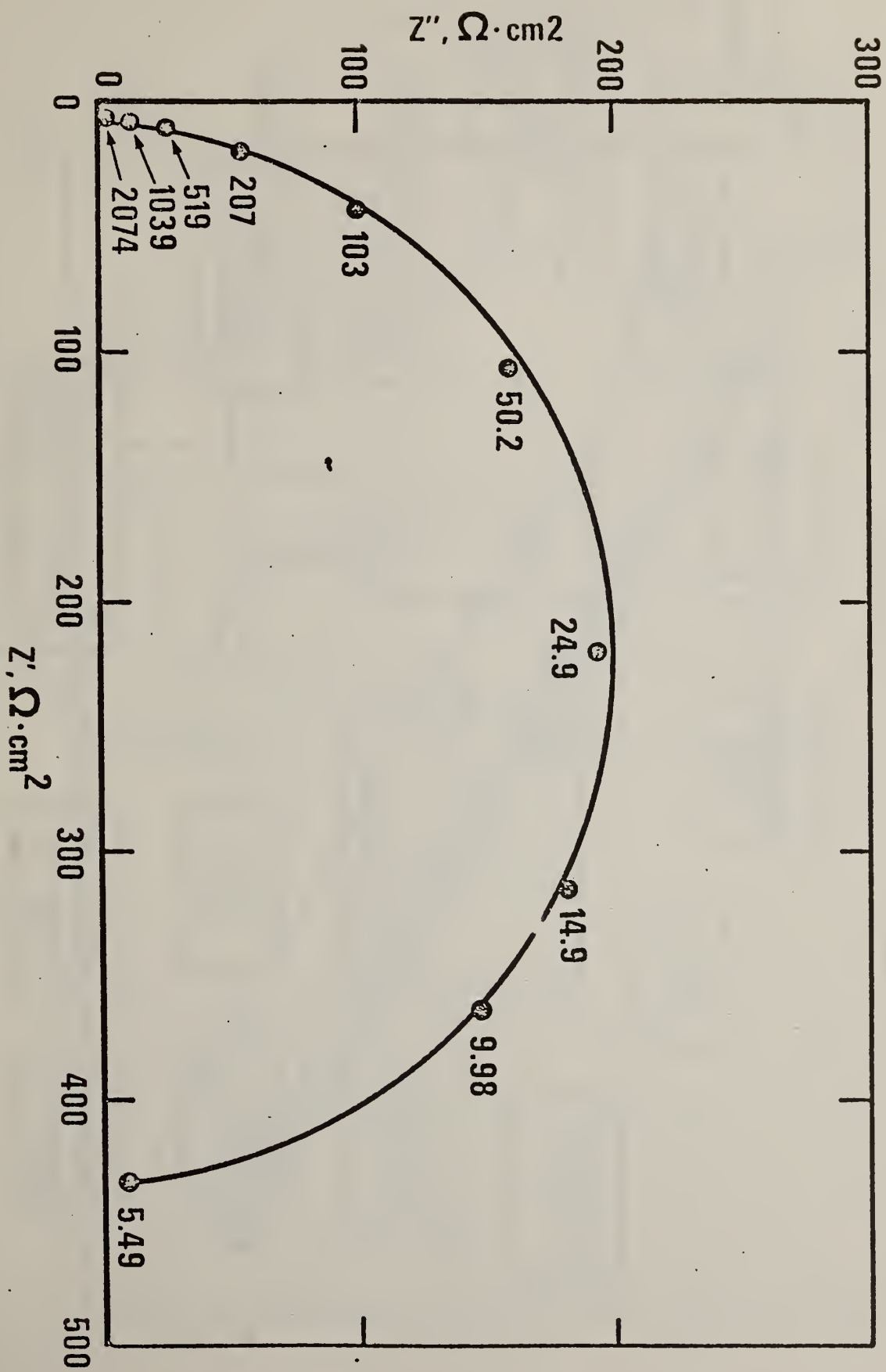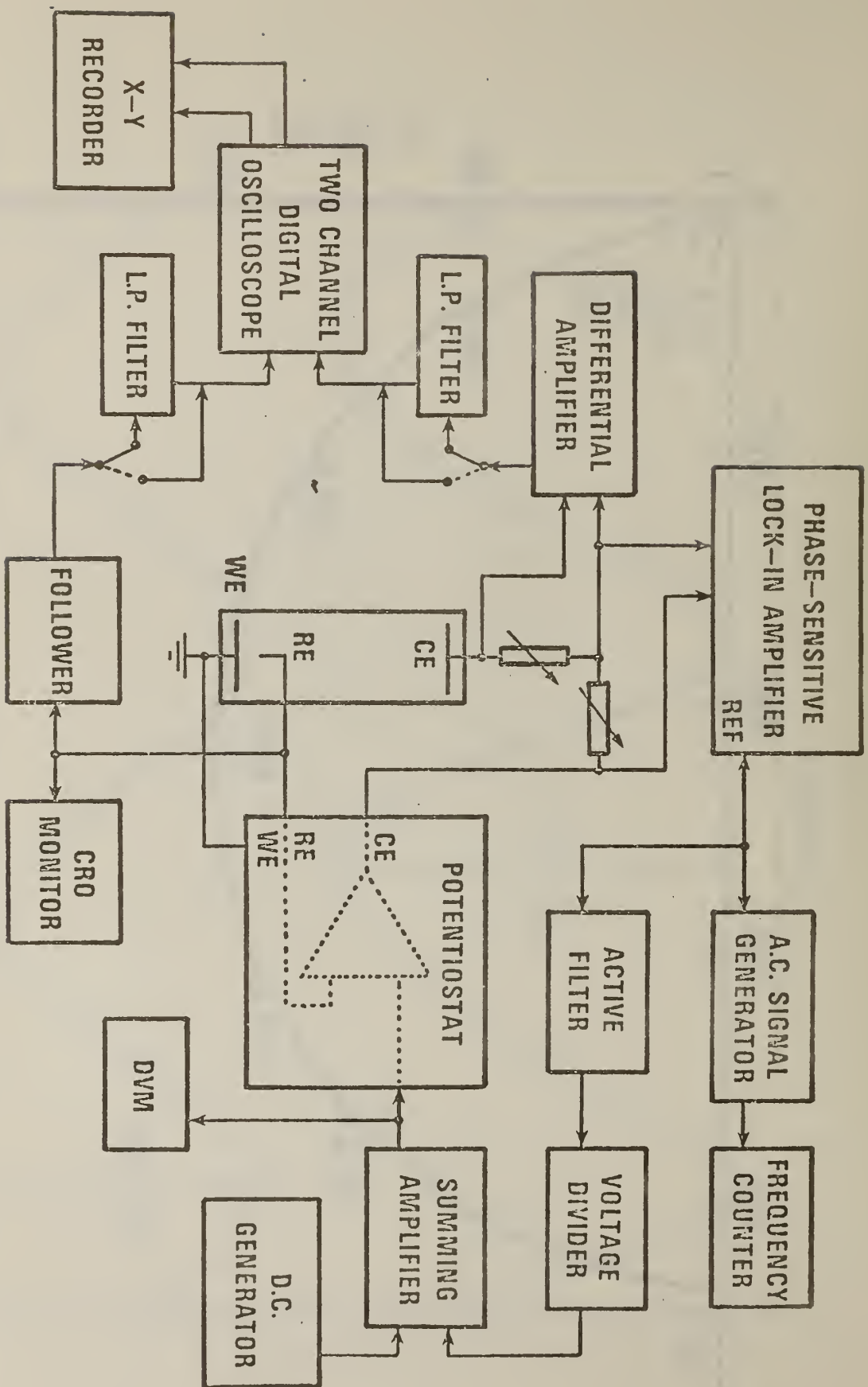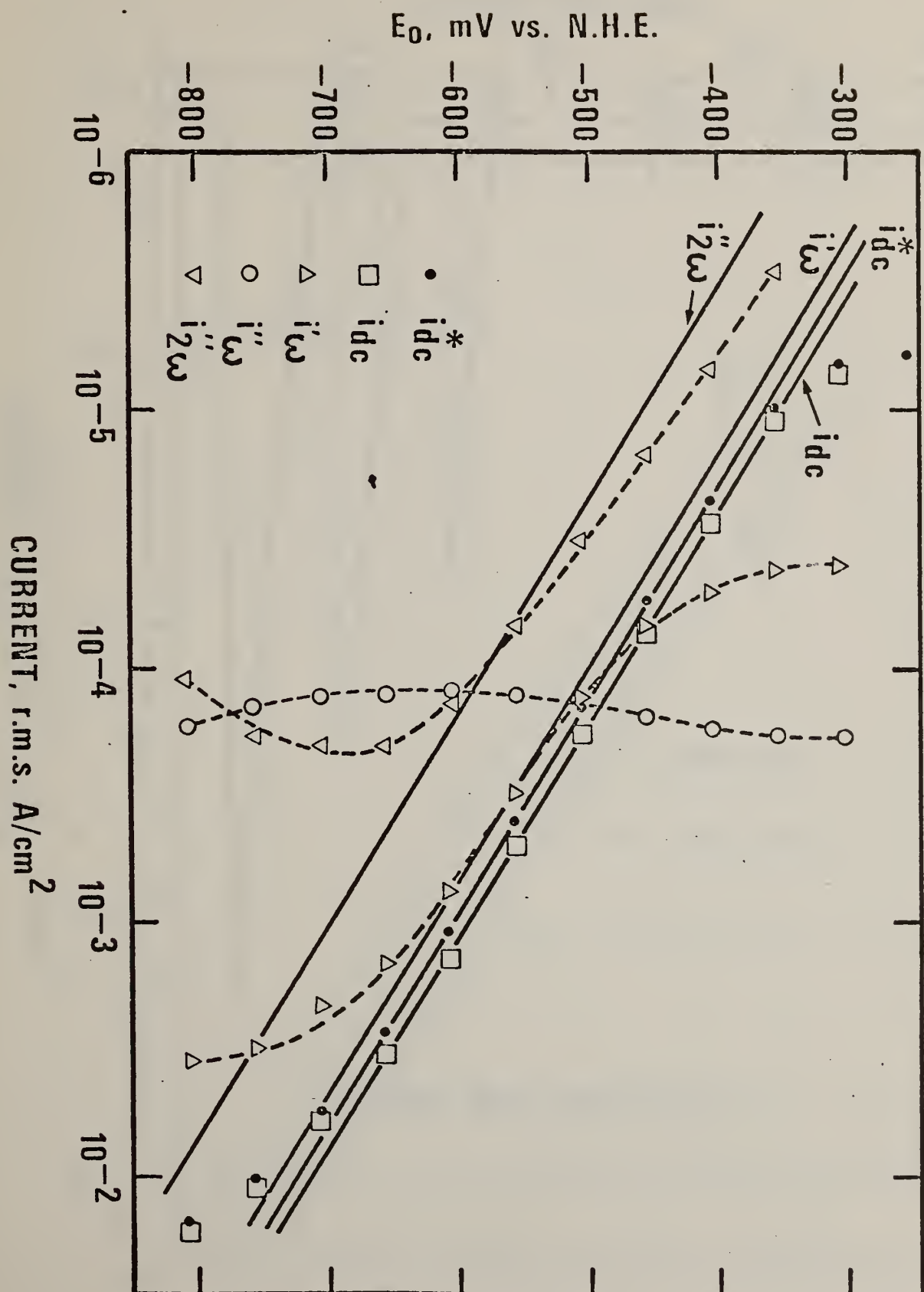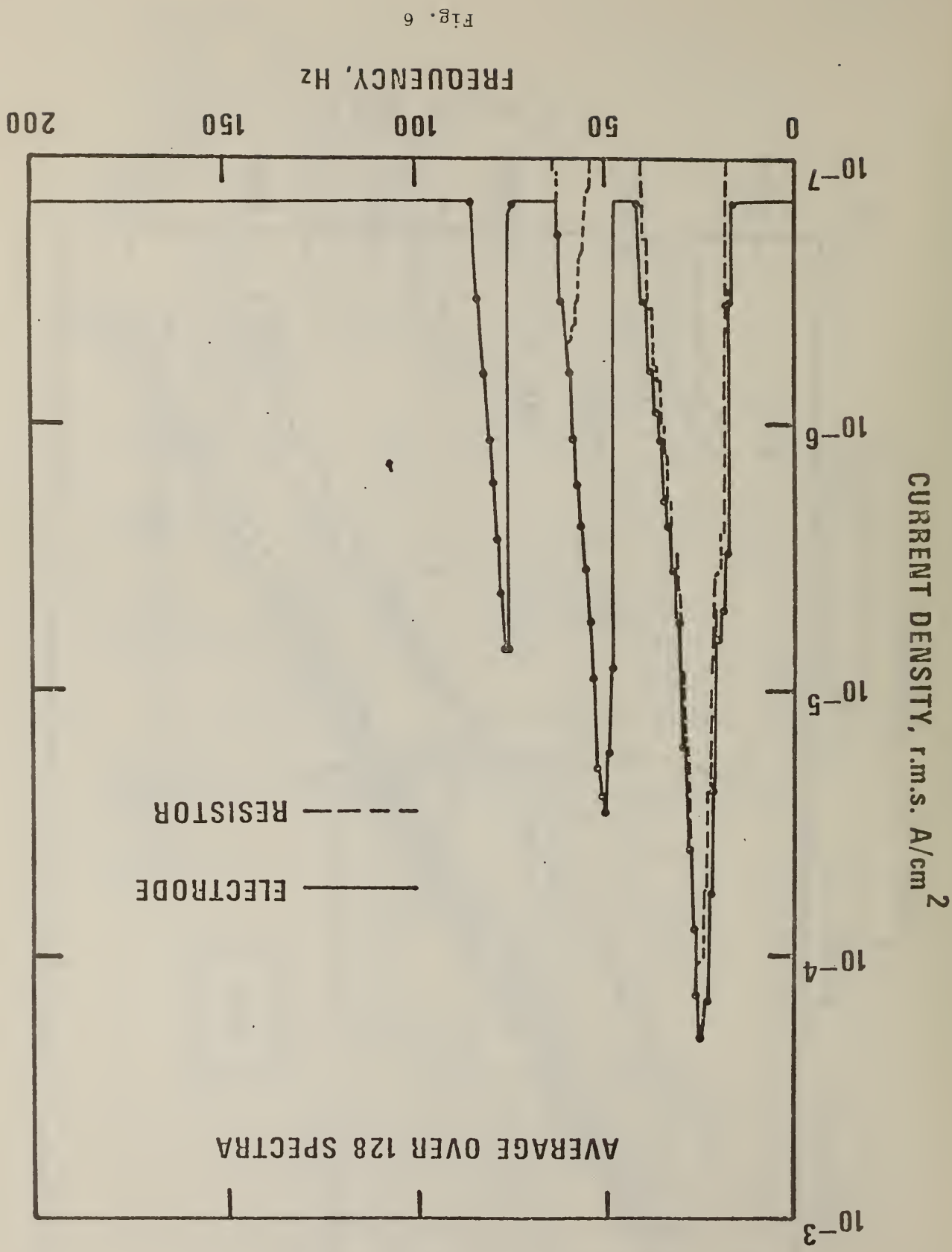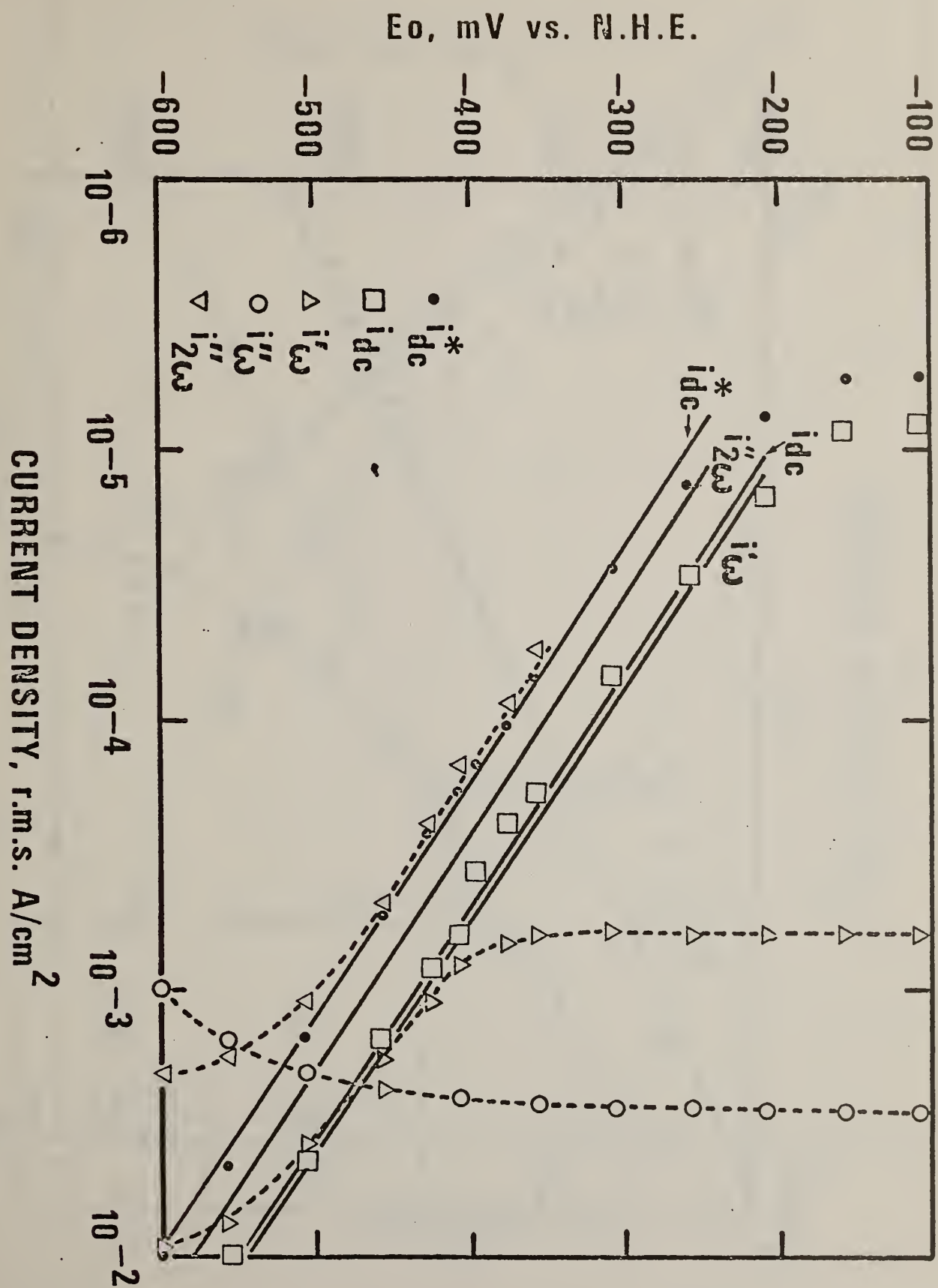
Fig. 1

Fig. 2

Fig. 3

Fig. 4
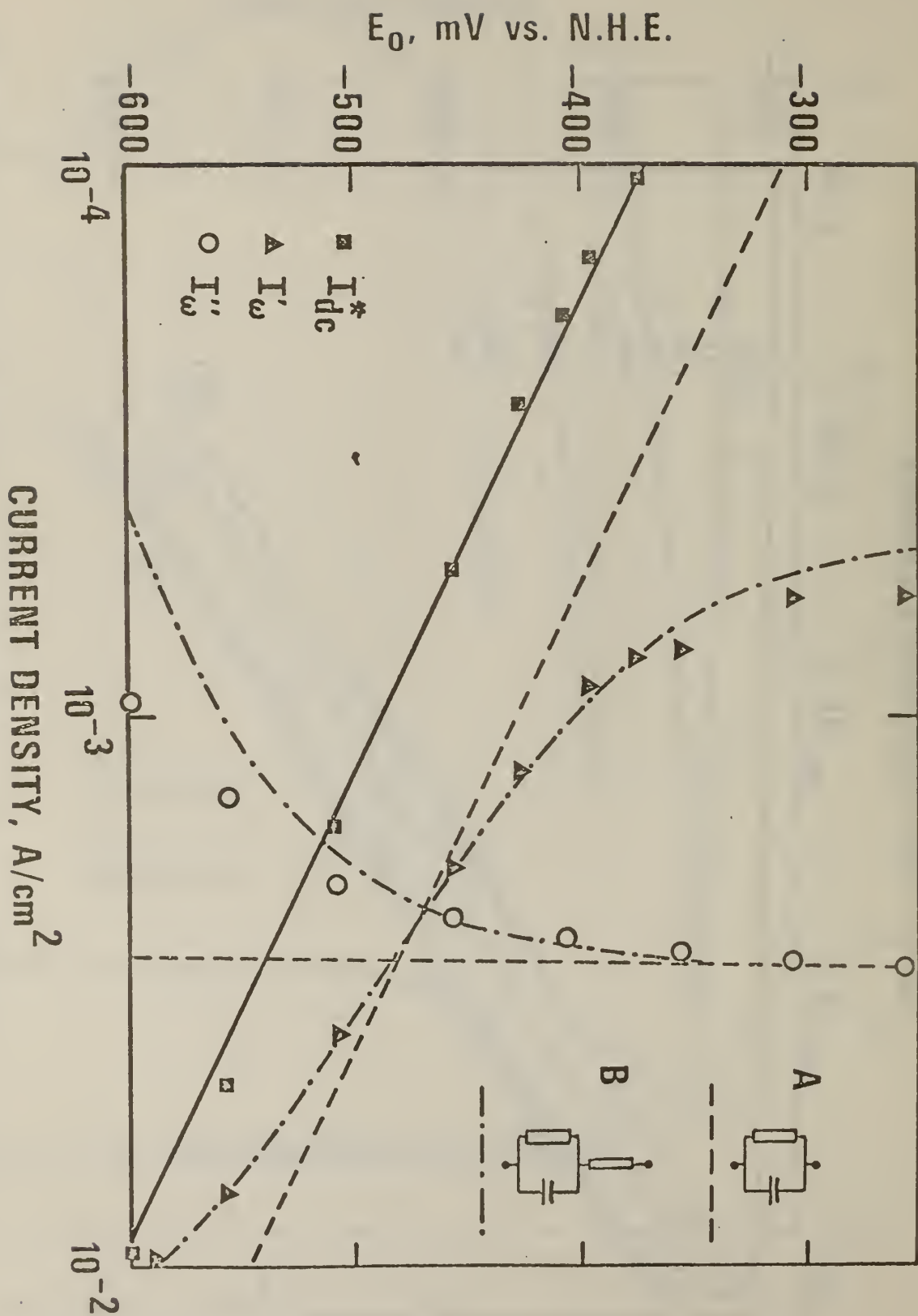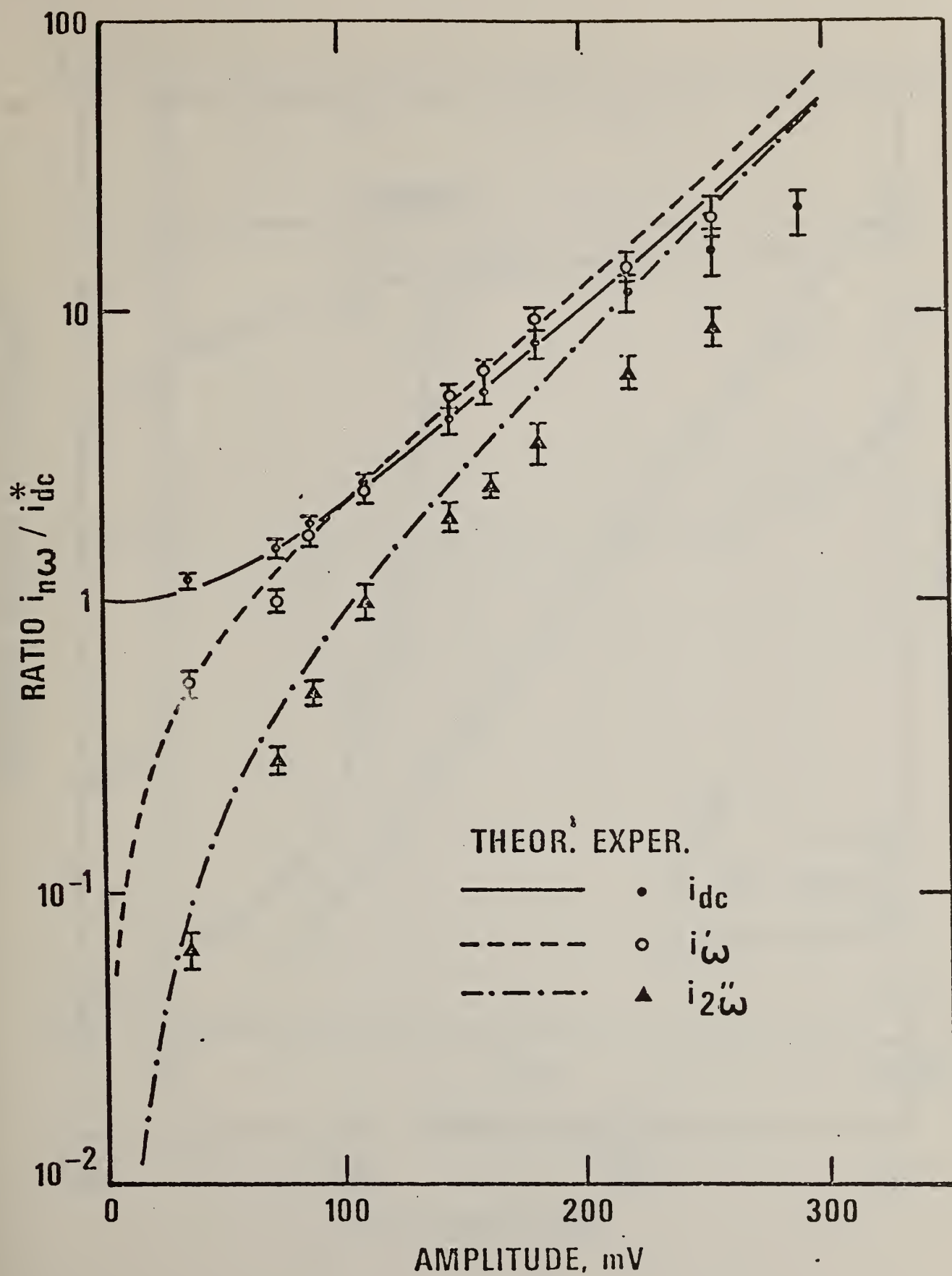
Fig. 5

Fig. 6

Fig. 7

Fig. 8

Fig. 9
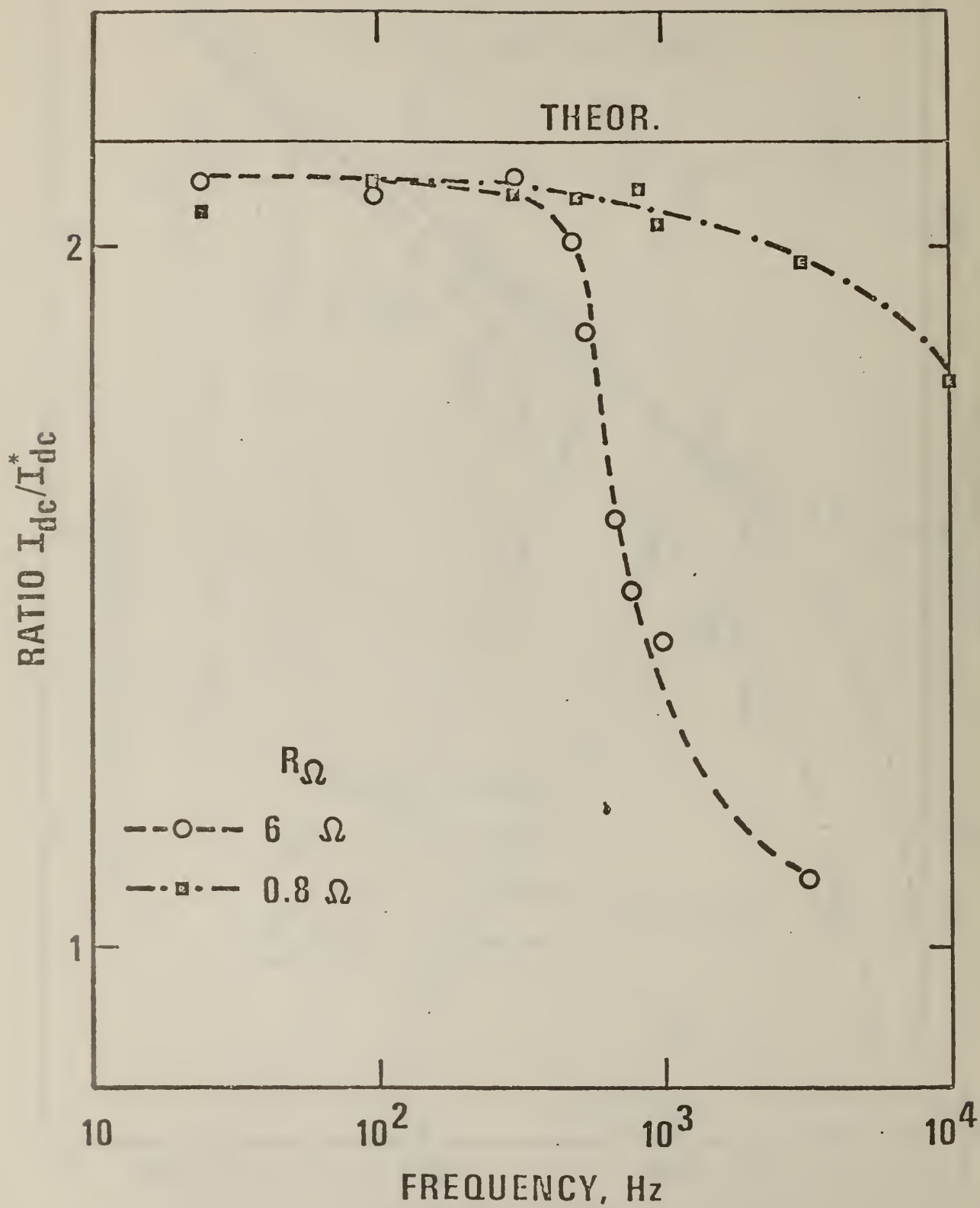
Fig. 10
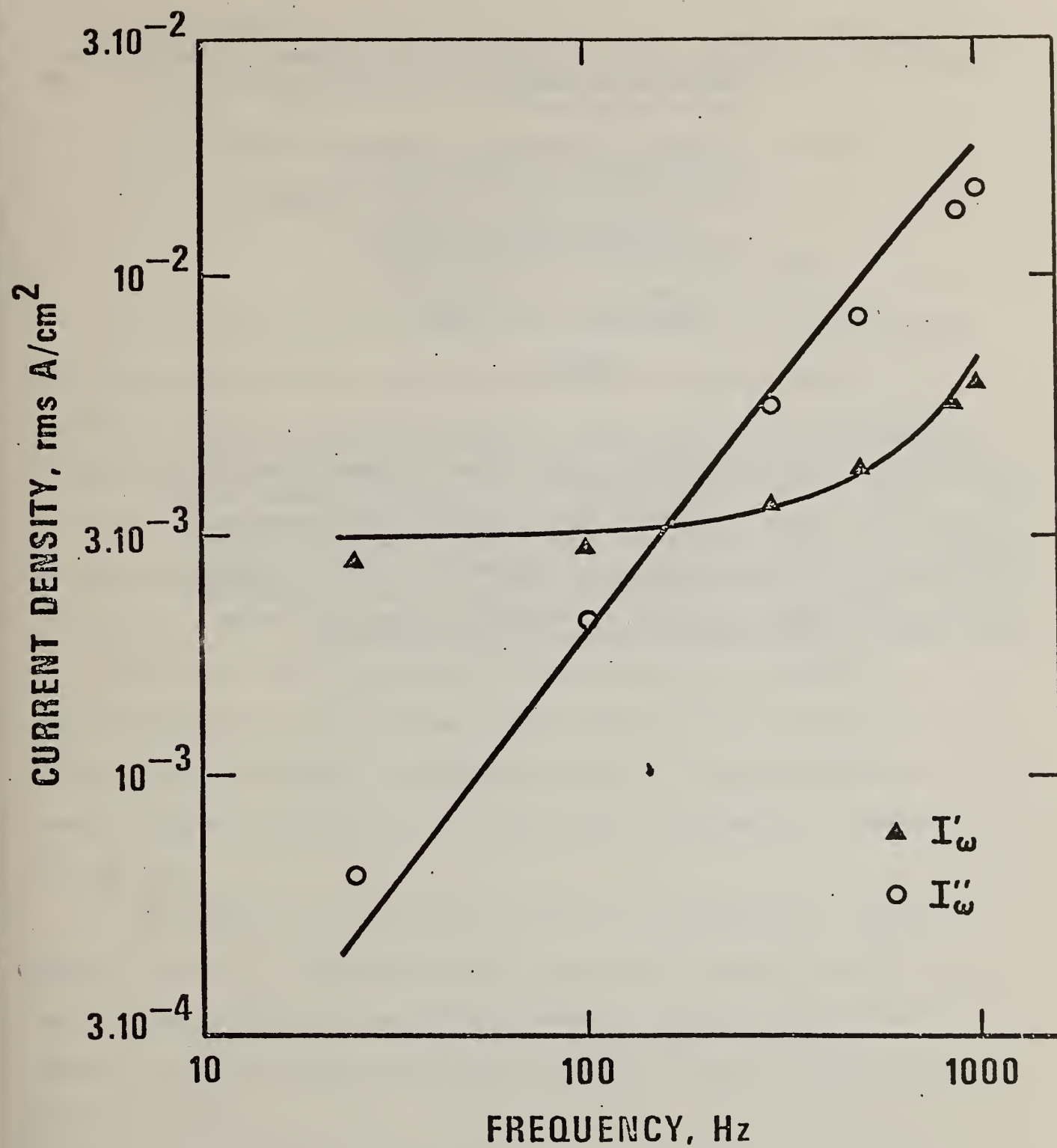
Fig. 11

Studies of Passive Film Breakdown by Detection and
Analysis of Electrochemical Noise

U. Bertocci and J. Kruger
National Measurement Laboratory
Chemical Stability and Corrosion Division
National Bureau of Standards
Washington, DC 20234

ABSTRACT

Random fluctuations in the passive current of electrodes under
potentiostatic conditions have been measured on aluminum in boric acid:
borate solution and on a Fe-Cr-Ni alloy, both in the amorphous and in
the crystalline state, in sulfuric acid. The onset of pitting can be
detected by the large increase in current noise. The noise level is
different in the amorphous and crystalline Fe-Cr-Ni alloy, indicating
that the breakdown of the passive film differs in the two conditions.
The experimental aspects involved in carrying out meaningful noise
measurements in electrochemical systems are also discussed.

Studies of Passive Film Breakdown by Detection and Analysis of Electrochemical Noise

U. Bertocci and J. Kruger
National Measurement Laboratory
Chemical Stability and Corrosion Division
National Bureau of Standards
Washington, DC 20234

The processes of passive film breakdown and healing are of fundamental importance in the understanding of the initiation and development of localized corrosion. A new approach which shows promise of producing new insights into these processes, is that of detecting and analyzing the fluctuations from the average values of the current and electrode potential. This has been recognized by a number of workers who have employed various techniques for the study of what is currently called "electrochemical noise" [1].

Use of this kind of measurement to study passive film breakdown acquires additional interest because there have been recent suggestions [2] that the event leading to breakdown consists of a dynamic breakdown-repair stochastic process which manifests itself as potential and current fluctuations.

In the present work, we report on some of the experimental aspects that are involved in making meaningful measurements, describe the use of these measurements to study metals covered by passive films and the changes in the signal that result when the passive film breaks down and pitting occurs.

EXPERIMENTAL APPROACH

Of the various methods of processing stationary or quasistationary random signals, the one employed in our laboratory has been that of transforming the output of the electrochemical cell in the frequency domain by means of a spectrum analyzer. Details of the experimental circuitry are given elsewhere [3].

As far as the conditions of the electrochemical cell are concerned, two main modes can be employed, that is the observation of the voltage fluctuations under galvanostatic conditions and the observation of the current fluctuations under potentiostatic conditions. Both methods have some specific advantages and the detection of the increases in noise level associated with pitting can be done in either mode. An example of noise levels under galvanostatic conditions is shown in Fig. 1, which gives the voltage spectra for Fe in borate buffer with a small concentration of chloride added. The noise level is larger when the potential of the electrode is above the pitting potential. The potentiostatic method, however, is preferable in most cases where passive films are being examined, because it maintains definite energy conditions at the electrode/electrolyte interface. The main problem, however, is to carry out the measurements so as to introduce the lowest possible level of instrumental noise maintaining the largest practicable bandwith. For this purpose, a battery-operated low-noise potentiostat has been built at the NBS. Its specific characteristics have been given elsewhere [4]. For the present purposes, its performance can be summarized as follows: the noise in the control voltage is about

10^{-7} V/$\sqrt{Hz}$ at 0.3 Hz and about constant at 2.5 10^{-8} V/$\sqrt{Hz}$ from 10 Hz to about 2000 Hz; the useful bandwith extends from 0.1 Hz to 2 kHz; the instrumental noise introduced by the ac amplifier which is driven by the current fluctuations at the working electorde is equivalent to about $3 \cdot 10^{-11}$ A/$\sqrt{Hz}$.

With the characteristics described, it follows that the potentiostatic generated noise can be used to obtain useful impedance data over a wide frequency range provided that the absolute impedance $|Z|$ of the electrode does not significantly exceed 1000 Ω. If the random fluctuations of the electrical characteristics of the electrode are negligibly small compared with the noise injected by the potentiostat, measurements of a deterministic nature can be carried out, the input being essentially white noise [5].

NOISE SOURCES IN POTENTIOSTATIC MEASUREMENTS

For the interpretation of the experimental results, it is useful to examine which sources of noise current may be contributing to the observed signal. The electrode can be represented by an equivalent circuit having a faradaic admittance Y_F in parallel with a capacitative Y_C, across which the potentiostat maintains a constant potential E plus a noise signal, which at any frequency takes the form V sin ωt. The two admittances may fluctuate causing the flow of an ac current even in the absence of an alternating signal in the control voltage. In order to simplify the argument, let us assume that the dc faradaic current can be described by a simple expression such as:

$$(I_F)_{dc} = Si_o \exp\left(\frac{\alpha FE}{RT}\right) \tag{1}$$

-3-

where S is the surface area of the electrode, i_o is a quantity proportional to the rate constant of the electrode reaction and which takes into account the choice of reference for the measurement of E. When the voltage E is applied, the faradaic admittance can be written as:

$$Y_F = \frac{(I_F)_{dc}}{E} = \frac{Si_o}{E} \exp(\frac{\alpha FE}{RT}).$$ (2)

Fluctuations in Y_F can be caused either by changes in surface area (during cathodic deposition of anodic dissolution) or in i_o, for instance, because of passive film breakdown. If Y_F fluctuates, it is obvious from (1) and (2) that also the faradaic current will do so. The amplitude of the fluctuations can be expressed as a fraction x of the average faradaic admittance (2) or as a fraction x of the dc current.

$$I_F = EY_F (1 + x \sin \omega t) = (I_F)_{dc} + x(I_F)_{dc} \sin \omega t$$ (3)

If the voltage applied in turn oscillates with amplitude V, the ac faradaic current consists of two main components, neglecting intermodulation terms, which is permissible when the fluctuations are sufficiently small. The first term, due to the fluctuations of the faradaic admittance at constant applied voltage is given by the last term in (3), whose amplitude is:

$$A_{F1} = x(I_F)_{dc}$$ (4)

The second term is the product of the voltage fluctuations and the differential admittance calculated for the average current given in (1)

$$A_{F2} = V\frac{d(I_F)_{dc}}{dE}$$ (5)

Since the phase difference between the two currents varies in a random fashion, the resulting amplitude is only little more than the larger of the two terms.

With similar reasoning it can be shown that there are two main terms for the capacitative current. The first is due to the fluctuations of

-4-

the electrode capacitance caused by the same processes that affect the
faradaic admittance. Assuming that the capacitance varies by a fraction
y at frequency ω,

$$C = C_{av} (1 + y \sin \omega t) \tag{6}$$

the capacitative current has an amplitude

$$A_{C1} = \omega y C_{av} \varepsilon \tag{7}$$

where $\varepsilon = E-E_{zc}$ is the difference between the average applied potential
and the potential of zero charge.

The second term of the capacitative current is due to the fluctuations
of the control voltage acting on the average value of the capacitance.
The amplitude is

$$A_{c2} = \omega C_{av} V \tag{8}$$

The phase difference between the second term of the faradaic current and
that of the capacitative current is fixed at $\pi/2$, but that between the
terms due to fluctuations in the electrode characteristics can vary. In
many cases a process causing an increase of electrode resistance, such as
an increase in thickness of a protecting film or a decrease in surface
area can cause a decrease of the capacitance, but this may not be always
true. Moreover, the size of the capacitative term depends on the size
of the difference ε between the electrode potential and the pzc.

Even this brief examination of the sources of noise current allows
one to estimate their relative importance in a typical situation, and
it is useful in interpreting the experimental results. For instance,
if we take an electrode whose differential faradaic admittance is $10^{-2}\Omega^{-1}$
and whose capacitance is $10^{-5}F$, the amplitude of the faradaic and
capacitative terms is shown in Table I. If the fluctuations of the faradaic
current are 0.1% of its average value of $10^{-5}A$ and the variations of the
capacitance are also of 0.1%, while $\varepsilon = 0.2$ V, the amplitude of the current

terms is also shown in Table I.

As the numbers show, the capacitative terms predominate at 1 kHz over the faradaic ones. What is also noteworthy is that fluctuations of the order of 0.1% in the electrode resistance and capacitance would cause much larger currents than those due to the potentiostat instability.

APPLICATION OF NOISE MEASUREMENTS TO B STUDY THE BREAKDOWN OF PASSIVITY

a) Aluminum in borate buffer.

The results obtained with 6061 Al in borate buffer solution to which 0.05M NaCl had been added, have shown that it is possible to determine the pitting potential by observing the significant increase of noise current that attends the formation of pits. An interesting example is given in Fig. 2, where are reported the noise spectra below the pitting potential (-700 mV vs. SCE) and at the pitting potential (-650 mV vs. SCE) during the initiation period and after development of pits (-600 mV vs. SCE). In the latter case, the noise current is more than two orders of magnitude greater than that below the pitting potential in the frequency range up to 50 Hz. The corresponding time record of Fig. 3 shows how the increase in noise covers the whole frequency range. On the contrary, Fig. 4 shows the time record taken during the induction period, and must be compared with spectrum 2 of Fig. 2. Here, isolated current bursts whose decay times range between 0.5 and 1.5 seconds, can be observed. Consequently, the increase in noise is largely limited to the low frequency end. The decay times of the current bursts correspond to the maximum repassivation times that still do not result in the formulation of a stable pit.

The noise in the current increases steadily with time: spectrum 3 was taken again at -650 mV about 10 min. after taking spectrum 2. However, the dc current was still cathodic, about 4 $\mu A/cm^2$.

The results indicate that while the very large noise levels, such as in spectrum 4 of Fig. 2 are associated with active pitting and are connected with hydrogen evolution from the pits [6], a significant increase in noise with respect to the passive state can be detected well in advance of pit formation, and is largely limited to the low frequency range, indicating that the fluctuations affect the resistive characteristics rather than the electrode capacitance. These results support the suggestions of Videm [2] that the pitting of Al involves repeated breakdown-repair events. Moreover, our results indicate that such events occur during pit initiation, assuming they are manifested as electrochemical noise. However, the character of the noise observed during pit initiation differs from that found during propagation.

b) Amorphous and crystalline Fe-Ni-Cr alloy

An amorphous passive film is generally considered more protective than a crystalline one, as shown by the fact that an increase in Cr in Fe-Ni alloys increases the resistance to attack as well as the tendency to form glassy oxide films. The passive film grown on an amorphous metal substrate is thought to have less tendency to localized breakdown because of its particularly uniform structure [7]. To gather more information on the differences in the properties of the passive films grown on amorphous and on crystalline substrates, an amorphous Fe-Ni-Cr alloy, to which P and B have been added to increase its tendency to cool in the glassy state, is being investigated. For comparison, specimens of the same alloy have been annealed in vacuum at 350°C for 3 months, so that the alloy became crystalline, as shown by the presence of broad x-ray diffraction peaks corresponding to the (110), (200) and (220) orientations, but without

-7-

phase separation because of the very low recrystallization temperature.

The current spectra of the amorphous alloy in 1 M H_2SO_4 at +550 mV vs. NHE do not show any features which can be attributed to fluctuations in the electrode characteristics. Dividing the current density by the voltage at each frequency gives the absolute impedance, as shown in Fig. 5. The relatively large value of the capacitance indicates that the passive film is thin. The spectra taken on the amorphous and on the crystalline alloy are shown in Fig. 6. Here the constant value of the current with frequency for the crystalline sample indicates that the oxide film developed on it is much thicker than on the amorphous crystal, so that the capacitance is very low.

Even more striking is the difference in behavior upon anodic polarization as shown in Fig. 7. Spectra 1 and 2 were taken on the amorphous alloy. Even polarizing at 1.59 V, where transpassive dissolution begins to occur and the dc current density increases more than 20 times to about $3.5 \cdot 10^{-3}$ A/cm^2, the fluctuations are small, so that the increase in noise at low frequency can be attributed to a moderate decrease in reaction resistance. The crystalline alloy, on the contrary, shows the characteristics of localized attack: an increase in potential of 70 mV from 1.37 V to 1.44 V causes only a modest increase in the dc current density, from 130 to 200 $\mu A/cm^2$, but has a spectacular effect in the noise level as shown by spectra 3 and 4 of Fig. 7. The monotonic decrease in noise current with frequency in spectrum 4 indicates that the fluctuations of the faradaic impedance are much larger than those of the capacitative terms. The results can be accounted for by fluctuations in the dc current density of the order of

-8-

$5 \cdot 10^{-4}$ at 50 Hz to $1.5 \cdot 10^{-4}$ at 500 Hz.

The remarkable difference in the noise spectra of the amorphous and crystallized alloy clearly shows that the latter has a much greater tendency to localized attack, no doubt due to structural inhomogenity of the passive film. Moreover, the noise measurements have revealed that the superior resistance to breakdown of the passive film in the amorphous alloy is not due to the static properties of this film because the overall current densities were observed not to differ greatly when comparing the crystallized and amorphous allo s. Rather, the greater resistance to breakdown of the amorphous alloy lay in the ability of its more homogeneous film to inhibit the dynamic processes (probably repeated breakdown-repair events) that result in electrochemical noise. These results with the amorphous and recrystallized alloys bolster the suggestions [2] that the breakdown mechanism i volves a dynamic fluctuating set of events rather than a steady deterioratio (by, for example, damaging species penetration) of the properties of the passive film.

REFERENCES

1. W. P. Iverson, J. Electrochem. Soc., 115, 617 (1968)

   G. Okamoto, T. Sugita, S. Nishiyama, K. Tachibana, Boshoku Gijutsu, 23, 439, 445 (1974).

   G. Blanc, I. Epelboin, C. Gabrielli, M. Keddam, J. Electroanal. Chem., 45, 97 (1977)

   U. Bertocci, 7th International Congress on Metallic Corrosion, Rio de Janeiro, 1978, in press.

2. K. Videm, Kjeller Report KR-149, Institutt for Atomenergi, Kjeller, Norway (1974)

   G. Okamoto, K. Tachibana, S. Nishiyama, and T. Sugita. Passivity and Its Breakdown on Iron and Iron Base Alloys, R. W. Staehle and H. Okada, Editors, NACE, Houston, Texas, P. 106 (1976).

   J. Kruger, Passivity and its Breakdown on Iron and Iron Base Alloys, R. W. Staehle, Ed., Nat. Assoc. Con. Eng., Houston, 1976, P. 94.

3. U. Bertocci, J. Electrochem. Soc., to be submitted.

4. U. Bertocci, R. W. Shideler, to be published.

5. G. Blanc, I. Epelboin, C. Gabrielli, M. Keddam, Electrochim. Acta, 20, 599 (1975)

6. C. B. Bergeron, R. B. Givens, J. Electrochem. Soc., 124, 1845 (1977) Corrosion Res. Conf. NACE, Atlanta (1979)

7. M. Naka, K. Hashimoto, T. Masumoto, Corrosion, 32, 146 (1976)

TABLE I

Amplitude of the faradaic and capacitative current components at two

frequencies, rms A.

$(I_F)_{dc} = 10^{-5}A$; $C_{av} = 10^{-5}F$; $d(I_F)_{dc}/dE = 10^{-2}\Omega^{-1}$

$\epsilon = 0.2$ V; $x = y = 10^{-3}$

Component	Formula	0.3 Hz $V = 10^{-7}$ V	1 kHz $V = 2.5^{-8}V$
A_{F2}	(5)	10^{-9}	10^{-9}
A_{C2}	(8)	$1.9 \cdot 10^{-12}$	$1.6 \cdot 10^{-9}$
A_{F1}	(4)	$7.1 \cdot 10^{-9}$	$7.1 \cdot 10^{-9}$
A_{C1}	(7)	$2.7 \cdot 10^{-9}$	$8.9 \cdot 10^{-6}$

-11-

FIGURE CAPTIONS

1. Noise voltage spectra of Fe in borate buffer + 0.01 M NaCl. Galvanostatic conditions.

2. Noise current spectra of 6061 Al in borate buffer + 0.01 M NaCl. Potentiostatic conditions. Reference: SCE. Averages over 64 spectra. 1) -700 mV.   2) -650 mV.   3) -650 mV after 10 min.   4) -600 mV.

3. Current-time signal taken with spectrum N.4. Fig. 2.
    Horizontal: 0.4 s/div. Vertical: $4.3 \cdot 10^{-7}$ $A/cm^2 \cdot$ div.

4. Current-time signal taken with spectrum N.2, Fig. 2.
    Horizontal: 0.4 s/div. Vertical: $8.6 \cdot 10^{-9}$ $A/cm^2 \cdot$ div.

5. Absolute impedance $|Z|$ vs. frequency derived from current and voltage spectra on $Fe_{32}Ni_{36}Cr_{14}P_{12}B_6$ in 1 M H_2SO_4. E = 0.57 V vs. NHE. Dashed line is calculated for R = 4200 $\Omega \cdot cm^2$, C = 5 $\mu F/cm^2$.

6. Current spectra for amorphous and crystalline $Fe_{32}Ni_{36}Cr_{14}P_{12}B_6$ in 1 M H_2SO_4. Dotted line: amorphous. Solid line: crystalline.

7. Current spectra for amorphous and crystalline $Fe_{32}Ni_{36}Cr_{14}P_{12}B_6$ in 1 M H_2SO_4. Amorphous: 1) E =1.14 V; i_{dc} = 1.5 $\cdot 10^{-4}$ A/cm^2; 2) E = 1.59; i_{dc} = 3.5 $\cdot 10^{-3}$ A/cm^2. Crystalline: 3) E = 1.37 V, i_{dc} = 1.3 $\cdot 10^{-4}$ A/cm^2.   4) E = 1.44 V, i_{dc} = 2.0 $\cdot 10^{-4}$ A/cm^2. Reference: NHE. Averages over 256 spectra.
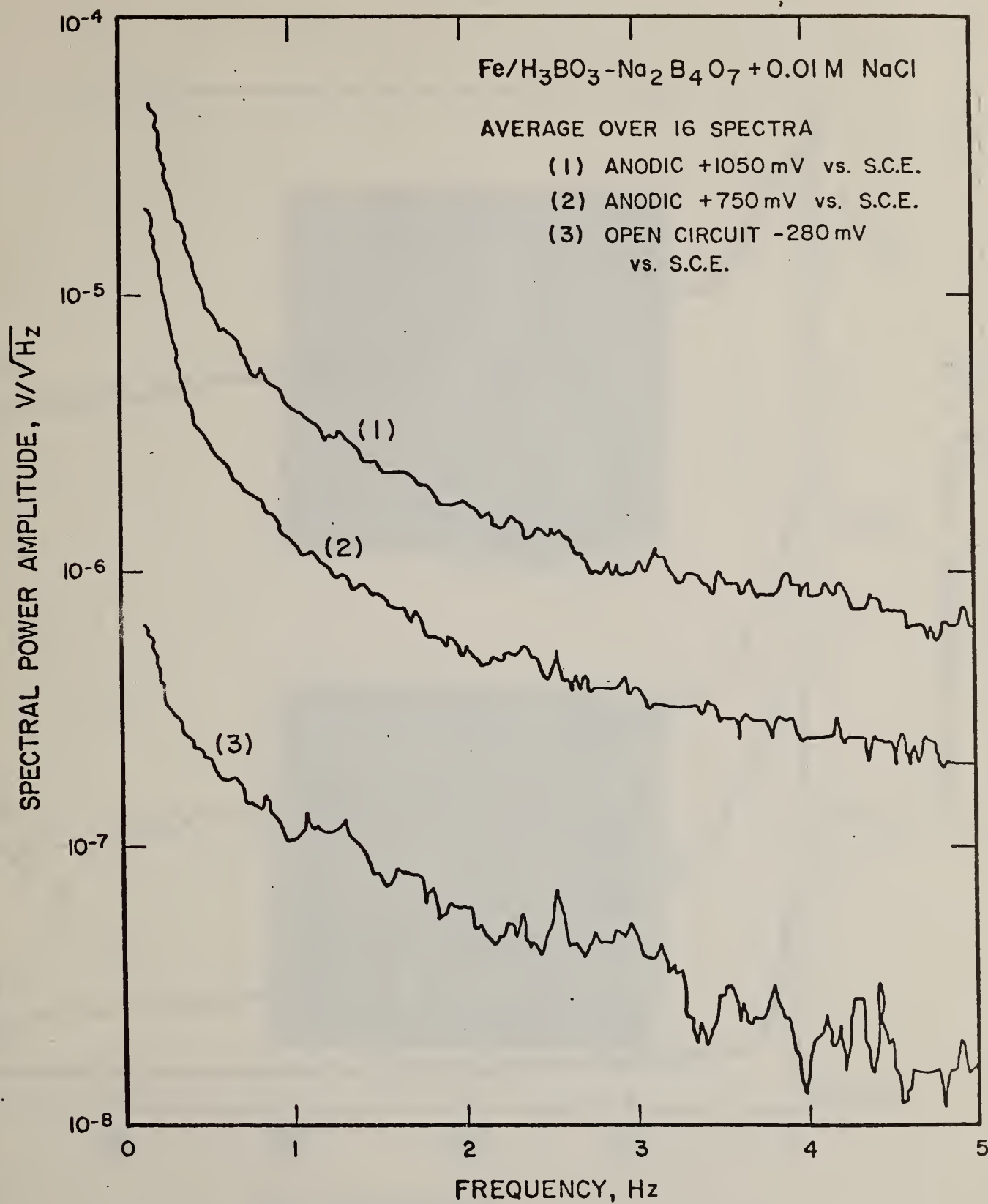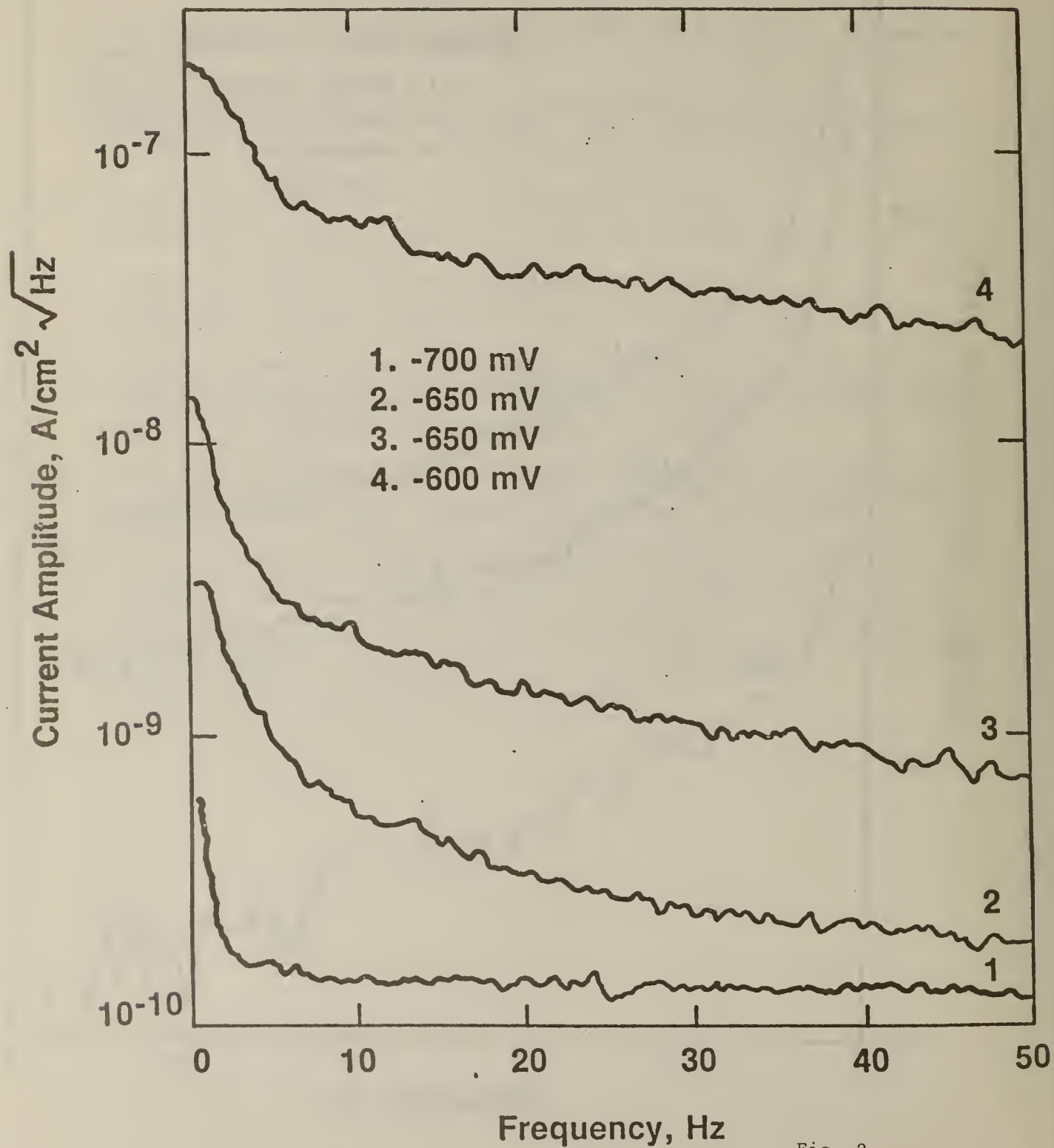
Fig. 1

Fig. 2

Fig. 3

Fig. 4

Fig. 5
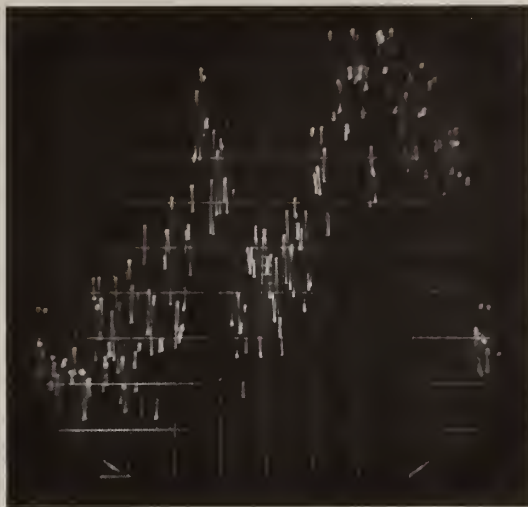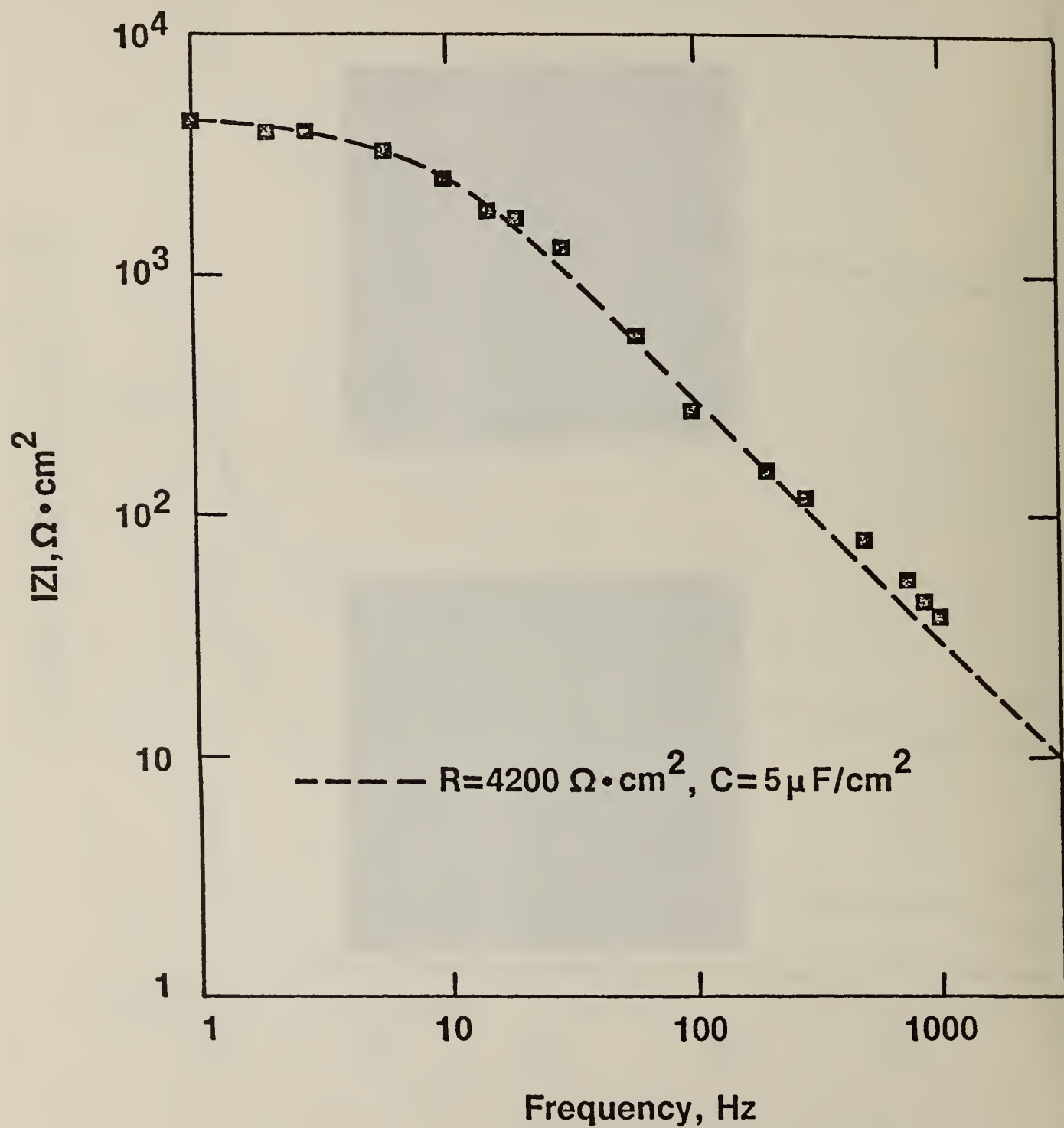
Fig. 6

$Fe_{32}Ni_{36}Cr_{14}P_{12}B_6$ in 1M H_2SO_4

Current Amplitude, $A/cm^2 \sqrt{Hz}$
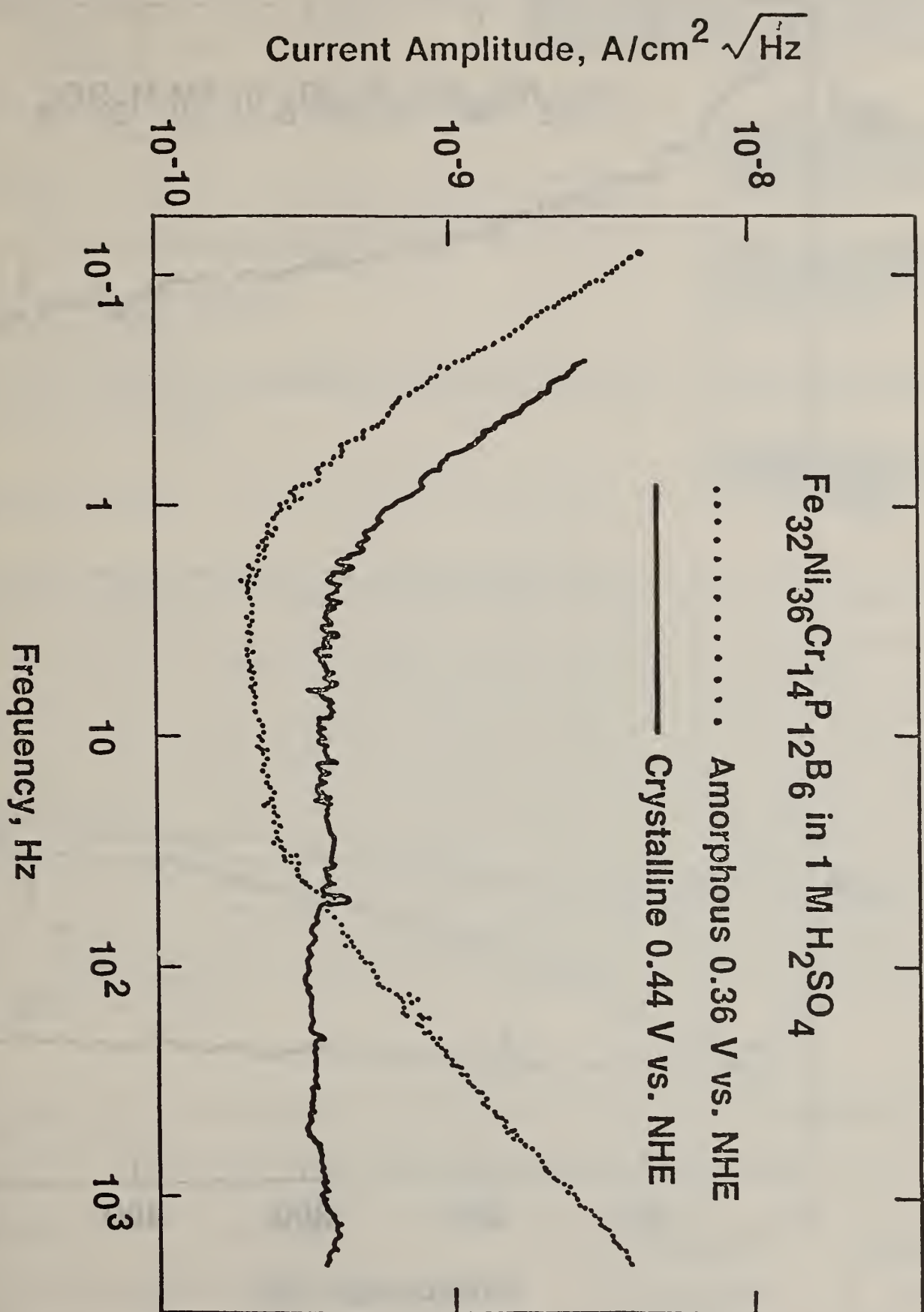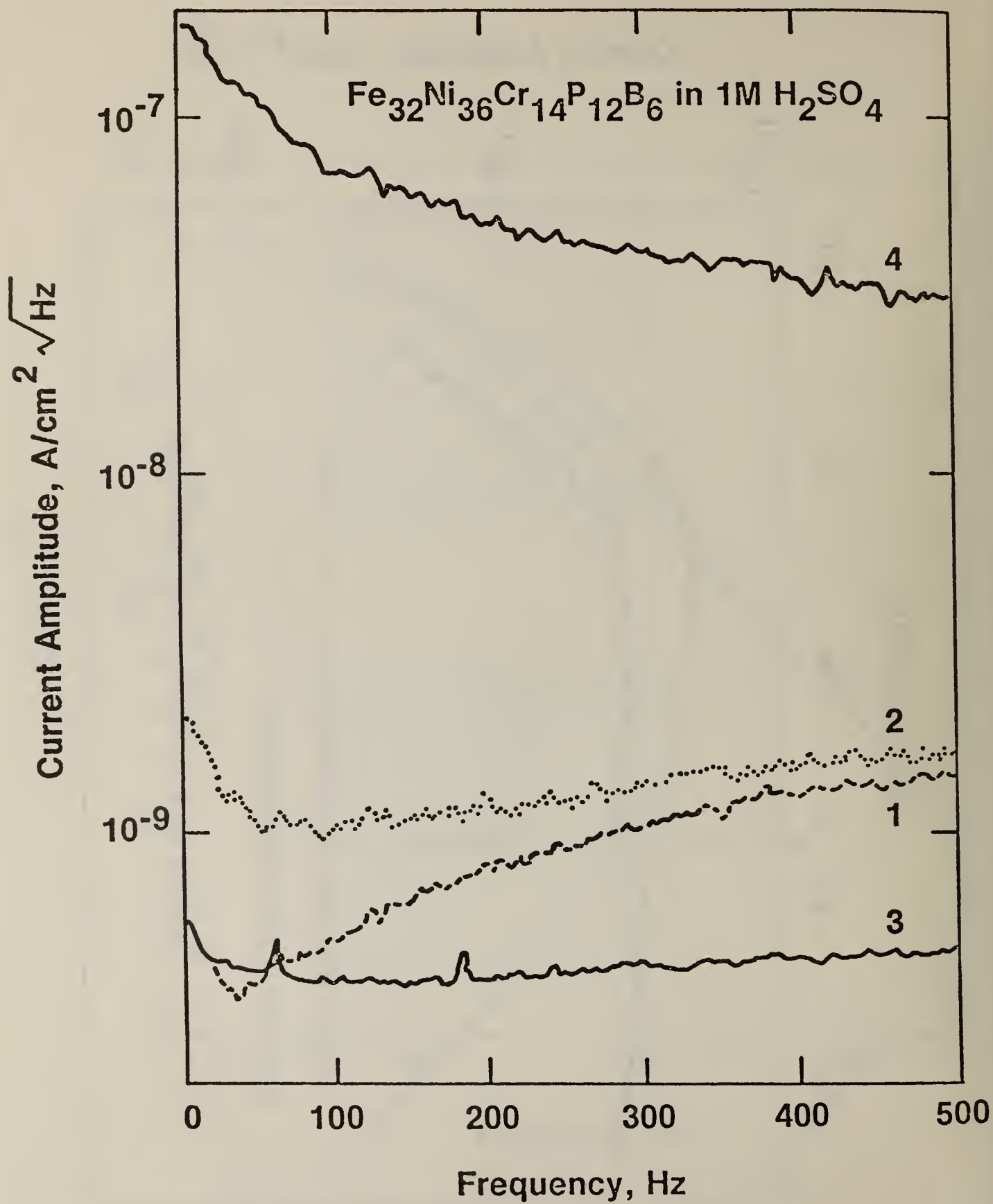
Frequency, Hz

Fig. 7

U.S. DEPT. OF COMM. BIBLIOGRAPHIC DATA SHEET	1. PUBLICATION OR REPORT NO. NBSIR 80-2083	2. Gov't. Accession No.	3. Recipient's Accession No.

4. TITLE AND SUBTITLE
Development of In-Situ Techniques for the Detection and Measurements of Corrosion of Copper Concentric Neutrals in Underground Environments

5. Publication Date
June 1980

6. Performing Organization Code

7. AUTHOR(S)
J. Kruger, U. Bertocci, E. Escalante, and J. L. Mullen

8. Performing Organ. Report No.

9. PERFORMING ORGANIZATION NAME AND ADDRESS

NATIONAL BUREAU OF STANDARDS
DEPARTMENT OF COMMERCE
WASHINGTON, DC 20234

10. Project/Task/Work Unit No.

11. Contract/Grant No.

12. SPONSORING ORGANIZATION NAME AND COMPLETE ADDRESS *(Street, City, State, ZIP)*
Department of Energy
Washington, DC 20545

13. Type of Report & Period Covered

14. Sponsoring Agency Code

15. SUPPLEMENTARY NOTES

☐ Document describes a computer program; SF-185, FIPS Software Summary, is attached.

16. ABSTRACT *(A 200-word or less factual summary of most significant information. If document includes a significant bibliography or literature survey, mention it here.)*

This is a final report on the Development of In-Situ Techniques for the Detection and Measurements of Corrosion of Copper Concentric Neutrals in Underground Environments which collects all of the papers written for the project. The titles of the papers included are: 1) Final Technical Report on the Development of In-Situ Techniques...Underground Environments; 2) Electrochemical and Corrosion Studies on Copper Concentric Neutral Wires; 3) Laboratory Corrosion Studies on Tinned Copper Concentric Neutral Wires; 4) Corrosion Induced by an Alternating Voltage. A Comparison Between Theoretical Predictions and Experimental Results; 5) Detection and Analysis of Electrochemical Noise for Corrosion Studies; 6) Applications of a Low-Noise Potentiostat in Electrochemical Measurements; 7) A Low-Noise Potentiostat for the Study of Small Amplitude Signals in Electrochemistry; 8) Corrosion Enhancement Due to Large Voltage Modulations. Frequency Analysis of the Response of Electrodes Under Charge-Transfer Control; 9) Studies of Passive Film Breakdown by Detection and Analysis of Electrochemical Noise; 10) A Field Study on the Corrosion of Concentric Neutral Cable; 11) AC Induced Corrosion. The Effect of an Alternating Voltage on Electrodes Under Charge-Transfer Control.

17. KEY WORDS *(six to twelve entries; alphabetical order; capitalize only the first letter of the first key word unless a proper name; separated by semicolons)*

Corrosion; corrosion noise; electrochemistry; polarization techniques; underground corrosion

18. AVAILABILITY	☒ Unlimited	19. SECURITY CLASS (THIS REPORT)	21. NO. OF PRINTED PAGES
☐ For Official Distribution. Do Not Release to NTIS		UNCLASSIFIED	135
☐ Order From Sup. of Doc., U.S. Government Printing Office, Washington, DC 20402, SD Stock No. SN003-003-		20. SECURITY CLASS (THIS PAGE)	22. Price
☒ Order From National Technical Information Service (NTIS), Springfield, VA. 22161		UNCLASSIFIED	$10.00